

NASA
TN
D-7428
c.1(R)

N74-11821

LOW-SPEED AERODYNAMIC CHARACTERISTICS
OF A 17-PERCENT-THICK AIRFOIL SECTION
DESIGNED FOR GENERAL AVIATION APPLICATIONS

Robert J. McGhee, et al

Langley Research Center
Hampton, Virginia

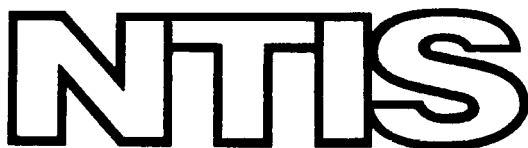
LOAN COPY: RETURN TO
AFWL TECHNICAL LIBRARY
KIRTLAND AFB, N. M.

December 1973

TECH LIBRARY KAFB, NM

0133579

DISTRIBUTED BY:

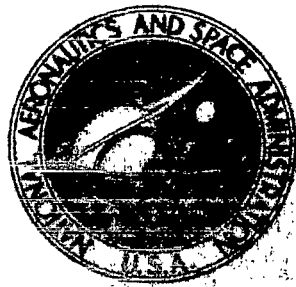


National Technical Information Service
U. S. DEPARTMENT OF COMMERCE



0133579

ASA TECHNICAL NOTE



NASA TM D-7428

N74-11821

(NASA-TM-D-7428) LOW SPEED AERODYNAMIC
CHARACTERISTICS OF A 17 PERCENT THICK
AIRFOIL SECTION DESIGNED FOR GENERAL
AVIATION APPLICATIONS (NASA)

IC

ISCL 01A 81/01

Unclassified
23743

LOW-SPEED AERODYNAMIC CHARACTERISTICS
OF A 17-PERCENT-THICK AIRFOIL SECTION
DESIGNED FOR GENERAL AVIATION APPLICATIONS

by Robert J. McGhee and William D. Beasley

Langley Research Center

Hampton, Va. 23665

Reproduced by
NATIONAL TECHNICAL
INFORMATION SERVICE
US Department of Commerce
Springfield, VA 22151

NATIONAL AERONAUTICS AND SPACE ADMINISTRATION • WASHINGTON, D. C. • DECEMBER 1973

1. Report No. NASA TN D-7428	2. Government Accession No.	3. Recipient's Catalog No.
4. Title and Subtitle LOW-SPEED AERODYNAMIC CHARACTERISTICS OF A 17-PERCENT-THICK AIRFOIL SECTION DESIGNED FOR GENERAL AVIATION APPLICATIONS		
7. Author(s) Robert J. McGhee and William D. Beasley		
9. Performing Organization Name and Address NASA Langley Research Center Hampton, Va. 23665		
12. Sponsoring Agency Name and Address National Aeronautics and Space Administration Washington, D.C. 20546		
15. Supplementary Notes		

16. Abstract

Wind-tunnel tests have been conducted to determine the low-speed two-dimensional aerodynamic characteristics of a 17-percent-thick airfoil designed for general aviation applications (GA(W)-1). The results were compared with predictions based on a theoretical method for calculating the viscous flow about the airfoil. The tests were conducted over a Mach number range from 0.10 to 0.28. Reynolds numbers based on airfoil chord varied from 2.0×10^6 to 20.0×10^6 . Maximum section lift coefficients greater than 2.0 were obtained and section lift-drag ratio at a lift coefficient of 1.0 (climb condition) varied from about 65 to 85 as the Reynolds number increased from about 2.0×10^6 to 6.0×10^6 .

PRICES SUBJECT TO CHANGE

17. Key Words (Suggested by Author(s)) Low-speed airfoil section Reynolds number effects Experimental-theoretical comparison GA(W)-1 airfoil General aviation aircraft	18. Distribution Statement Unclassified - Unlimited
19. Security Classif. (of this report) Unclassified	20. Security Classif. (of this page) Unclassified

LOW-SPEED AERODYNAMIC CHARACTERISTICS OF A
17-PERCENT-THICK AIRFOIL SECTION DESIGNED
FOR GENERAL AVIATION APPLICATIONS

By Robert J. McGhee and William D. Beasley
Langley Research Center

SUMMARY

An investigation was conducted in the Langley low-turbulence pressure tunnel to determine the low-speed two-dimensional aerodynamic characteristics of a 17-percent-thick airfoil designed for general aviation applications. The results are compared with a typical older NACA 65 series airfoil section. Also, a comparison between experimental data and predictions, based on a theoretical method for calculating the viscous flow about the airfoil, is presented. The tests were conducted over a Mach number range from 0.10 to 0.28 and an angle-of-attack range from -10° to 24° . Reynolds numbers, based on the airfoil chord, were varied from about 2.0×10^6 to 20.0×10^6 .

The results of the investigation indicate that maximum section lift coefficients increased rapidly at Reynolds numbers from about 2.0×10^6 to 6.0×10^6 and attained values greater than 2.0 for the plain airfoil and greater than 3.0 with a 20-percent-chord split flap deflected 60° . Stall characteristics were generally gradual and of the trailing-edge type either with or without the split flap. At a lift coefficient of 1.0 (climb condition) the section lift-drag ratio increased from about 65 to 85 as the Reynolds number increased from about 2.0×10^6 to 6.0×10^6 . Maximum section lift coefficients were about 30 percent greater than that of a typical older NACA 65 series airfoil section and the section lift-drag ratio at a lift coefficient of 0.90 was about 50 percent greater. Agreement of experimental results with predictions based on a theoretical method which included viscous effects was good for the pressure distributions as long as no boundary-layer flow separation was present, but the theoretical method predicted drag values greatly in excess of the measured values.

INTRODUCTION

Research on advanced aerodynamic technology airfoils has been conducted over the last several years at the Langley Research Center. Results of this research have been applied to the design of a 17-percent-thick airfoil suitable for a propeller driven light airplane.

The subcritical characteristics of thick supercritical airfoil section research of reference 1 indicated performance increases over conventional airfoil sections. Some of the features that produce these favorable aerodynamic characteristics have been applied in the design of a new low-speed airfoil section. This new airfoil is one of several being developed by NASA for light airplanes and has been designated as General Aviation (Whitcomb)-number one airfoil (GA(W)-1).

The present investigation was conducted to determine the basic low-speed two-dimensional aerodynamic characteristics of the NASA GA(W)-1 airfoil section. In addition, the results are compared to a comparable NACA 65 series airfoil section. Such sections are presently used on some light airplanes. Also, the experimental results are compared with results obtained from an analytical aerodynamic performance prediction method.

The investigation was performed in the Langley low-turbulence pressure tunnel over a Mach number range from 0.10 to 0.28. The Reynolds number, based on airfoil chord, varied from about 2.0×10^6 to 20.0×10^6 . The geometrical angle of attack varied from about -10° to 24° .

SYMBOLS

Values are given both in SI and the U.S. Customary Units. The measurements and calculations were made in the U.S. Customary Units.

a mean-line designation

C_p pressure coefficient, $\frac{p_L - p_\infty}{q_\infty}$

c chord of airfoil, cm (in.)

c_c section chord-force coefficient,

$$\int_{\text{forward } (t/c)_{\max}} C_p d\left(\frac{z}{c}\right) - \int_{\text{aft } (t/c)_{\max}} C_p d\left(\frac{z}{c}\right)$$

c_d section profile-drag coefficient determined from wake measurements,

$$\int_{\text{wake}} c_d' d\left(\frac{h}{c}\right)$$

c_d'	point drag coefficient, $2\left(\frac{\rho_1}{\rho_2}\right)^{1/2}\left(\frac{q_1}{q_\infty}\right)^{1/2}\left[\left(\frac{\rho_2}{\rho_\infty}\right)^{1/2} - \left(\frac{q_2}{q_\infty}\right)^{1/2}\right]$
c_l	section lift coefficient, $c_n \cos \alpha - c_c \sin \alpha$
$c_{l,i}$	design section lift coefficient
c_m	section pitching-moment coefficient about quarter chord, $\int_{l.s.} C_p \left(0.25 - \frac{x}{c}\right) d\left(\frac{x}{c}\right) - \int_{u.s.} C_p \left(0.25 - \frac{x}{c}\right) d\left(\frac{x}{c}\right)$
c_n	section normal-force coefficient, $\int_{l.s.} C_p d\left(\frac{x}{c}\right) - \int_{u.s.} C_p d\left(\frac{x}{c}\right)$
h	vertical distance in wake profile, cm (in.)
l/d	section lift-drag ratio, c_l/c_d
M	free-stream Mach number
p	static pressure, N/m ² (lb/ft ²)
q	dynamic pressure, N/m ² (lb/ft ²)
R	Reynolds number based on free-stream conditions and airfoil chord
t	airfoil thickness, cm (in.)
x	airfoil abscissa, cm (in.)
z	airfoil ordinate, cm (in.)
z_c	mean line ordinate, cm (in.)
α	angle of attack of airfoil, angle between chord line and airstream axis, deg
ρ	density, kg/m ³ (slugs/ft ³)

Subscripts:

L	local point on airfoil
max	maximum
t	thickness
1	tunnel station 1 chord length downstream of model
2	tunnel station downstream of model where static pressure is equal to free-stream static pressure
∞	undisturbed stream conditions

Abbreviations:

GA(W)-1 General Aviation (Whitcomb)-number one

l.s.	lower surface
u.s.	upper surface

AIRFOIL DESIGN

The airfoil section (fig. 1) was developed by employing some of the favorable characteristics of the thick supercritical airfoil of reference 1, which indicated performance increases over conventional airfoils at subcritical conditions. In order to expedite the airfoil development, the computer program of reference 2 was used to predict the results of various design modifications. The final airfoil shape was defined after 17 iterations on the computer. The airfoil is 17 percent thick with a blunt nose and a cusped lower surface near the trailing edge. The design cruise lift coefficient was about 0.40 at a Reynolds number of about 6×10^6 . In defining the airfoil emphasis was placed on providing good lift-drag ratios at $c_l = 1.0$ for improved climb performance, and on providing a maximum lift coefficient of about 2.0. Several key design features of the airfoil are:

1. A large upper surface leading-edge radius (about $0.06c$) was used to attenuate the peak negative pressure coefficients and therefore delay airfoil stall to high angles of attack.

2. The airfoil was contoured to provide an approximate uniform chordwise load distribution near the design lift coefficient of 0.40. To account for viscous effects this airfoil incorporated more camber in the rear of the airfoil than the NACA mean camber line (fig. 2).

3. A blunt trailing edge was provided with the upper and lower surface slopes approximately equal to moderate the upper surface pressure recovery and thus postpone the stall.

The airfoil thickness distribution and camber line are presented in figure 2. Table I presents the measured airfoil coordinates.

APPARATUS AND PROCEDURE

Model Description

The airfoil model was machined from an aluminum billet and had a chord of 58.42 cm (23 in.) and a span of 91.44 cm (36 in.). The airfoil surface was fair and smooth. Figure 3 shows a photograph of the model. The model was equipped with both upper and lower surface orifices located at the chord stations indicated in table II. A base pressure orifice was included in the blunt trailing edge of the airfoil ($x/c = 1.0$). In order to provide data for a simple flap deflection, an aluminum wedge was installed on the model to simulate a split flap deflected 60° . Orifices were installed on this simulated flap as indicated in table II.

Wind Tunnel

The Langley low-turbulence pressure tunnel (ref. 3) is a closed-throat single-return tunnel which can be operated at stagnation pressures from 101.3 to 1013 kN/m² (1 to 10 atm) with tunnel-empty test-section Mach numbers up to 0.46 and 0.23, respectively. The maximum unit Reynolds number is about 49×10^6 per meter (15×10^6 per foot) at a Mach number of 0.23. The test section is 91.44 cm (3 ft) wide by 228.6 cm (7.5 ft) high.

Circular end plates provided attachment for the two-dimensional model. The end plates are 101.6 cm (40 in.) in diameter and are flush with the tunnel wall. They are hydraulically rotated to provide for model angle-of-attack changes. The airfoil was mounted so that the center of rotation of the circular plates was at 0.25c on the model chord line. The air gaps at the tunnel walls were sealed with flexible-sliding metal seals (fig. 4).

Wake Survey Rake

A fixed wake survey rake (fig. 5) at the model midspan was mounted from the tunnel sidewall and located 1 chord length rearward of the trailing edge of the airfoil. The wake rake utilized 91 total-pressure tubes and five static-pressure tubes 0.1524 cm (0.060 in.) in diameter. The total-pressure tubes were flattened to 0.1016 cm (0.040 in.) for 0.6096 cm (0.24 in.) from the tip of the tubes. The static pressure tubes had four flush orifices drilled 90° apart and located 8 tube diameters from the tip of the tube and in the measurement plane of the total-pressure tubes. Three tunnel sidewall static pressures were also measured from orifices located in the measurement plane of the total-pressure tubes. One static orifice was located on the center line of the tunnel and the other two orifices were about 0.35c above and below the center line of the tunnel.

Instrumentation

Measurements of the static pressures on the airfoil surfaces and the wake rake pressures were made by an automatic pressure-scanning system utilizing variable capacitance type precision transducers. Basic tunnel pressures were measured with precision quartz manometers. Angle of attack was measured with a calibrated potentiometer operated by a pinion gear and rack attached to the circular plates. Data were obtained by a high-speed data-acquisition system and recorded on magnetic tape.

TESTS AND METHODS

The airfoil was investigated at Mach numbers from 0.10 to 0.28 over an angle-of-attack range from about -10° to 24°. Reynolds number based on the airfoil chord was varied from about 2.0×10^6 to 20.0×10^6 , primarily by varying the tunnel stagnation pressure. The model was tested both with the wake rake installed and removed to determine its influence on the flow over the airfoil. Figure 6 shows typical lift coefficient and pitching-moment-coefficient data and no effects were indicated. The pressure distribution data also indicated no effect of the wake rake on the flow over the airfoil. The airfoil was tested both smooth (natural boundary-layer transition) and with roughness located on both upper and lower surfaces at 0.08c. The roughness was sized according to reference 4 which indicated a nominal roughness particle height of 0.0107 cm (0.0042 in.) at a Reynolds number of 6×10^6 and 0.0257 cm (0.0101 in.) at a Reynolds number of 2×10^6 . The corresponding commercial grit numbers required are number 120 and number 60. The transition strips were 0.25 cm (0.10 in.) wide. The roughness was sparsely spaced and attached to the airfoil surface with lacquer. Several different roughness sizes were used for the same test conditions and these results are shown in figure 7. For several runs the standard NACA method of applying roughness (number 60 grit wrapped around leading edge on both surfaces back to 0.08c) was employed (ref. 5). For several test runs

oil was spread over the airfoil upper surface to determine if any local flow separation was present. Tufts were attached to the airfoil and tunnel sidewalls with plastic tape to determine stall patterns on both the airfoil and adjacent sidewalls.

The static-pressure measurements at the airfoil surface were reduced to standard pressure coefficients and then machine integrated to obtain section normal-force and chord-force coefficients and section pitching-moment coefficients about the quarter chord. Section profile-drag coefficient was computed from the wake rake measurements by the method of reference 6. The wake rake static-pressure measurements indicated some influence on the static pressures due to the presence of the rake body; therefore, the tunnel sidewall static pressures were used in computing the section profile-drag coefficients.

An estimate of the standard low-speed wind-tunnel boundary corrections as calculated by the method of reference 7 is shown in figure 8. These corrections amount to about 2 percent of the measured coefficients and have not been applied to the data. An estimate of the total head tube displacements effects on the values of c_d showed these effects to be negligible.

RESULTS

The results of this investigation have been reduced to coefficient form and are presented in the following figures:

	Figure
Tuft photographs of NASA GA(W)-1 airfoil	9
Effect of Reynolds number on section characteristics, model smooth	10
Effect of Mach number on section characteristics, model smooth, $R \approx 6 \times 10^6$	11
Effect of Reynolds number on section characteristics, roughness located at $0.08c$	12
Effect of Mach number on section characteristics, roughness located at $0.08c$, $R \approx 6 \times 10^6$	13
Effect of roughness on section characteristics	14
Comparison of section characteristics between NASA GA(W)-1 and NACA 65 ₂ -415 and 65 ₃ -418 airfoils	15
Variation of maximum section lift coefficient with Reynolds number for various airfoils without flaps	16

Figure

Section characteristics for 0.20c simulated split flap deflected 60°	17
Effect of angle of attack on chordwise pressure distributions	18
Comparison of experimental and theoretical aerodynamic characteristics	19
Comparison of experimental and theoretical chordwise pressure distributions . .	20

DISCUSSION OF RESULTS

Experimental Results

Lift.- Figure 10 shows that with the airfoil smooth (natural boundary-layer transition) a lift-curve slope of about 0.12 per degree and a lift coefficient of about 0.52 at $\alpha = 0^\circ$ was obtained for all Mach numbers and Reynolds numbers investigated. Maximum lift coefficients increased from about 1.64 to about 2.12 as the Reynolds number was increased from about 2×10^6 to 12×10^6 at $M = 0.15$ (fig. 16), with the most rapid increase occurring between Reynolds numbers of 2×10^6 and 6×10^6 . Increasing the Reynolds number above 12×10^6 had no additional effect on maximum lift coefficient as shown by figure 10(b) ($M = 0.20$).

The GA(W)-1 airfoil section encounters a gradual type stall (fig. 10), particularly in the lower Reynolds number ranges. Tuft pictures (fig. 9) indicated the stall is of the turbulent or trailing-edge type. (See also pressure data of fig. 18.)

At a Reynolds number of 6.0×10^6 , increasing the Mach number from 0.10 to 0.28 had only a minor effect on the lift characteristics as shown by the results presented in figure 11(a). The stall angle of attack was decreased about 2° and maximum lift coefficient about 5 percent.

The addition of roughness at $0.08c$ (figs. 12 and 14) did alter the effective airfoil shape because of changes in boundary-layer thickness, particularly for $R = 2.0 \times 10^6$ as shown in figure 14(a). For example, the angle of attack for zero lift coefficient changed from about -4° to -3.6° . No measurable change in lift-curve slope was indicated; therefore, the lift coefficient at $\alpha = 0^\circ$ decreased from about 0.52 to about 0.43. These effects on the lift characteristics decreased as the Reynolds number was increased above 2.0×10^6 as might be expected because of the related decrease in boundary-layer thickness. Figure 13(a) indicates that the effects of Mach number with roughness applied to the airfoil were similar to those with the model smooth.

Comparisons of the values of $(c_l)_{\max}$ for the NASA GA(W)-1 airfoil with other NACA airfoils without flaps are shown in figure 16. Substantial improvements in $(c_l)_{\max}$ for the GA(W)-1 airfoil throughout the Reynolds number range are indicated when compared

to the NACA 4 and 5 digit airfoils and 65 series airfoils. Both the GA(W)-1 and 65₃-418 airfoils have the same design lift coefficient (0.40) and figure 2 indicates both airfoils have roughly the same mean thickness distribution in the region of the structural box (0.15c to 0.60c). At a Reynolds number of 6.0×10^6 , a 30-percent improvement in $(c_l)_{max}$ is shown for the GA(W)-1 airfoil over the comparable 65₃-418 airfoil. Typical operating ranges of Reynolds numbers for general aviation airplanes are from about 2×10^6 to 6×10^6 . These improvements result from two primary considerations of the design; first, attenuating of the peak negative pressure coefficients on the upper surface near the leading edge by use of a large leading-edge radius, and second, the attainment of increased aft loading by using the greater aft camber. Figure 15(a) shows a comparison of the lift characteristics of the NACA 65 series airfoils and NASA GA(W)-1 airfoil at a Reynolds number of about 6×10^6 with roughness located near the leading edge of the airfoils. Even when the large wraparound roughness was employed on the new airfoil, it exhibited superior lift characteristics to the older NACA 65 series airfoils although it stalled about 4° earlier than with the narrow strip roughness now usually employed.

In order to obtain some preliminary information on the new airfoil section in a high-lift configuration, a simple 0.20c split flap deflected 60° was installed on the model. The increment in c_l at a Reynolds number of about 6.0×10^6 between the basic airfoil and flapped airfoil was about 1.46 at $\alpha = 0^\circ$ and about 1.2 at $(c_l)_{max}$. (Compare figs. 10(b) and 17.) The data of reference 5 indicate an increment in c_l of about 1.40 at $\alpha = 0^\circ$ and about 1.2 at $(c_l)_{max}$ for the NACA 65₃-418 airfoil. Comparison of the values of $(c_l)_{max}$ for the two airfoils with the simulated split flap deflected 60° shows about a 17-percent increase for the GA(W)-1 airfoil (3.16 compared to 2.70). Similar improvements are also indicated when compared to the NACA 4418 airfoil with simulated split flap deflected 60°. The stall characteristics of the GA(W)-1 airfoil with the simulated flap were gradual as indicated by the lift characteristics and tuft studies.

Pitching moment. - The pitching-moment-coefficient data (fig. 10) were generally insensitive to Reynolds number in the low angle-of-attack range. However, for angles of attack greater than about 4° the low Reynolds number data indicate less negative values of c_m . Increasing the Reynolds number, which results in a decrease in boundary-layer thickness, caused negative increments in c_m up to airfoil stall. At a Reynolds number of 6.0×10^6 increasing the Mach number from 0.10 to 0.28 (fig. 11(a)) caused no effect on the pitching-moment data up to about 12°. At higher angles of attack a positive increment in c_m is shown.

The addition of roughness (figs. 12 and 14) at 0.08c resulted in a positive increment in c_m at Reynolds numbers of 2×10^6 and 4×10^6 . However, at a Reynolds number of 6×10^6 this increment had essentially disappeared.

Comparison of the pitching-moment data of the GA(W)-1 airfoil with that of the 653-418 airfoil (fig. 15(a)) at a Reynolds number of about 6×10^6 indicates a more negative c_m of about 0.04 for the GA(W)-1 section. This is expected because of the aft loading of the GA(W)-1 airfoil section as illustrated by the camber distribution of figure 2.

Drag. - The profile drag data of figure 10 generally show, at moderate lift coefficients, the expected decrease in c_d with increases in Reynolds number. This drag reduction is associated with the related decreases in boundary-layer thickness and accompanying reduction in skin friction drag. An increased amount of laminar flow is indicated at a Reynolds number of about 2×10^6 (fig. 10(a)) by the low values of c_d obtained in the low lift-coefficient range (typical laminar bucket). In practical applications no laminar bucket, such as shown here, should be expected since the design velocity characteristics were not selected for this purpose. Laminar flow designs are generally impractical for general aviation airplanes since transition is usually fixed near the leading edge of the airfoil by the roughness of construction or insect remains gathered in flight.

For general aviation application, the drag data of most practical interest are those obtained with a turbulent boundary layer over most of the airfoil chord in the Reynolds number range from about 2×10^6 to 6×10^6 . Figure 12(b) illustrates the drag data with fixed transition at $0.08c$ for this Reynolds number range. The drag coefficient at the design lift coefficient ($c_l = 0.40$) at a typical cruise Reynolds number of 6×10^6 is about 0.0108. However, figures 7(b) and 12(b) indicate a large lift-coefficient range where the values of c_d remain approximately constant. This is of particular importance from a safety standpoint for light general aviation airplanes where large values of section lift-drag ratio at high lift coefficients result in improved climb performance. Thus, at $c_l = 1.0$ section lift-drag ratios vary from about 65 at $R = 2.1 \times 10^6$ to about 85 at $R = 6.3 \times 10^6$ (fig. 12(b)).

A comparison between the section lift-drag characteristics of the GA(W)-1 airfoil and the older NACA 65 series airfoils is shown in figure 15(b). For the older type airfoils a coarse size grit was extensively applied (0.08c) over the airfoil in order to achieve transition in the wind tunnel. This older method of applying large wrap-around roughness (NACA standard) results in an increment in c_d of about 0.0010 at $c_l = 0.40$ for the GA(W)-1 airfoil when compared to the narrow roughness strip now usually employed (NASA standard). However, in order to obtain a direct comparison of the drag coefficients between the airfoils the comparison is made with the older NACA standard method of employing roughness.

On this basis figure 15(b) shows at $R \approx 6.0 \times 10^6$ that the section drag coefficient, at a cruise lift coefficient of about 0.40, for the 17-percent-thick GA(W)-1 airfoil is about

0.0010 higher than that for the 65₃-418 airfoil. However, comparison of the section lift-drag ratios at a lift coefficient of 0.90, the highest c_l for which data were available, indicates about a 50-percent improvement for the GA(W)-1 airfoil section ($l/d = 47$ for 65₃-418 airfoil compared to $l/d = 70$ for GA(W)-1 airfoil). The figure also indicates that even greater improvements would probably occur at higher climb lift coefficients.

Pressure distributions.- The chordwise pressure data of figure 18 illustrate the effects of angle of attack for a Reynolds number of 6.3×10^6 . The data at $\alpha = 0^\circ$ ($c_l = 0.47$) indicate approximately constant values of C_p from about $x/c = 0.05$ to $x/c = 0.55$ for both the upper and lower surfaces of the airfoil (design condition). Upper and lower surface pressure coefficients at the airfoil trailing edge are slightly positive. Some upper surface trailing-edge separation is first indicated at an angle of attack of about 8° by the constant pressure region on the upper surface of the airfoil and is also indicated by the nonlinear lift curves above this angle of attack. Increases in angle of attack above 8° resulted in this constant pressure region moving forward along the airfoil and at maximum lift coefficient ($\alpha = 19.06^\circ$) trailing-edge separation was present from about $x/c = 0.70$ to the airfoil trailing edge. The airfoil stall is of the turbulent, or trailing edge, type as indicated by figure 18(k) ($\alpha = 20.05^\circ$) and as observed by means of tuft studies.

Comparison of Experimental and Theoretical Data

Predictions of the aerodynamic characteristics by the viscous flow method of reference 2 are compared with the experimental results at $R = 6.3 \times 10^6$ in figure 19. As previously mentioned, this viscous flow method was employed during the development of the GA(W)-1 airfoil shape. The theoretical method predicts the lift and pitching-moment data well for angles of attack where no boundary-layer flow separation is present (up to about 8°). However, the theoretical method overpredicts the drag data throughout this same lift-coefficient range. Examples of pressure distributions calculated by the theoretical method are compared with the experimental pressures in figure 20. The agreement between experiment and theory is good over most of the chord length of the airfoil, as long as no boundary-layer flow separation is present.

CONCLUDING REMARKS

Wind-tunnel tests have been conducted to determine the low-speed two-dimensional aerodynamic characteristics of a 17-percent-thick airfoil section designed for general aviation applications. The results were compared with a typical older NACA 65 series airfoil section. Also, the experimental data are compared with predictions based on a theoretical method for calculating the viscous flow about the airfoil. The tests were

conducted over a Mach number range from 0.10 to 0.28. Reynolds number based on the airfoil chord was varied from about 2×10^6 to 20×10^6 . The following results were determined from this investigation:

1. Maximum section lift coefficients increased rapidly at Reynolds number from about 2.0×10^6 to 6.0×10^6 and attained values greater than 2.0 for the plain airfoil and greater than 3.0 with a 20-percent-chord split flap deflected 60°.
2. Stall characteristics were generally gradual and of the trailing-edge type either with or without the split flap.
3. Section lift-drag ratio at a lift coefficient of 1.0 (climb condition) increased from about 65 to 85 as the Reynolds number increased from about 2.0×10^6 to 6.0×10^6 .
4. Maximum section lift coefficients were about 30 percent greater than a typical older NACA 65 series airfoil and the section lift-drag ratio at a lift coefficient of 0.90 was about 50 percent greater.
5. Comparison of experiment with predictions based on a theoretical method which included viscous effects was good for the pressure distributions as long as no boundary-layer flow separation was present, but the predicted drag values were much greater than measured values.

Langley Research Center,
National Aeronautics and Space Administration,
Hampton, Va., October 16, 1973.

REFERENCES

1. Ayers, Theodore G.: Supercritical Aerodynamics: Worthwhile Over a Range of Speeds. *Astronaut. & Aeronaut.*, vol. 10, no. 8, Aug. 1972, pp. 32-36.
2. Stevens, W. A.; Goradia, S. H.; and Braden, J. A.: Mathematical Model for Two-Dimensional Multi-Component Airfoils in Viscous Flow. NASA CR-1843, 1971.
3. Von Doenhoff, Albert E.; and Abbott, Frank T., Jr.: The Langley Two-Dimensional Low-Turbulence Pressure Tunnel. NACA TN 1283, 1947.
4. Braslow, Albert L.; and Knox, Eugene C.: Simplified Method for Determination of Critical Height of Distributed Roughness Particles for Boundary-Layer Transition at Mach Numbers From 0 to 5. NACA TN 4363, 1958.
5. Abbott, Ira H.; and Von Doenhoff, Albert E.: Theory of Wing Sections. Dover Publ., Inc., c.1959.
6. Baals, Donald D.; and Mourhess, Mary J.: Numerical Evaluation of the Wake-Survey Equations for Subsonic Flow Including the Effect of Energy Addition. NACA WR L-5, 1945. (Formerly NACA ARR L5H27.)
7. Allen, H. Julian; and Vincenti, Walter G.: Wall Interference in a Two-Dimensional-Flow Wind Tunnel, With Consideration of the Effects of Compressibility. NACA Rep. 782, 1944. (Supersedes NACA WR A-63.)

TABLE I.- NASA GA(W)-1 AIRFOIL COORDINATES

 $[c = 58.42 \text{ cm (23 in.)}]$

x/c	$(z/c)_{\text{upper}}$	$(z/c)_{\text{lower}}$
0.0	0.0	0.0
.002	.01300	-.00974
.005	.02035	-.01444
.0125	.03069	-.02052
.025	.04165	-.02691
.0375	.04974	-.03191
.05	.05600	-.03569
.075	.06561	-.04209
.100	.07309	-.04700
.125	.07909	-.05087
.150	.08413	-.05426
.175	.08848	-.05700
.20	.09209	-.05926
.25	.09778	-.06265
.30	.10169	-.06448
.35	.10409	-.06517
.40	.10500	-.06483
.45	.10456	-.06344
.50	.10269	-.06091
.55	.09917	-.05683
.575	.09674	-.05396
.60	.09374	-.05061
.625	.09013	-.04678
.65	.08604	-.04265
.675	.08144	-.03830
.700	.07639	-.03383
.725	.07096	-.02930
.750	.06517	-.02461
.775	.05913	-.02030
.800	.05291	-.01587
.825	.04644	-.01191
.850	.03983	-.00852
.875	.03313	-.00565
.900	.02639	-.00352
.925	.01965	-.00248
.950	.01287	-.00257
.975	.00604	-.00396
1.000	-.00074	-.00783

TABLE II.- AIRFOIL ORIFICE LOCATIONS

Upper surface		Lower surface	
x/c	z/c	x/c	z/c
0.0	0.00030	0.00678	0.01635
.00630	.00228	.01204	-.02035
.01248	.03083	.01722	-.02326
.01730	.03543	.02596	-.02683
.02461	.04143	.03726	-.03187
.03713	.04957	.04970	-.03583
.04961	.05583	.06196	-.03909
.06222	.06109	.07422	-.04200
.07522	.06570	.09957	-.04700
.10013	.07313	.14961	-.05426
.14970	.08409	.19943	-.05930
.20004	.09209	.24965	-.06265
.24991	.09778	.30004	-.06452
.29965	.10170	.34983	-.06517
.34991	.10409	.39991	-.06487
.39978	.10500	.45009	-.06348
.44974	.10457	.49983	-.06100
.50004	.10270	.54970	-.05691
.55035	.09917	.59983	-.05070
.60017	.09374	.65022	-.04270
.64996	.08609	.70022	-.03387
.70004	.07643	.75000	-.02483
.75000	.06522	.80013	-.01596
.79987	.05296	.85004	-.00857
.85004	.03987	.89987	-.00357
.90004	.02643	.94970	-.00261
.95026	.01287	.99004	-.00613
.99004	.00204	1.0	-.00430

Lower surface orifices for 0.20c simulated
split flap deflected 60°

x/c	z/c
0.81304	-0.03913
.82609	-.06087
.83478	-.07696
.84565	-.09565
.85652	-.11413
.86739	-.13304
.87826	-.15217
.88696	-.17065

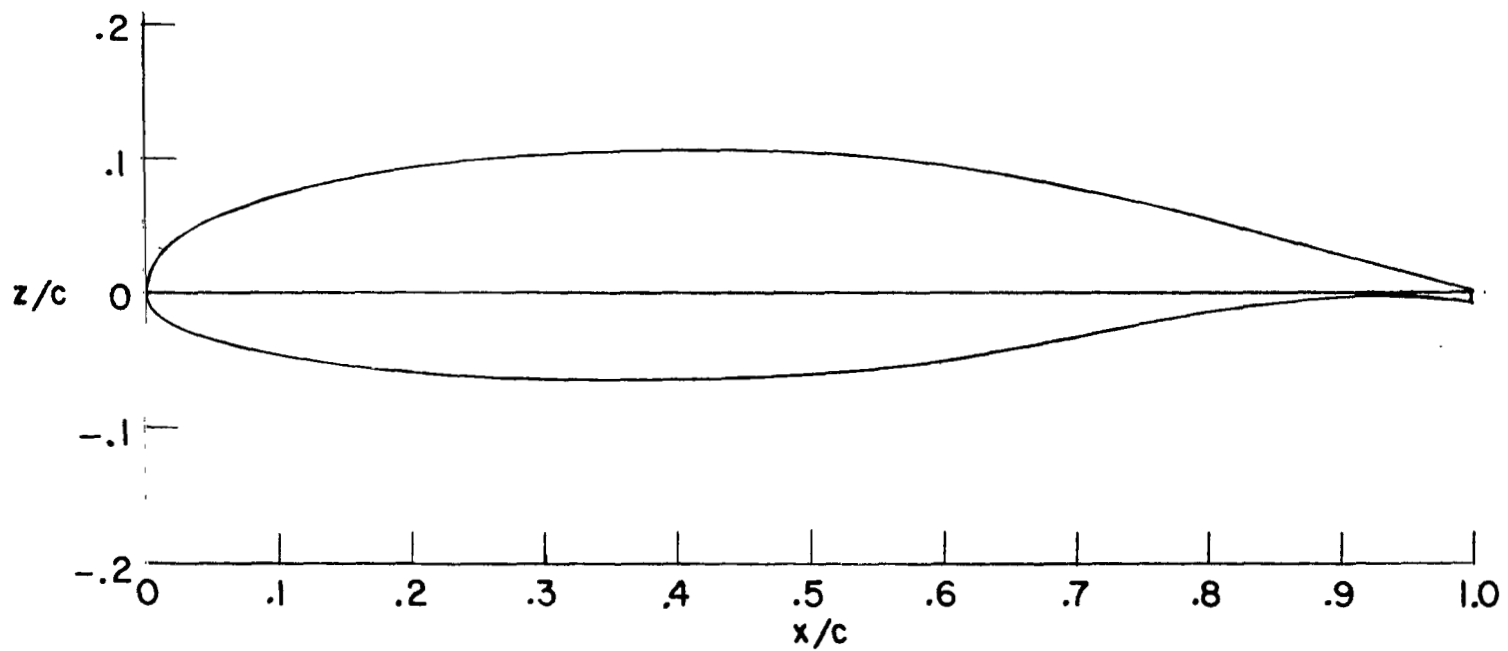


Figure 1.- Section shape for NASA GA(W)-1 airfoil.

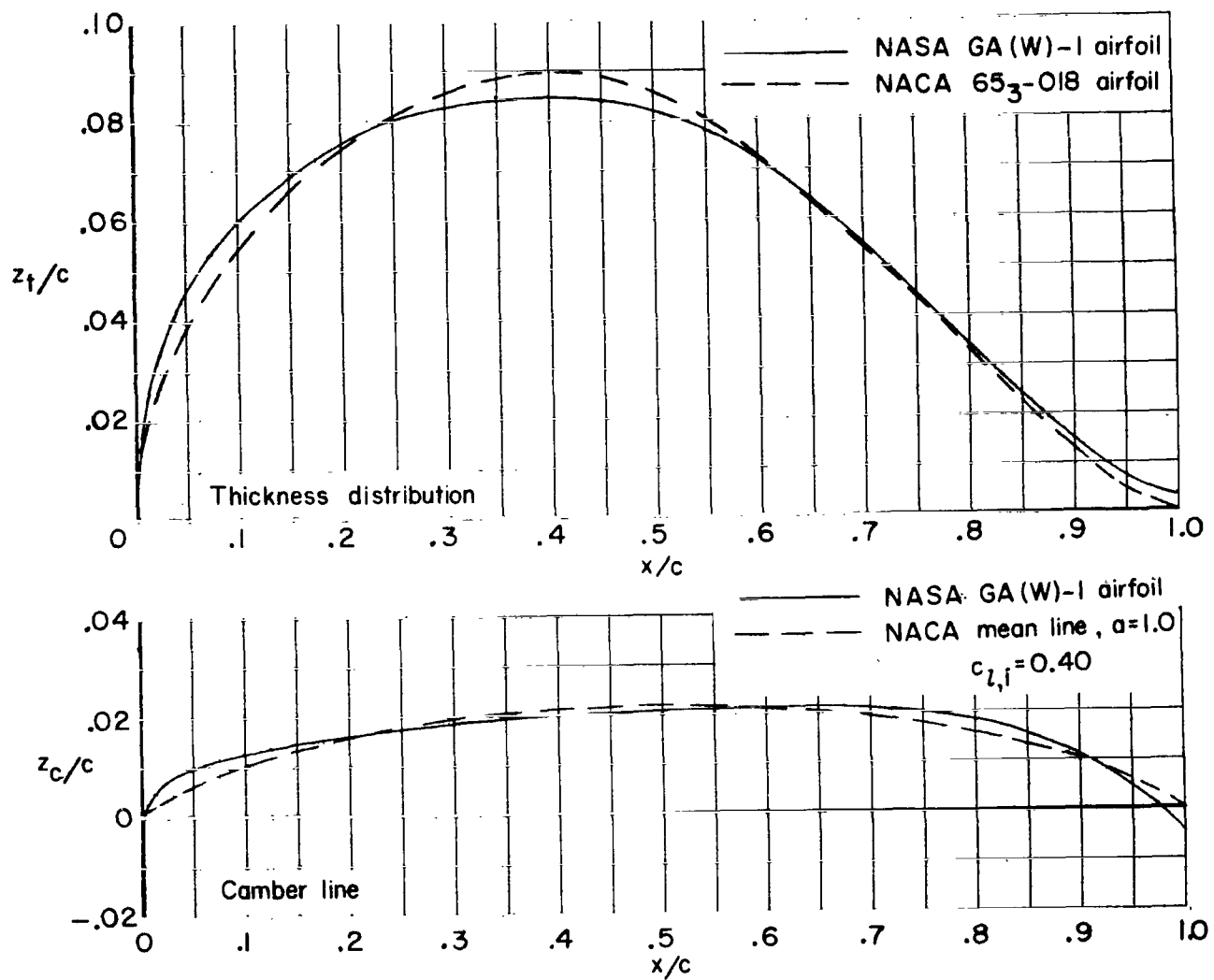
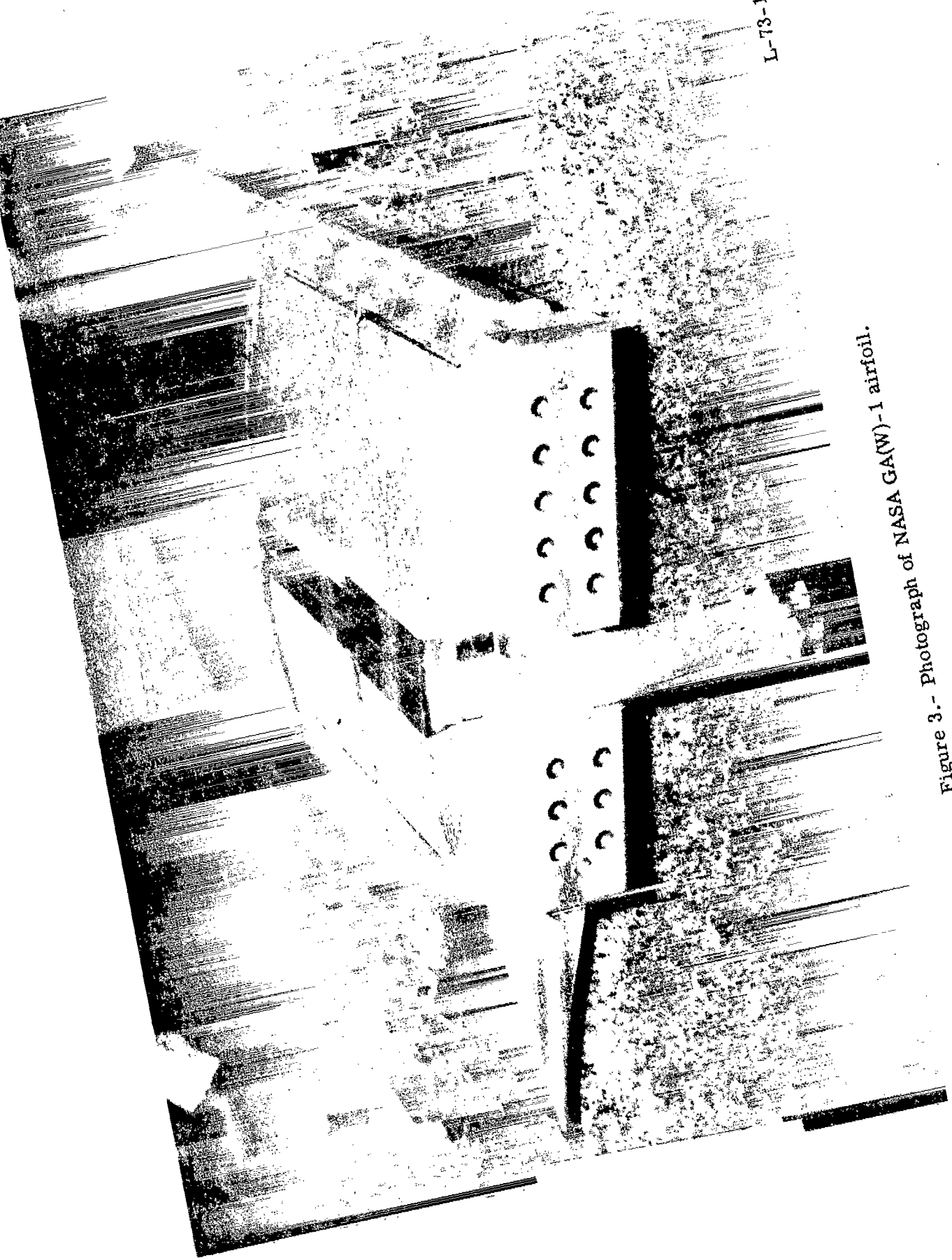


Figure 2.- Comparison of camber lines and thickness distribution.

L-73-1668

Figure 3.- Photograph of NASA GA(N)-1 airfoil.



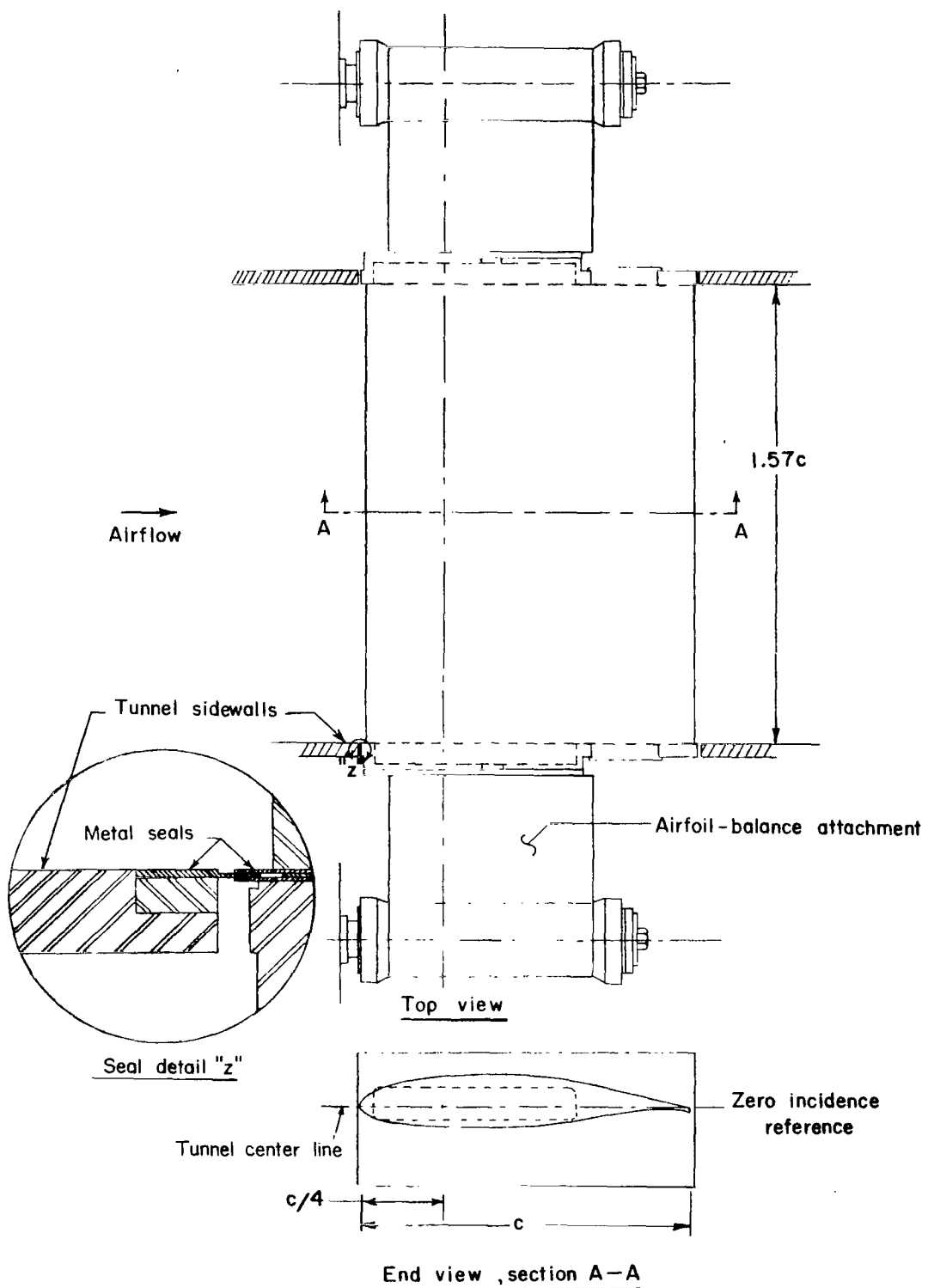


Figure 4.- Airfoil mounted in wind tunnel. All dimensions in terms of airfoil chord. $c = 58.42$ cm (23 in.).

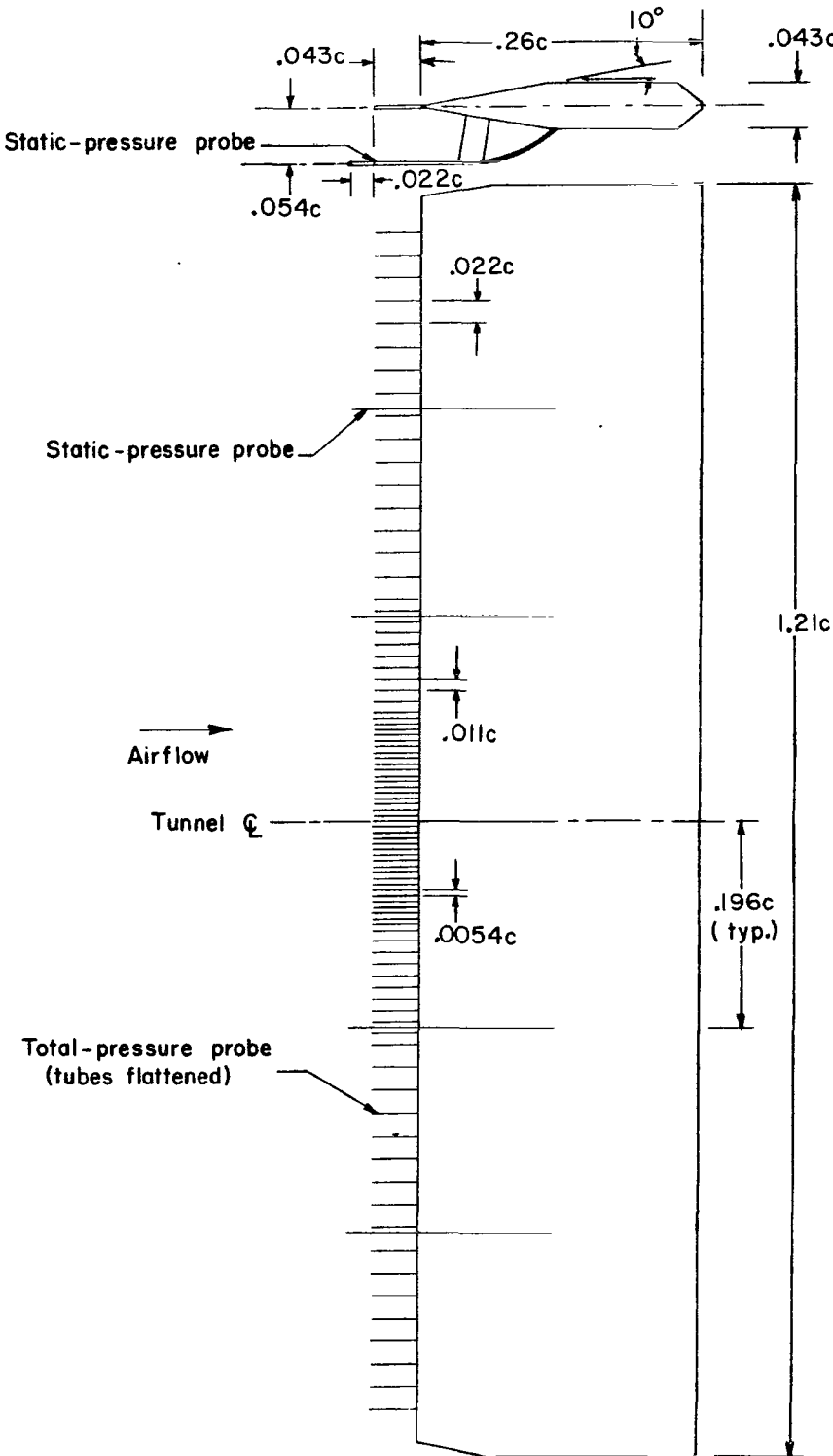


Figure 5.- Drawing of wake rake. All dimensions in terms of airfoil chord.
 $c = 58.42 \text{ cm (23 in.)}$.

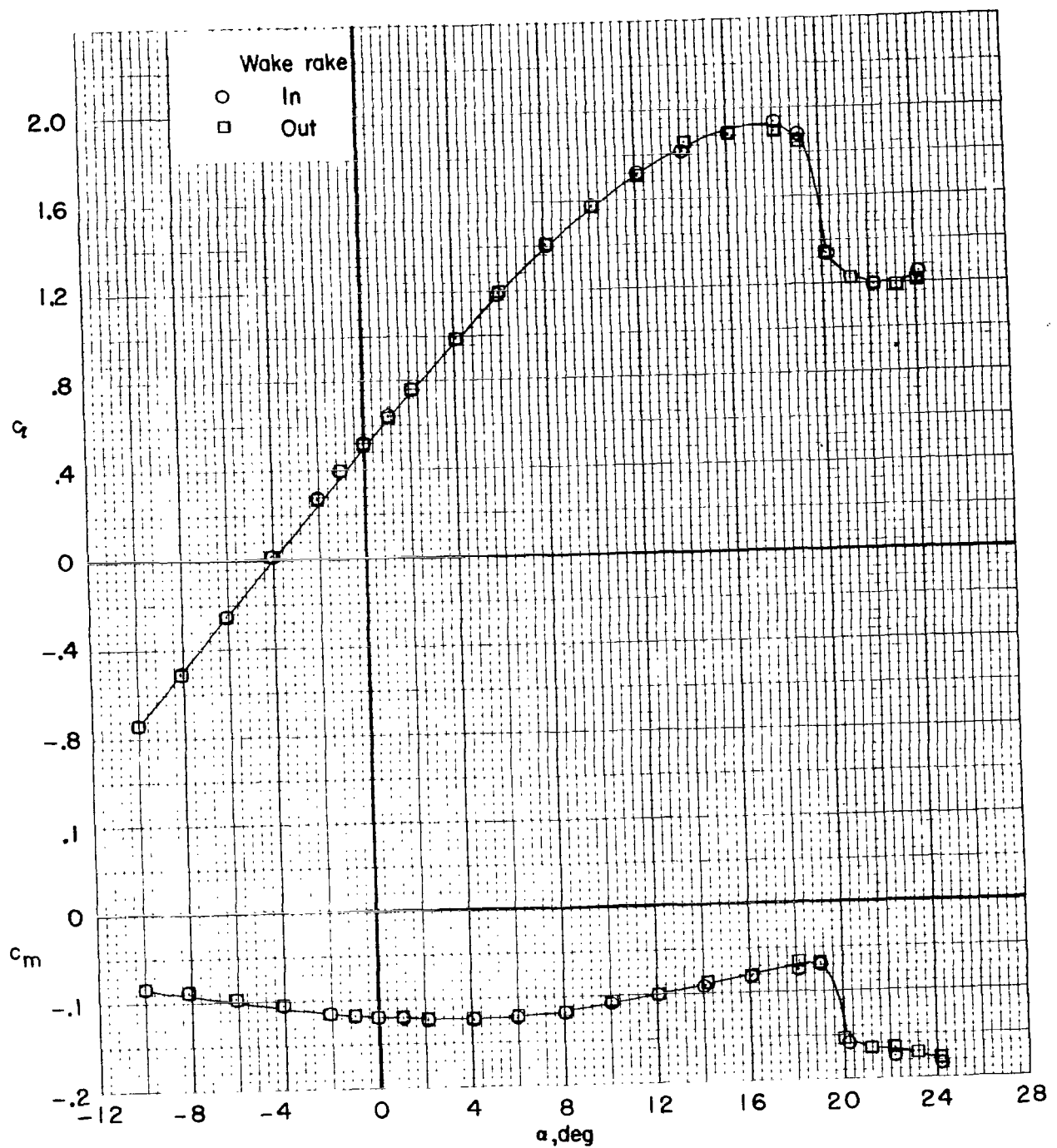
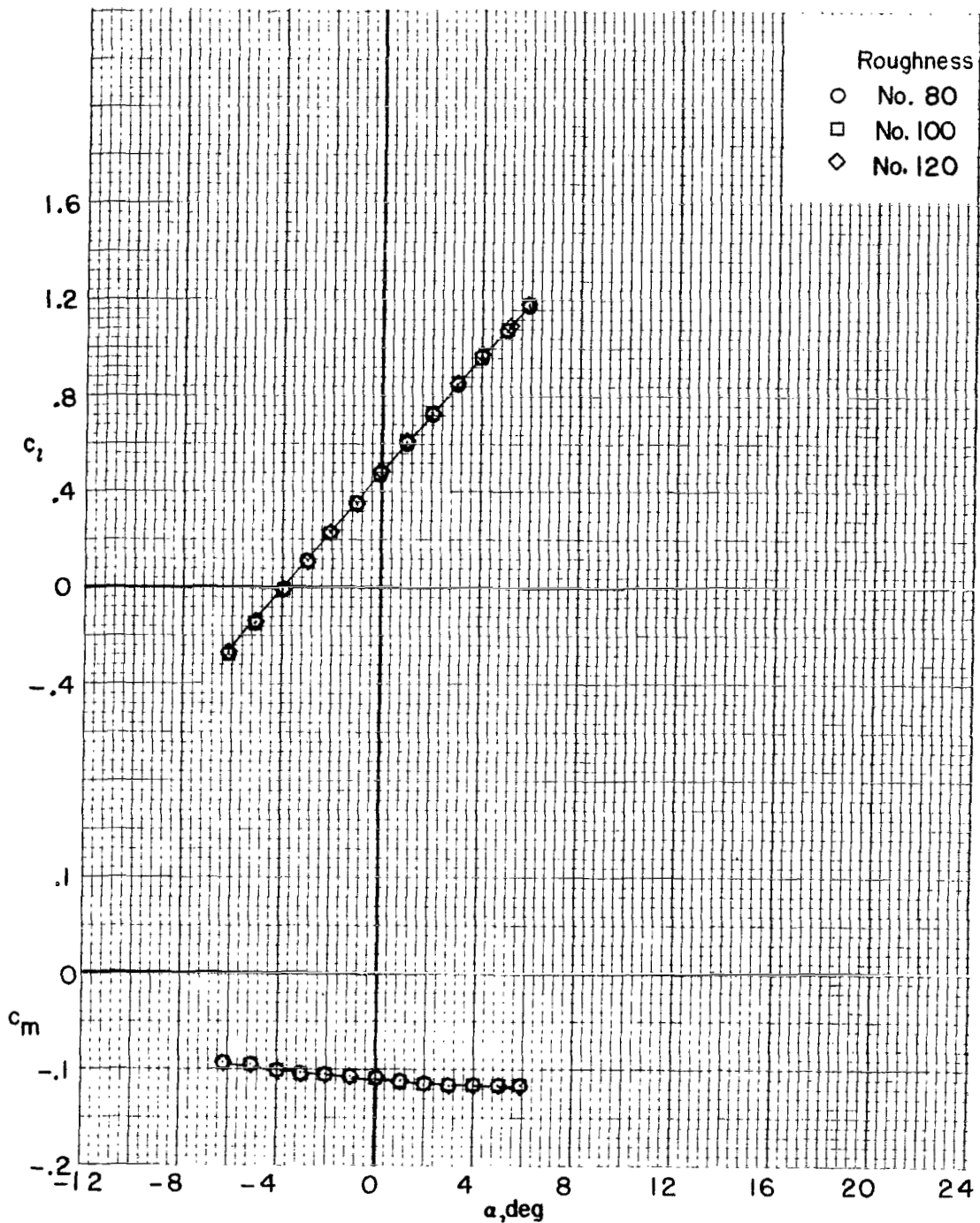


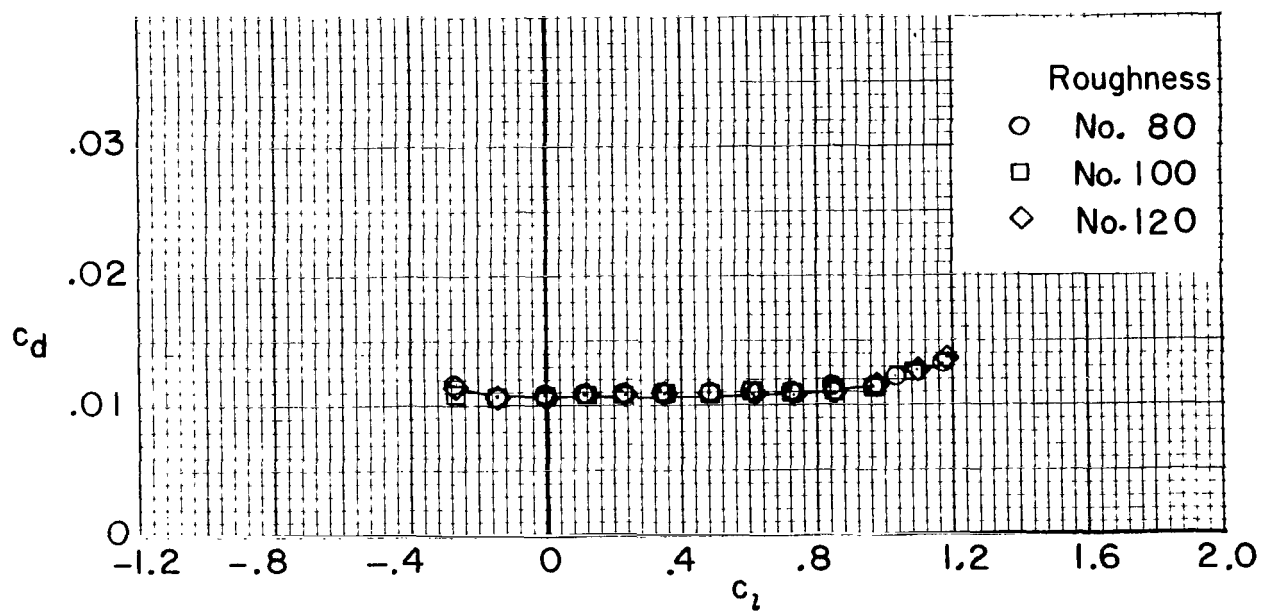
Figure 6.- Effect of wake rake on section characteristics. Model smooth;
 $M = 0.20$; $R \approx 6 \times 10^6$.



(a) Variation of c_l and c_m with α .

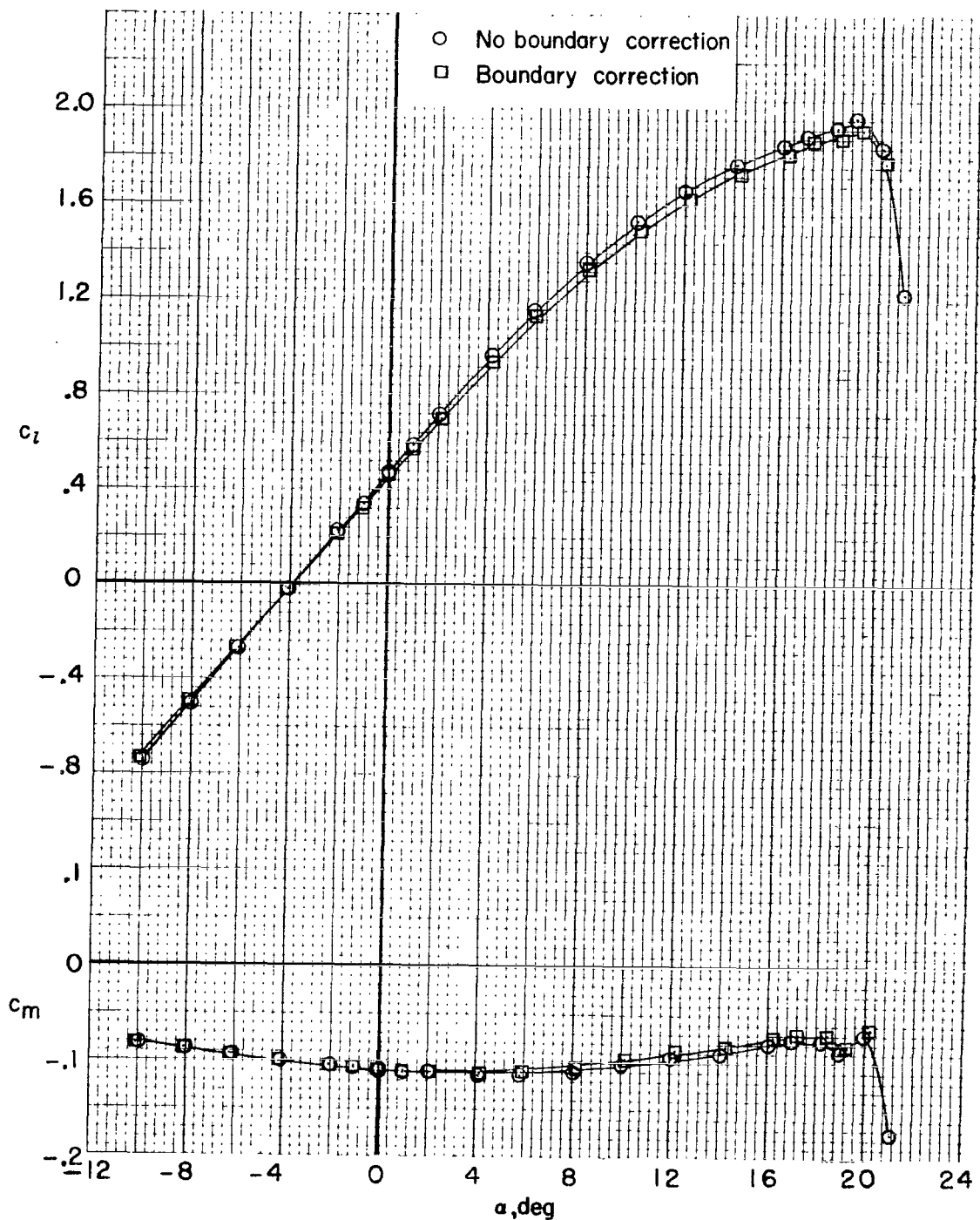
Figure 7.- Effect of roughness size on section characteristics.

$M = 0.20$; $R \approx 6 \times 10^6$.



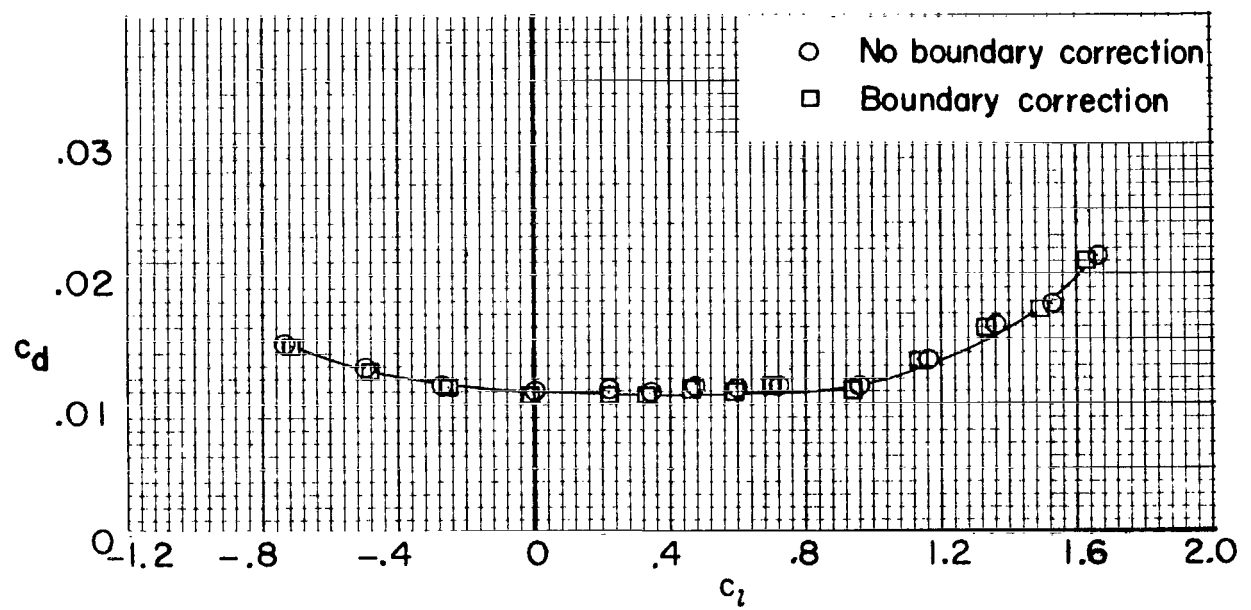
(b) Variation of c_d with c_l .

Figure 7.- Concluded.



(a) Variation of c_l and c_m with α .

Figure 8.- Effect of standard low-speed wind-tunnel boundary corrections on section data. Number 80 roughness located at $0.08c$; $M = 0.15$; $R \approx 6 \times 10^6$.



(b) Variation of c_d with c_l .

Figure 8.- Concluded.

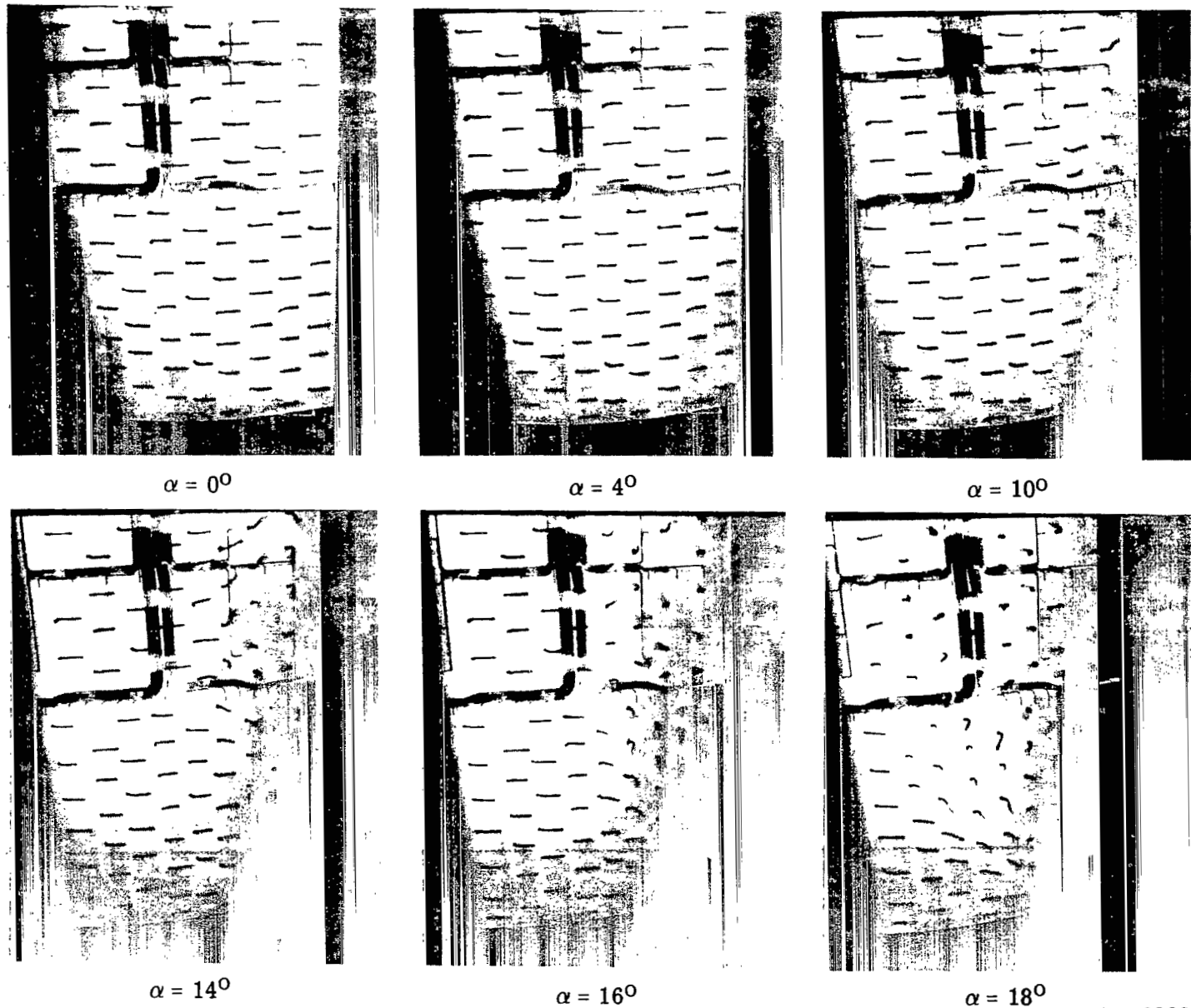
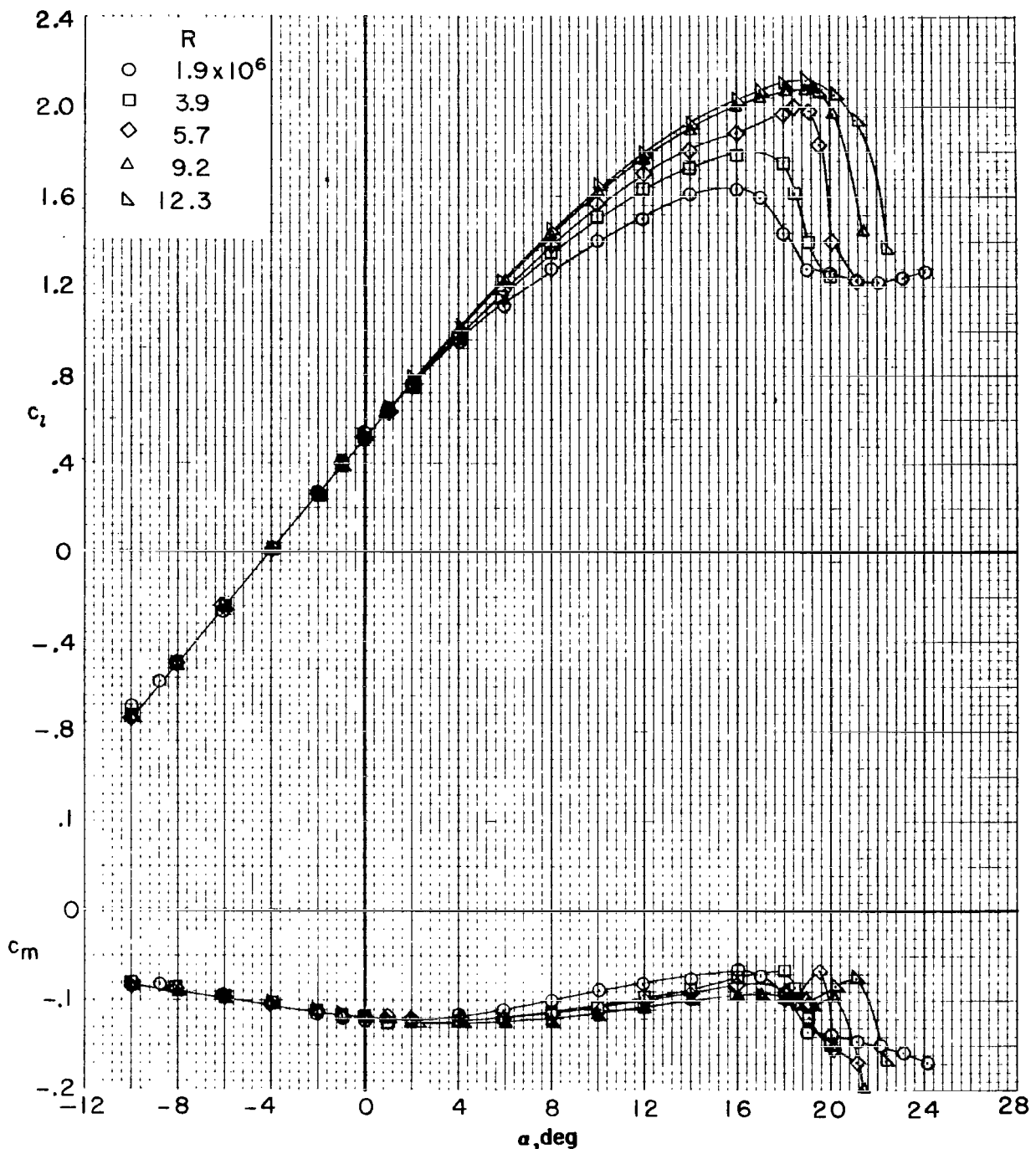


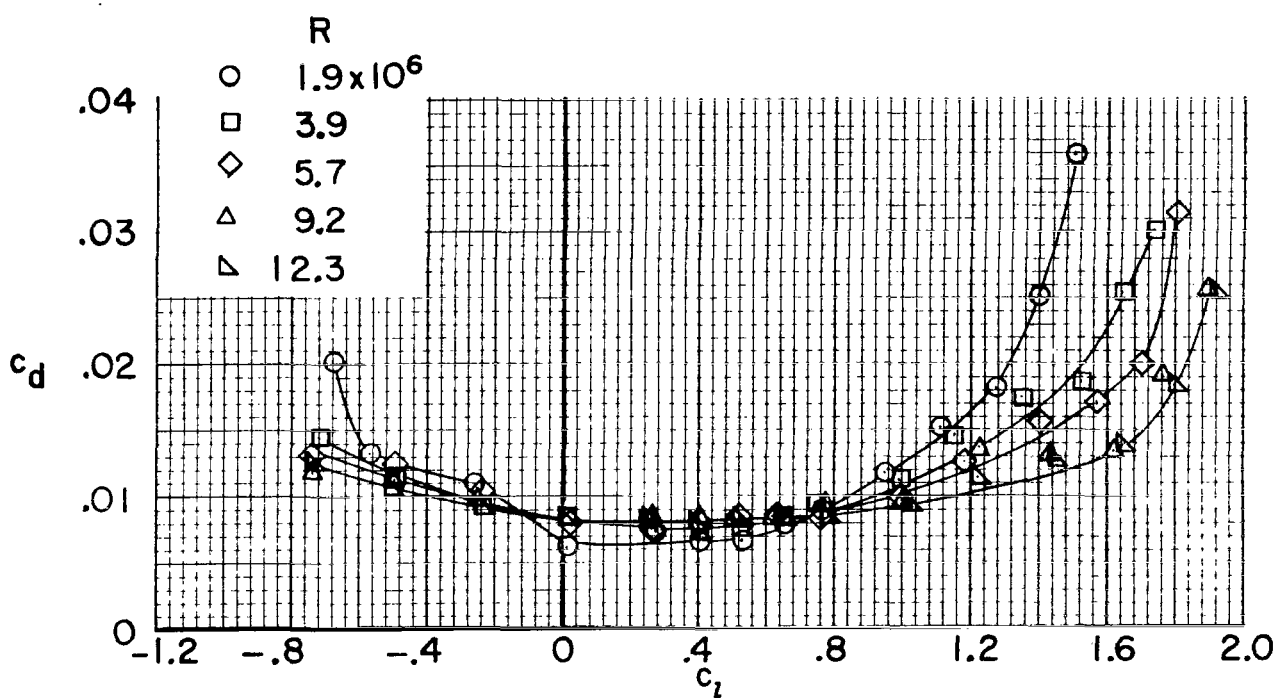
Figure 9.- Tuft photographs of NASA GA(W)-1 airfoil. $M = 0.20$; $R \approx 2.70 \times 10^6$.

L-73-6898



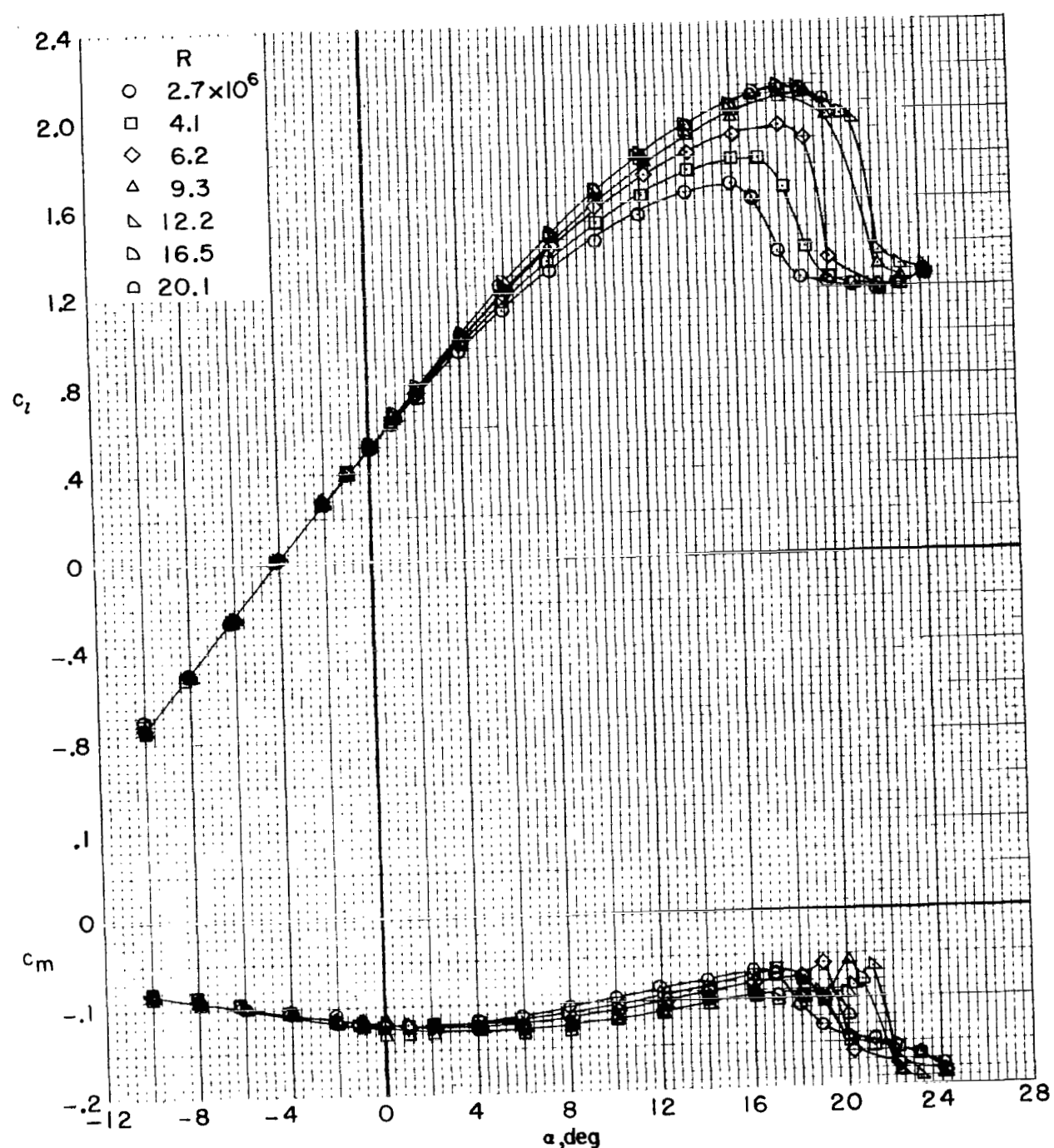
(a) $M = 0.15$.

Figure 10.- Effect of Reynolds number on section characteristics. Model smooth.



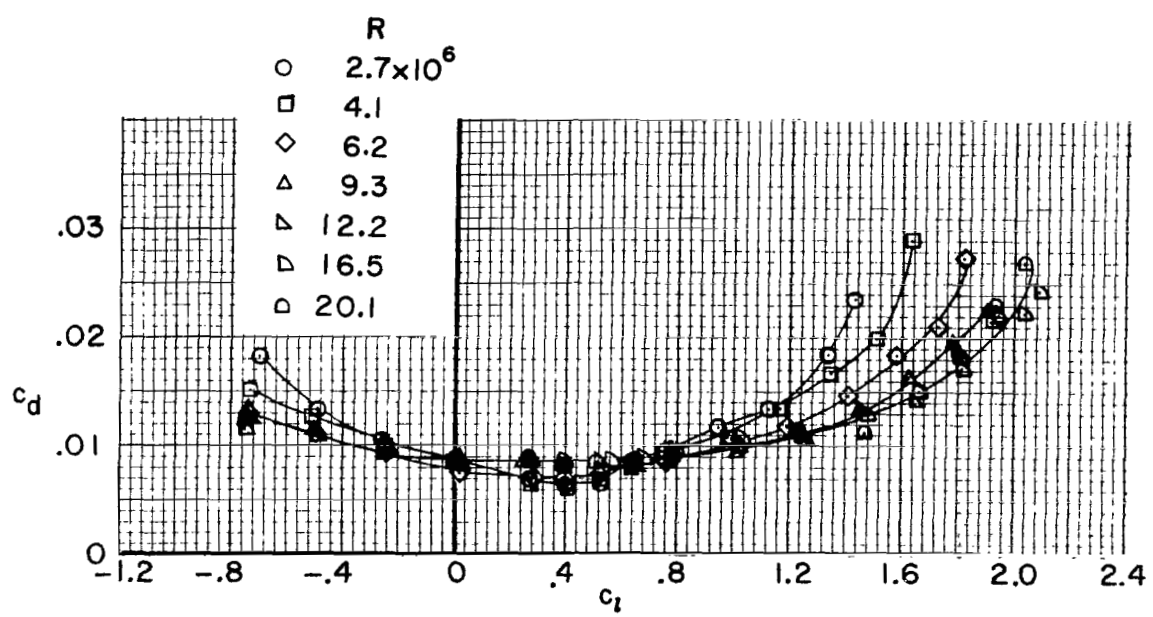
(a) $M = 0.15$. Concluded.

Figure 10.- Continued.



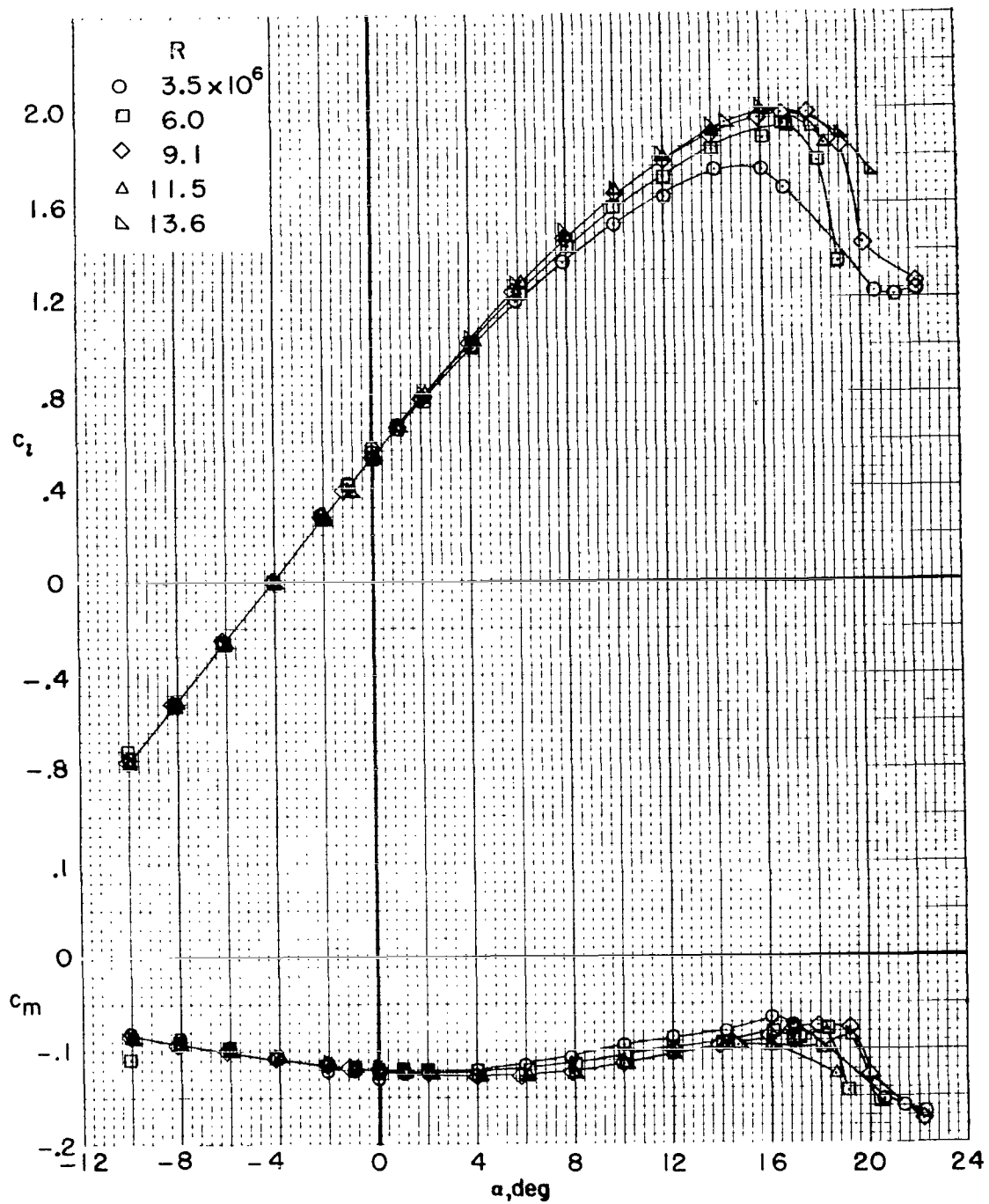
(b) $M = 0.20$.

Figure 10.- Continued.



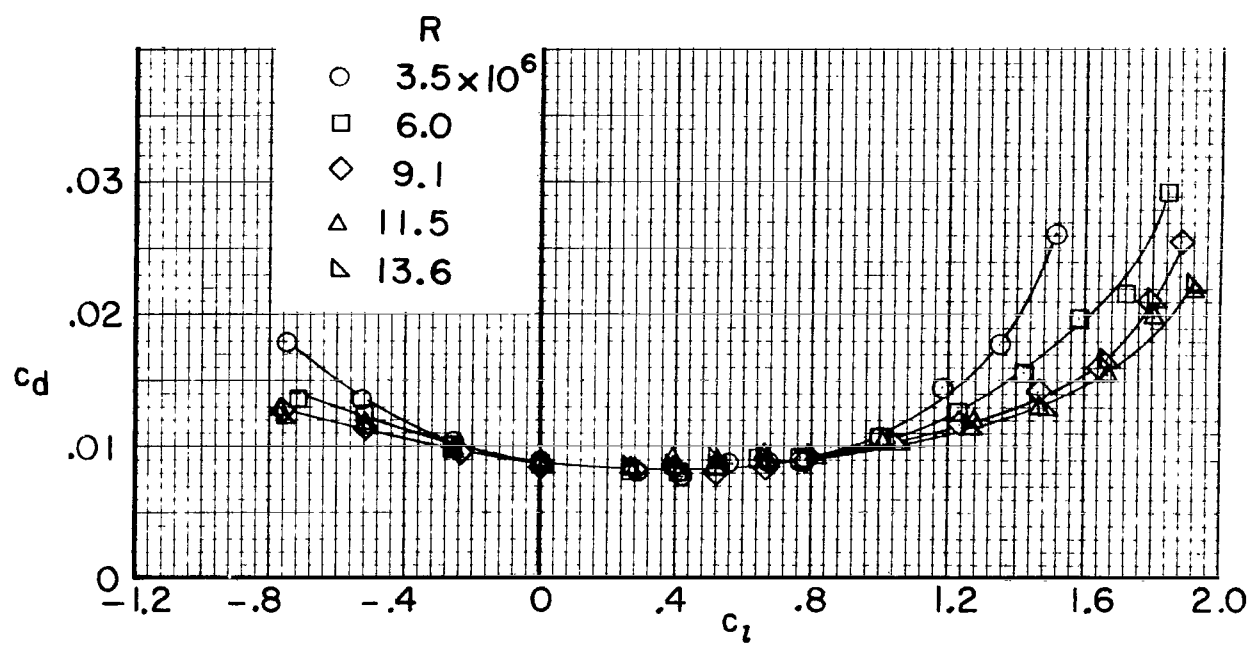
(b) $M = 0.20$. Concluded.

Figure 10.- Continued.



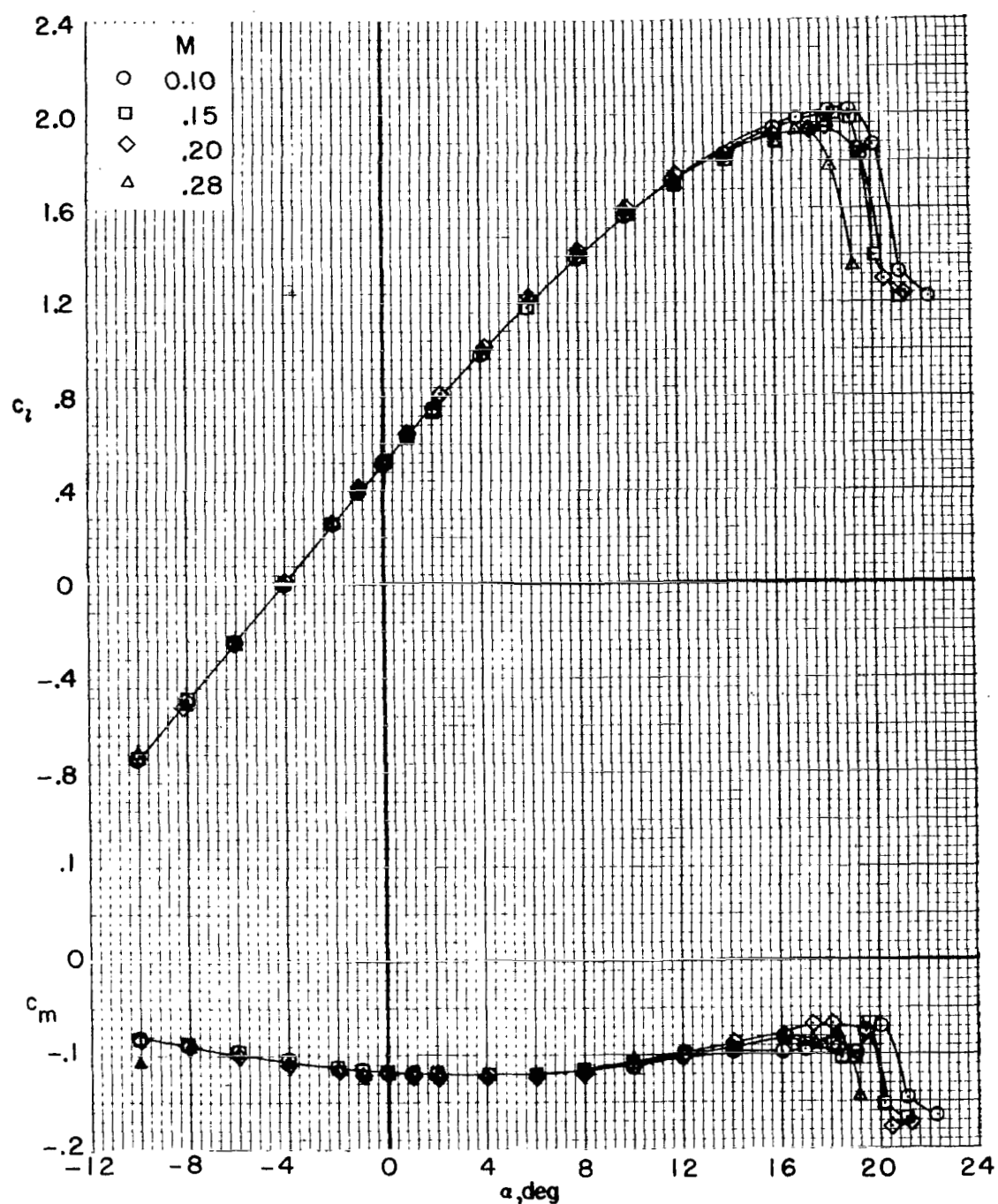
(c) $M = 0.28$.

Figure 10.- Continued.



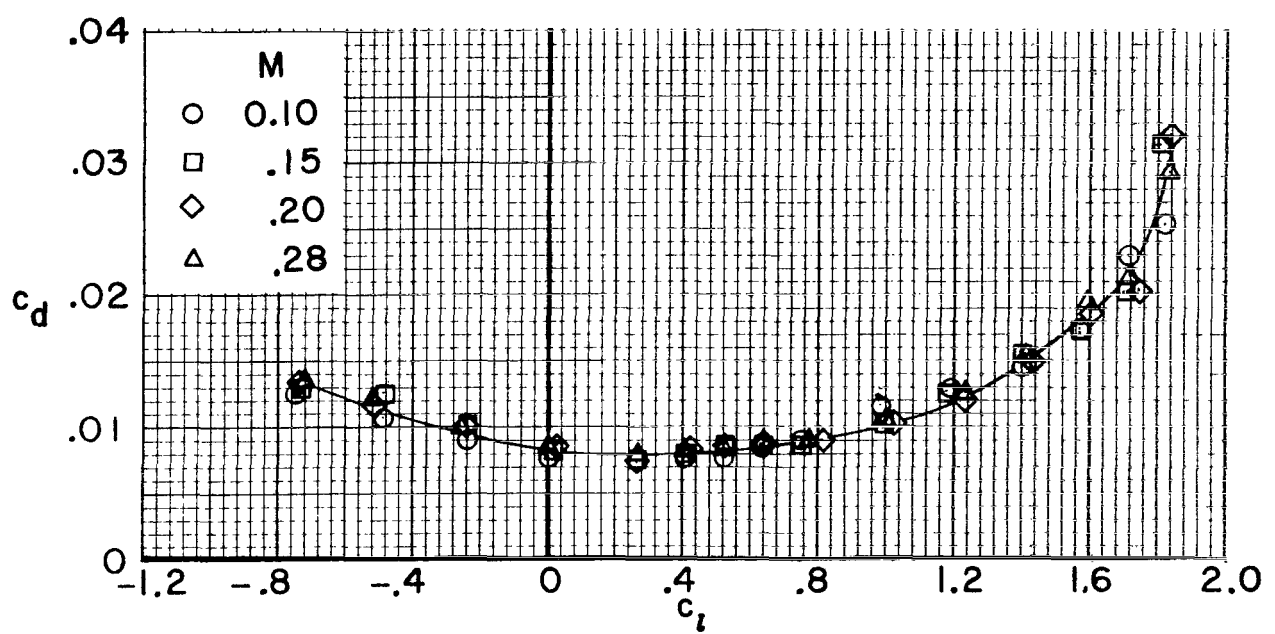
(c) $M = 0.28$. Concluded.

Figure 10.- Concluded.



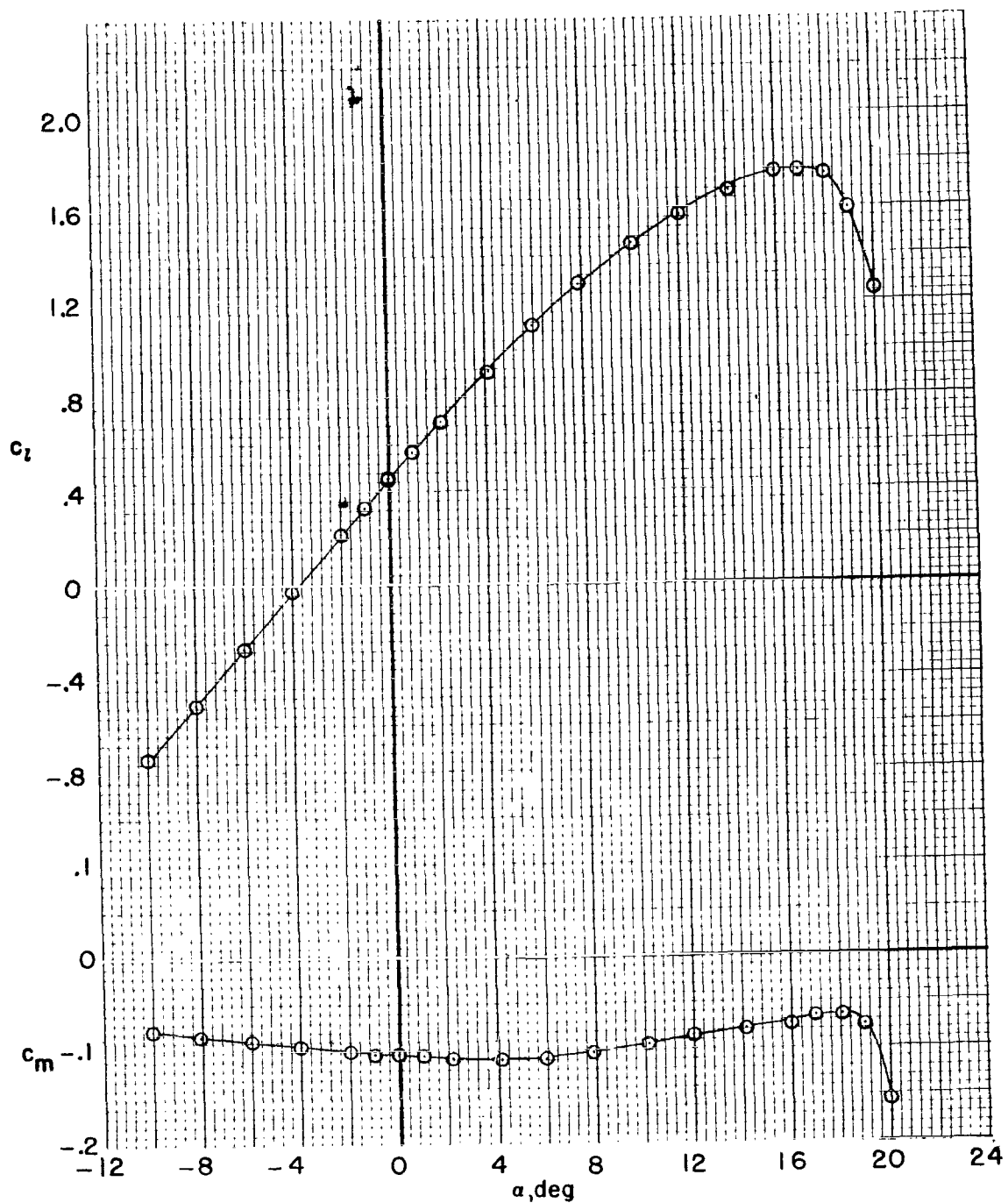
(a) Variation of c_l and c_m with α .

Figure 11.- Effect of Mach number on section characteristics.
Model smooth; $R \approx 6 \times 10^6$.



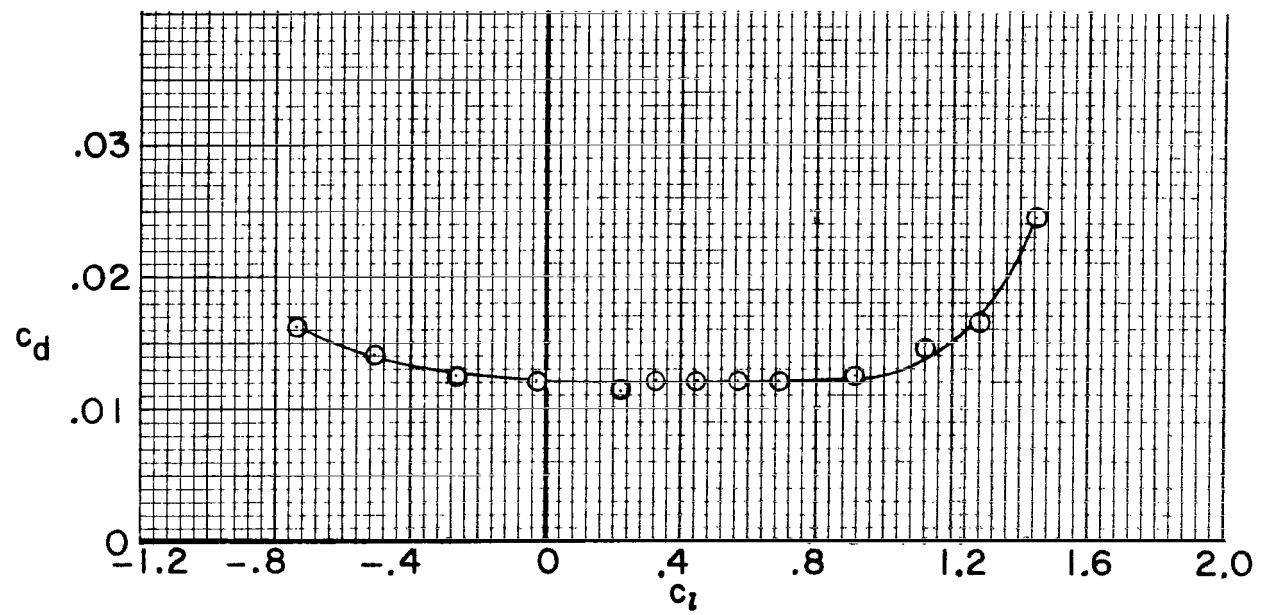
(b) Variation of c_d with c_l .

Figure 11.- Concluded.



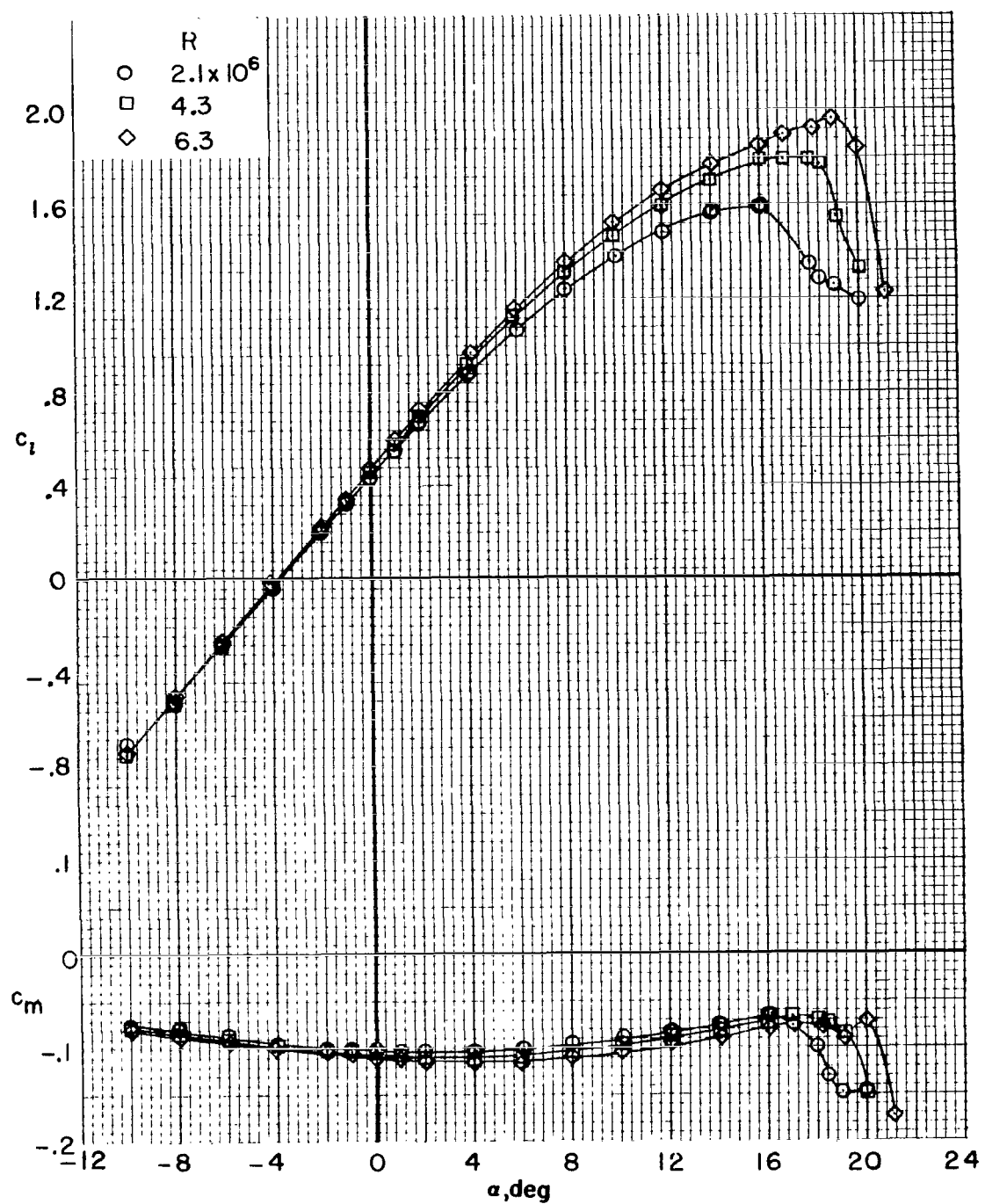
(a) $M = 0.10; R = 3.7 \times 10^6$.

Figure 12.- Effect of Reynolds number on section characteristics.
Number 80 roughness located at $0.08c$.



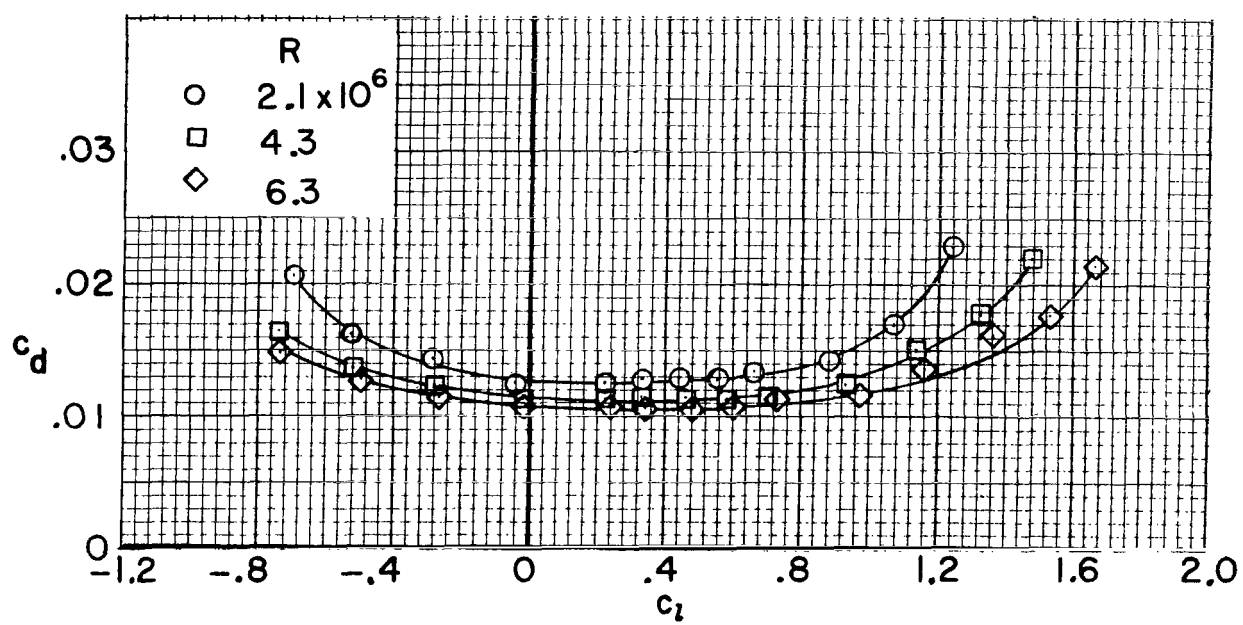
(a) $M = 0.10$; $R = 3.7 \times 10^6$. Concluded.

Figure 12.- Continued.



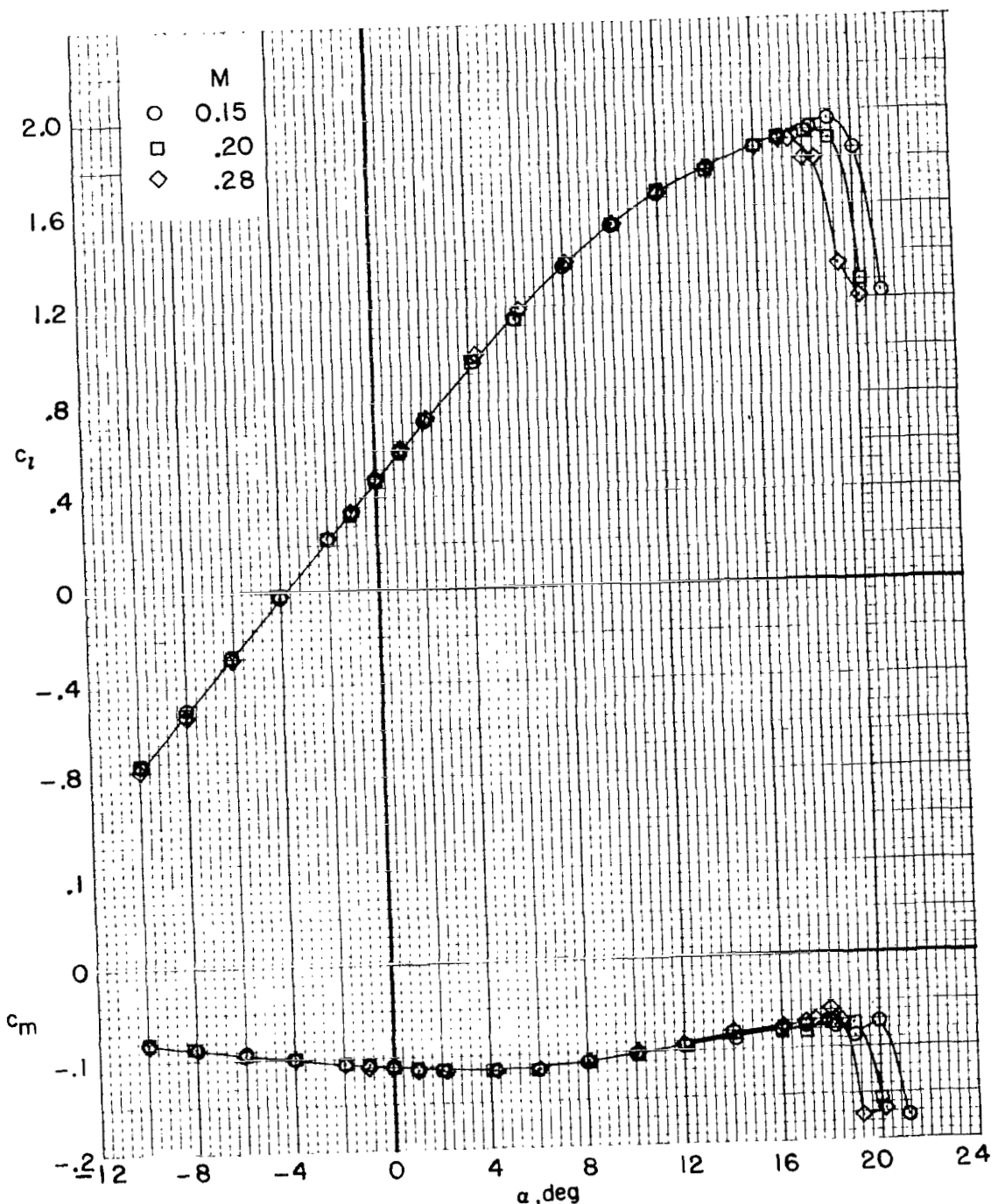
(b) $M = 0.15$.

Figure 12.- Continued.



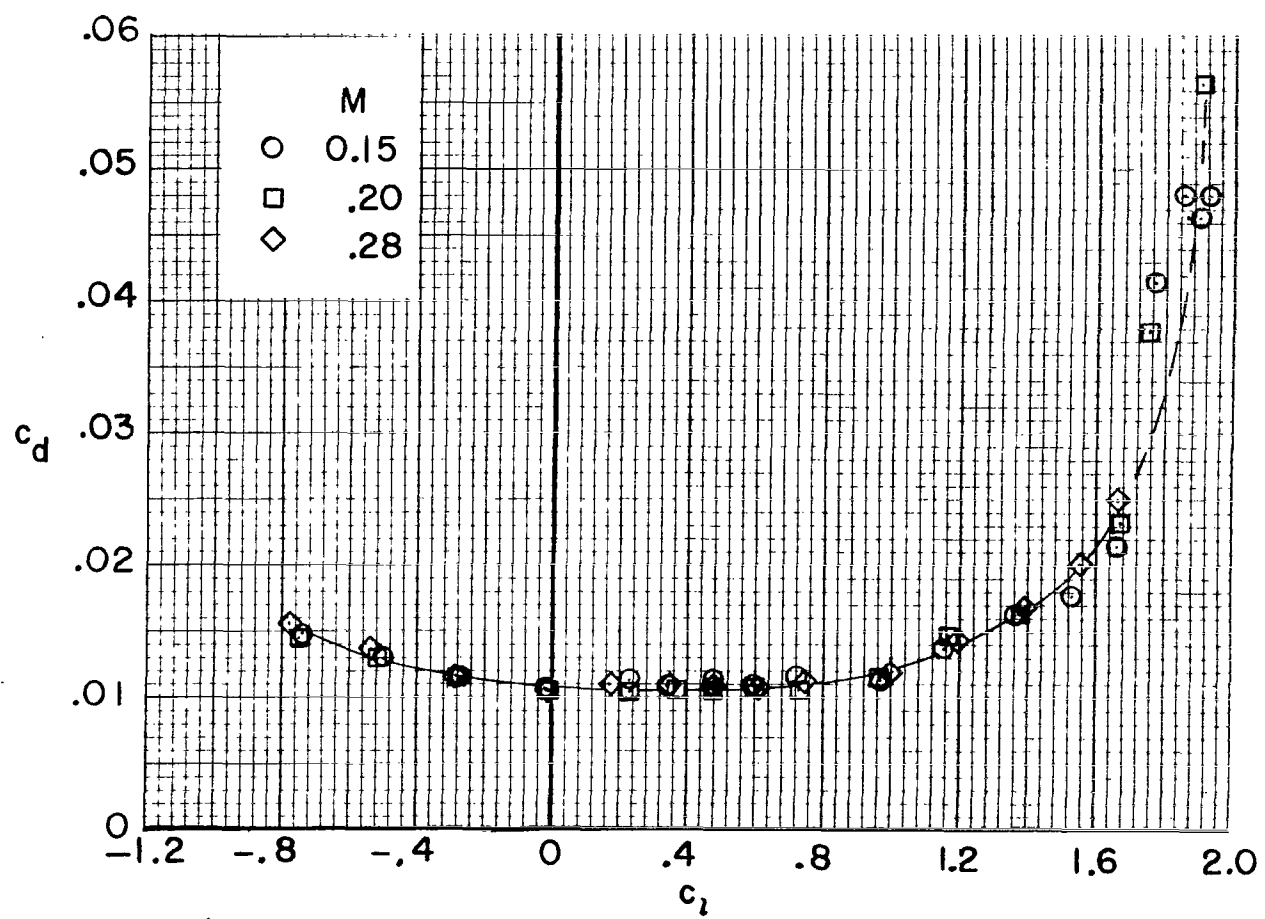
(b) $M = 0.15$. Concluded.

Figure 12.- Concluded.



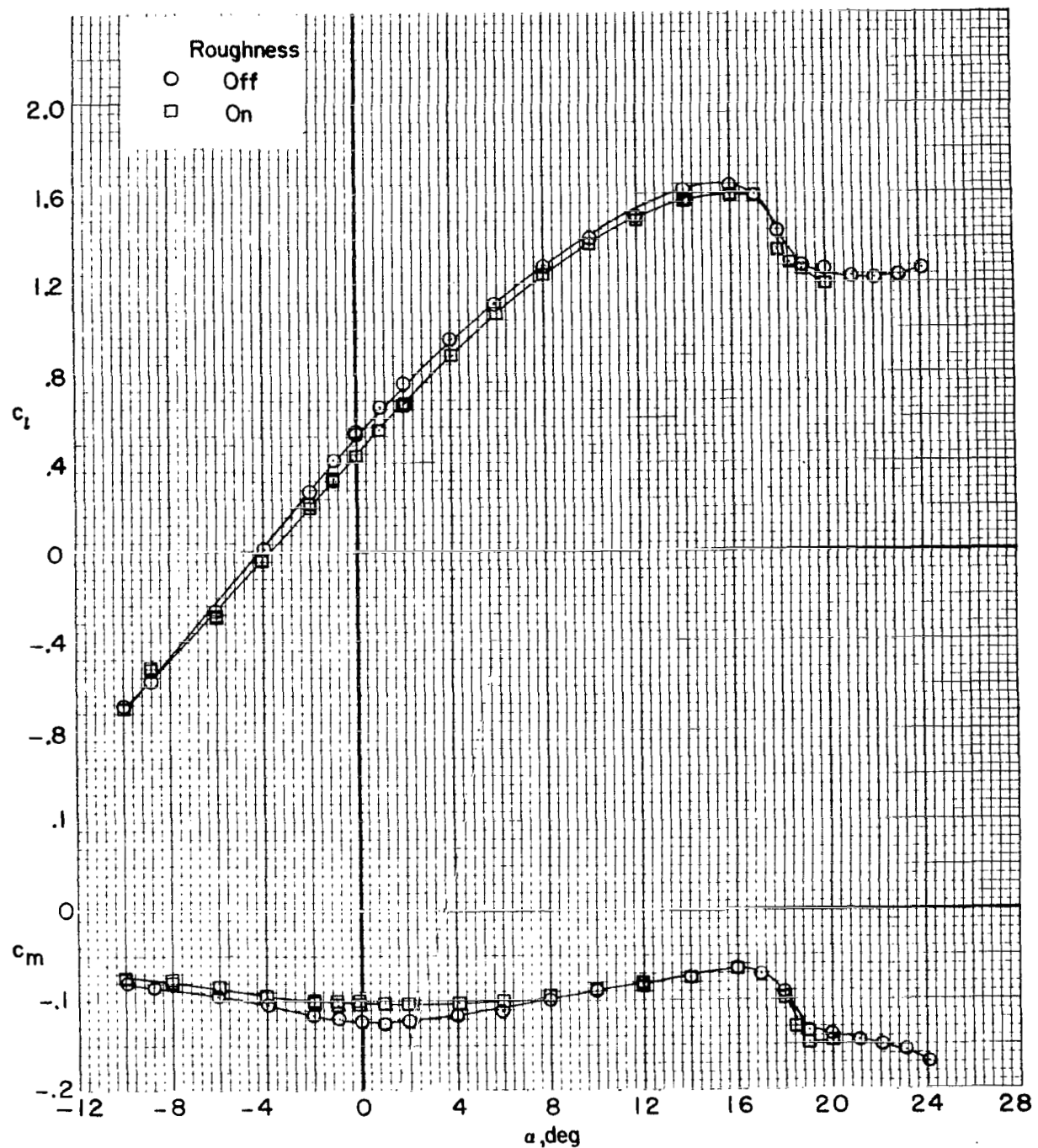
(a) Variation of c_l and c_m with α .

Figure 13.- Effect of Mach number on section characteristics. Number 80
 roughness located at $0.08c$. $R \approx 6 \times 10^6$.



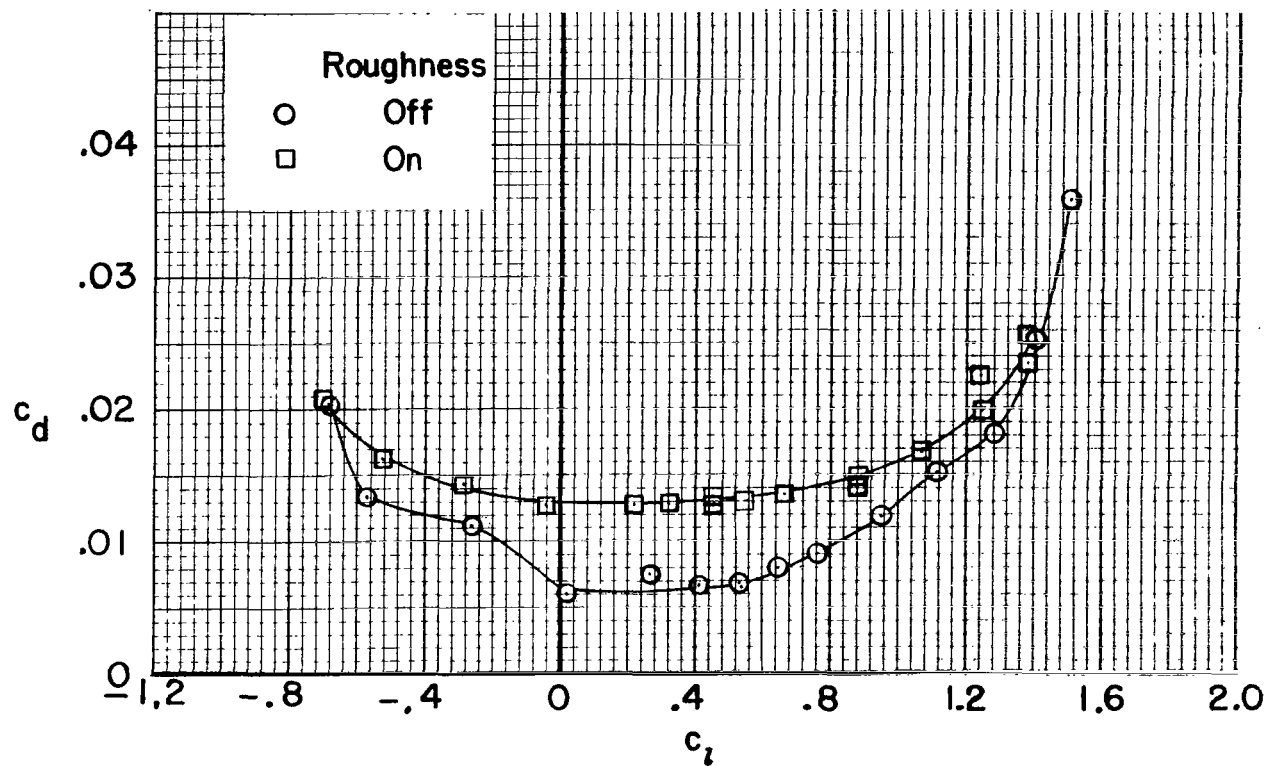
(b) Variation of c_d with c_l .

Figure 13.- Concluded.



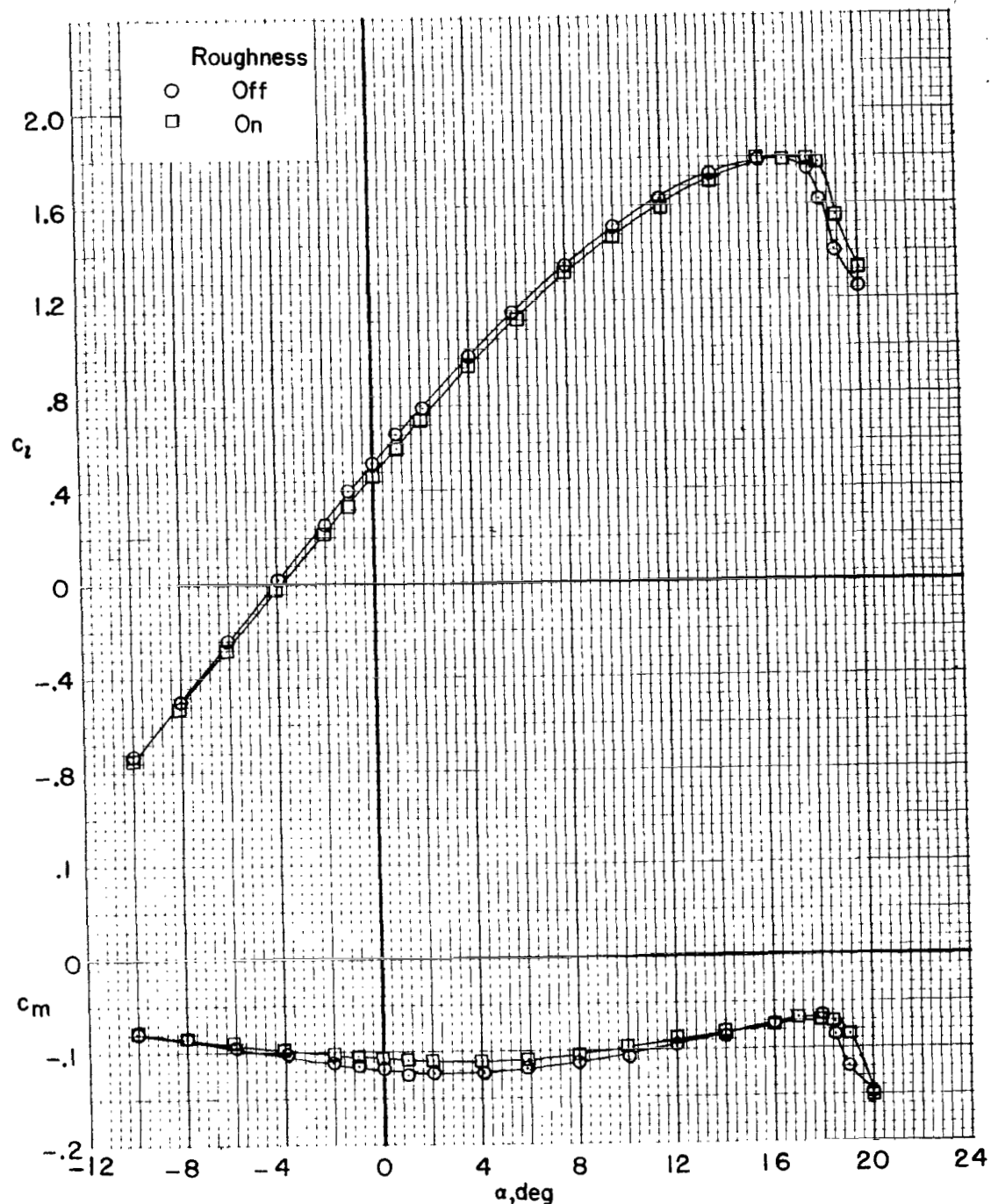
(a) $R \approx 2 \times 10^6$.

Figure 14.- Effect of roughness on section characteristics. $M = 0.15$.
Number 80 roughness located at $0.08c$.



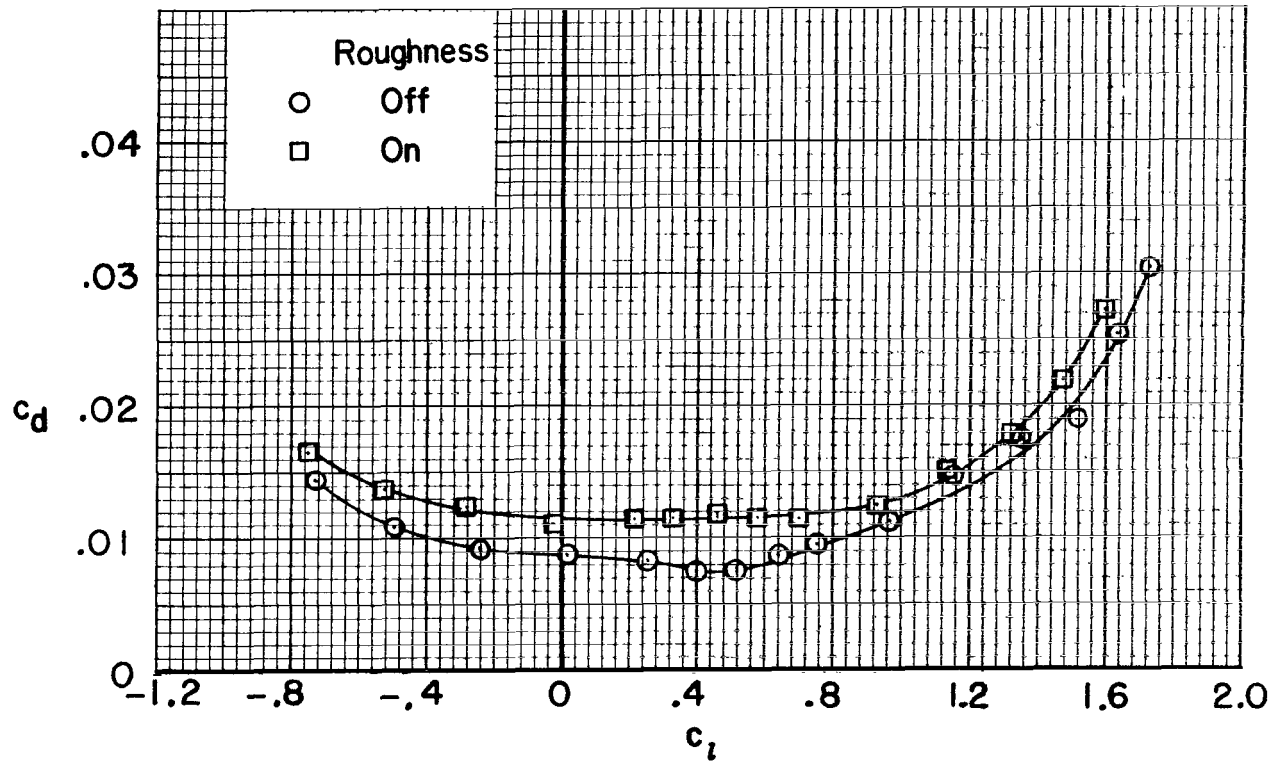
(a) $R \approx 2 \times 10^6$. Concluded.

Figure 14.- Continued.



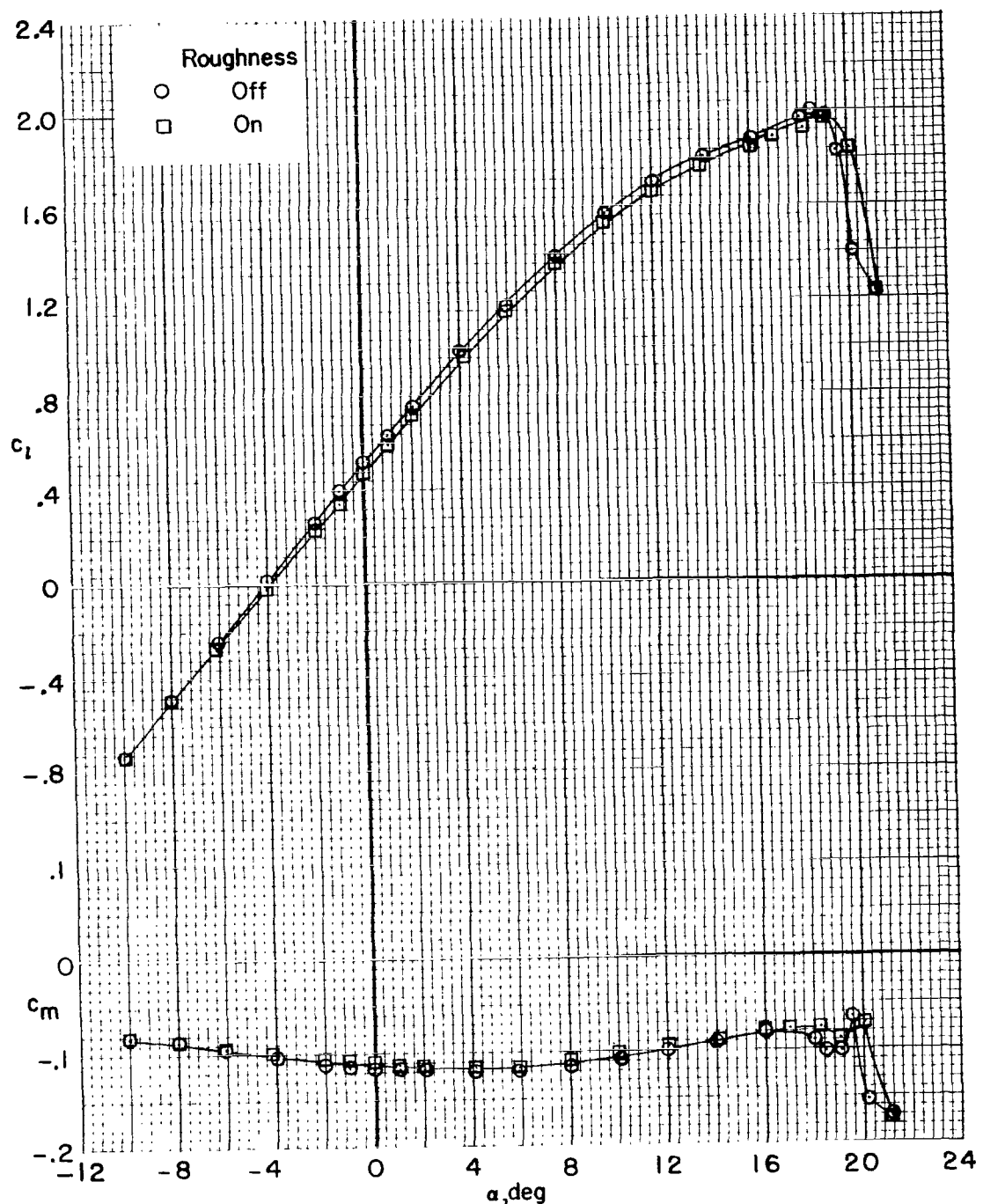
(b) $R \approx 4 \times 10^6$.

Figure 14.- Continued.



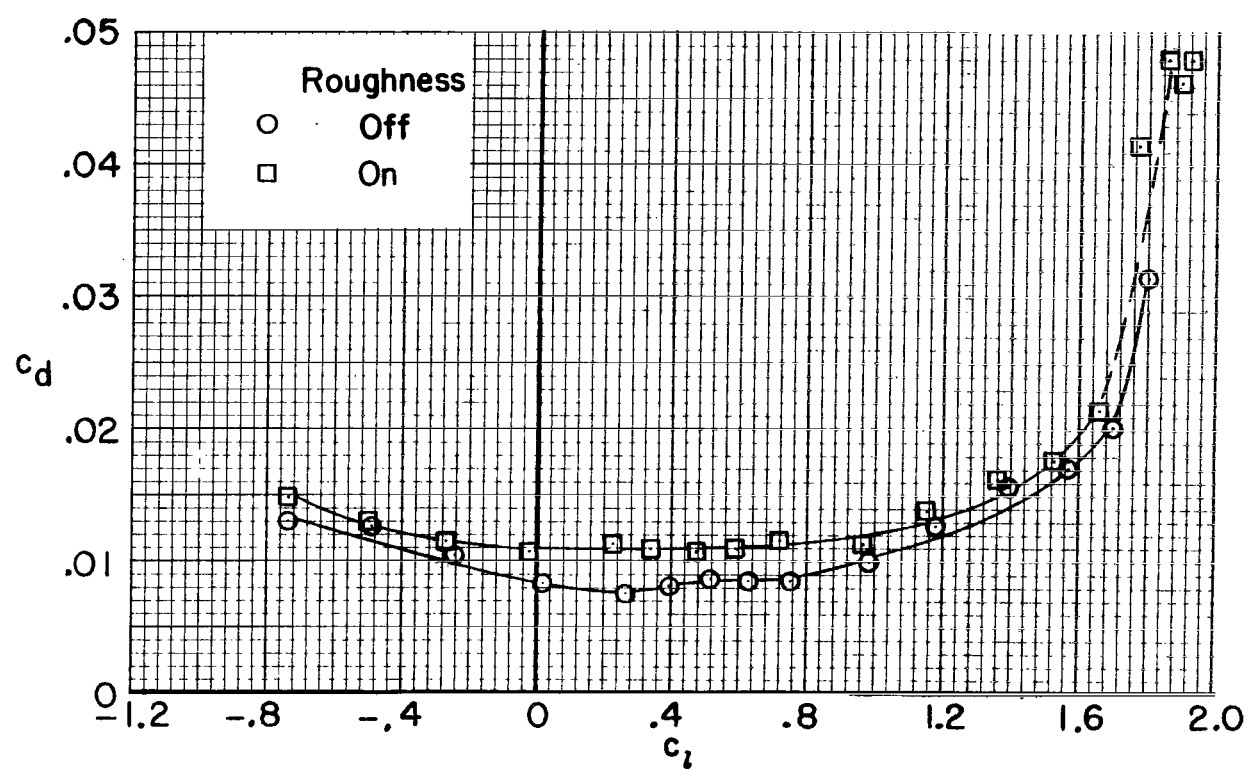
(b) $R \approx 4 \times 10^6$. Concluded.

Figure 14.- Continued.



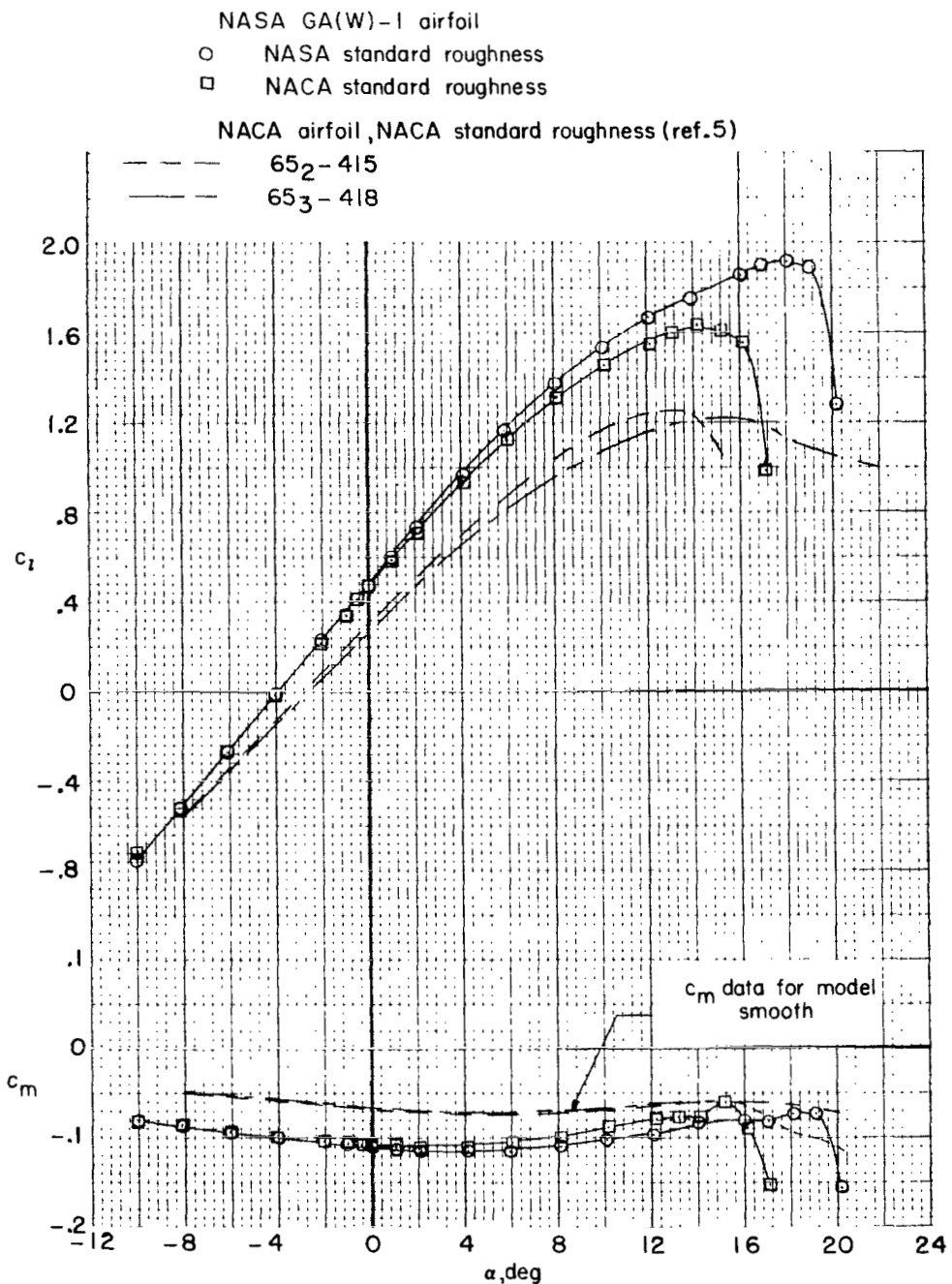
(c) $R \approx 6 \times 10^6$.

Figure 14.- Continued.



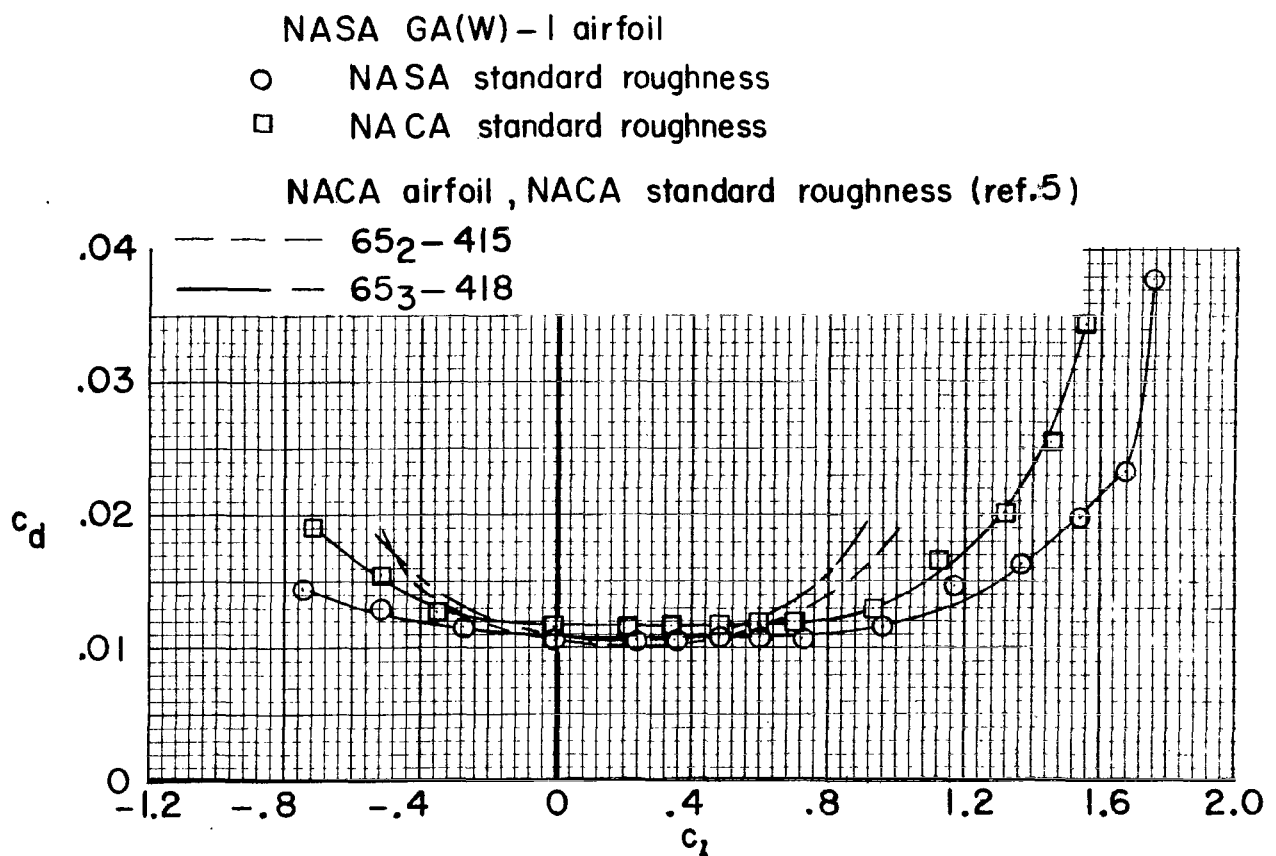
(c) $R \approx 6 \times 10^6$. Concluded.

Figure 14.- Concluded.



(a) Variation of c_l and c_m with α .

Figure 15.- Comparison of section characteristics of NASA GA(W)-1 airfoil and NACA 65₂-415 and 65₃-418 airfoils. $M = 0.20$; $R \approx 6 \times 10^6$.



(b) Variation of c_d with c_l .

Figure 15.- Concluded.

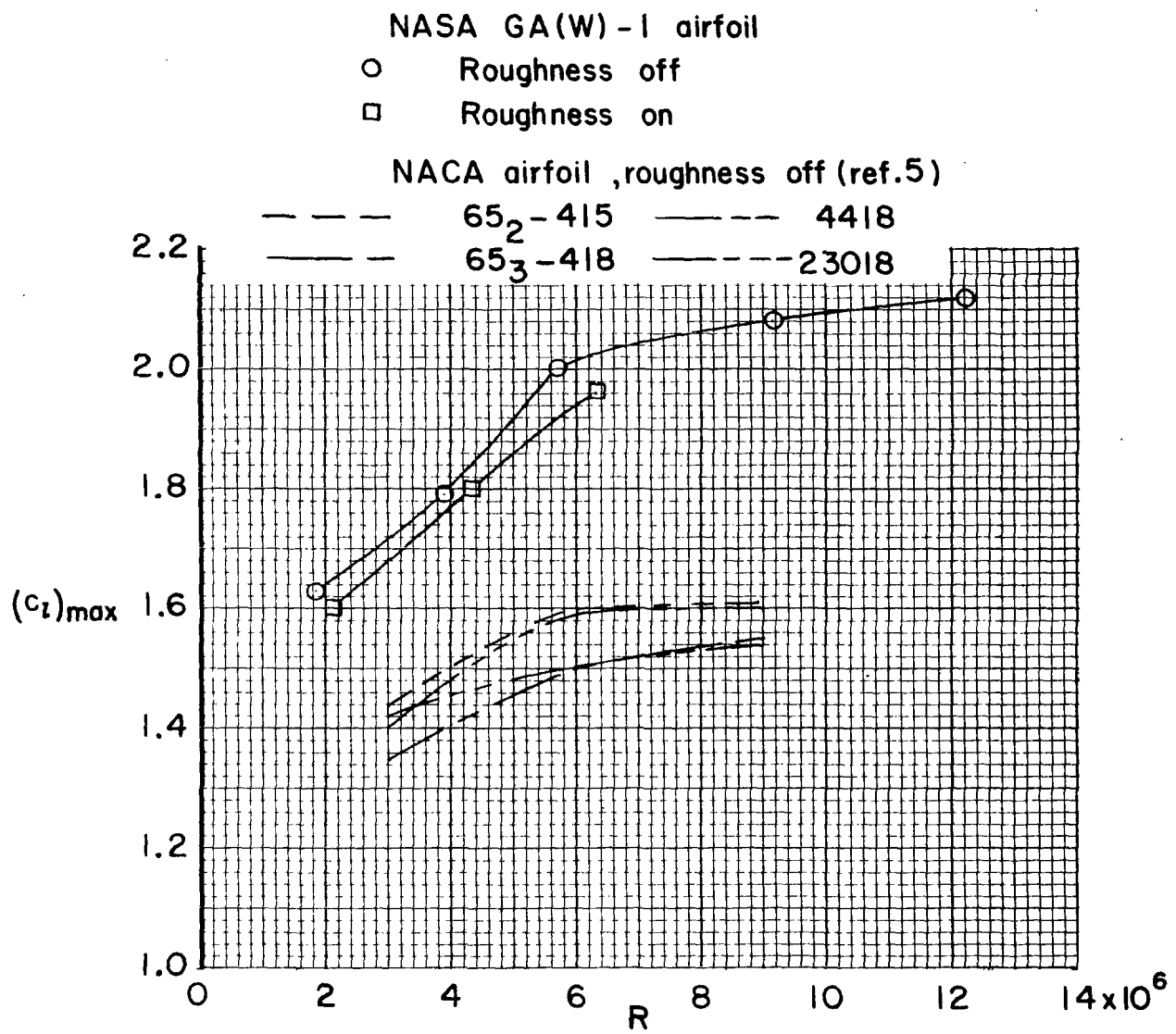


Figure 16.- Variation of maximum section lift coefficient with Reynolds number for various airfoils without flaps. $M = 0.15$.

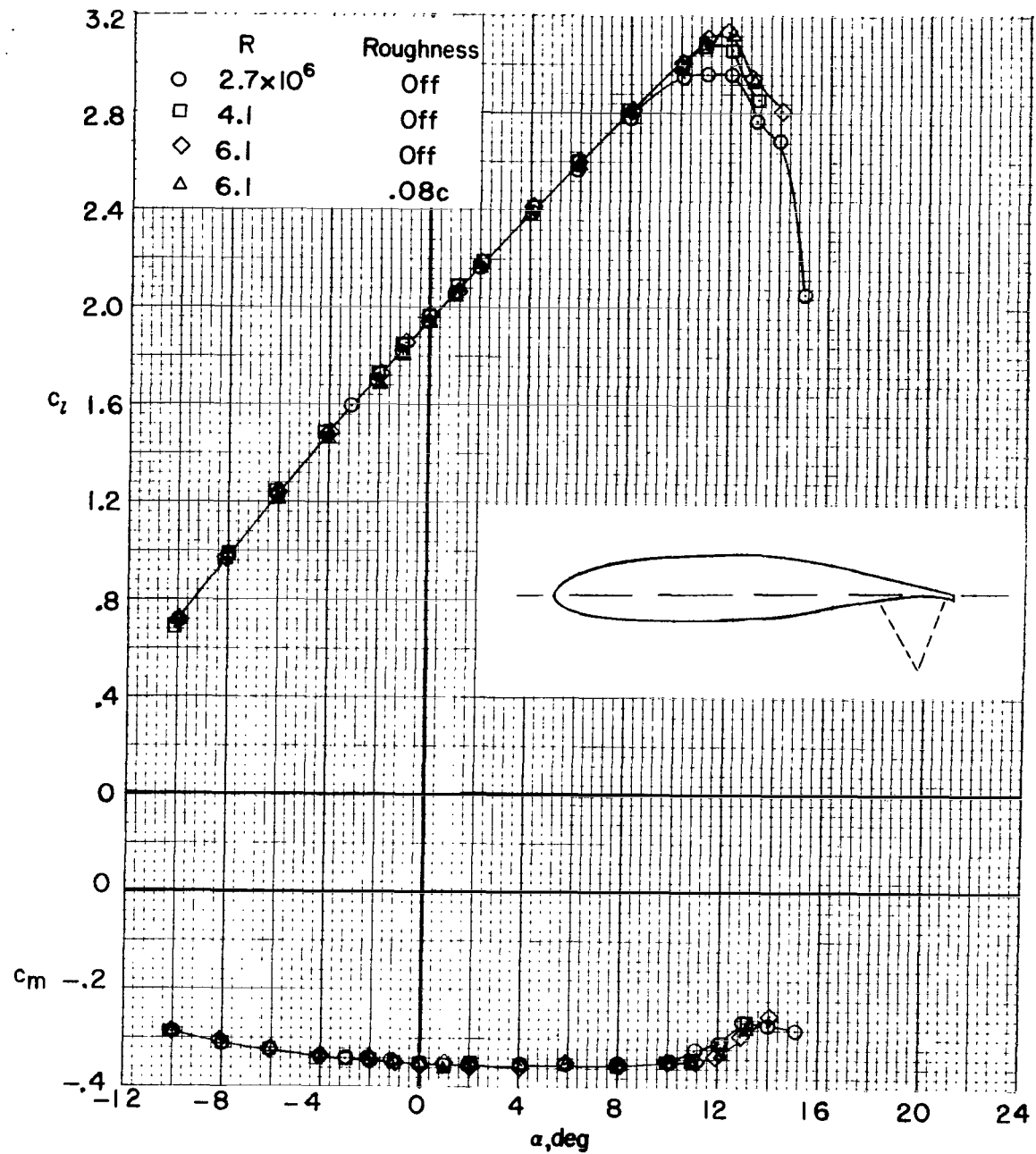
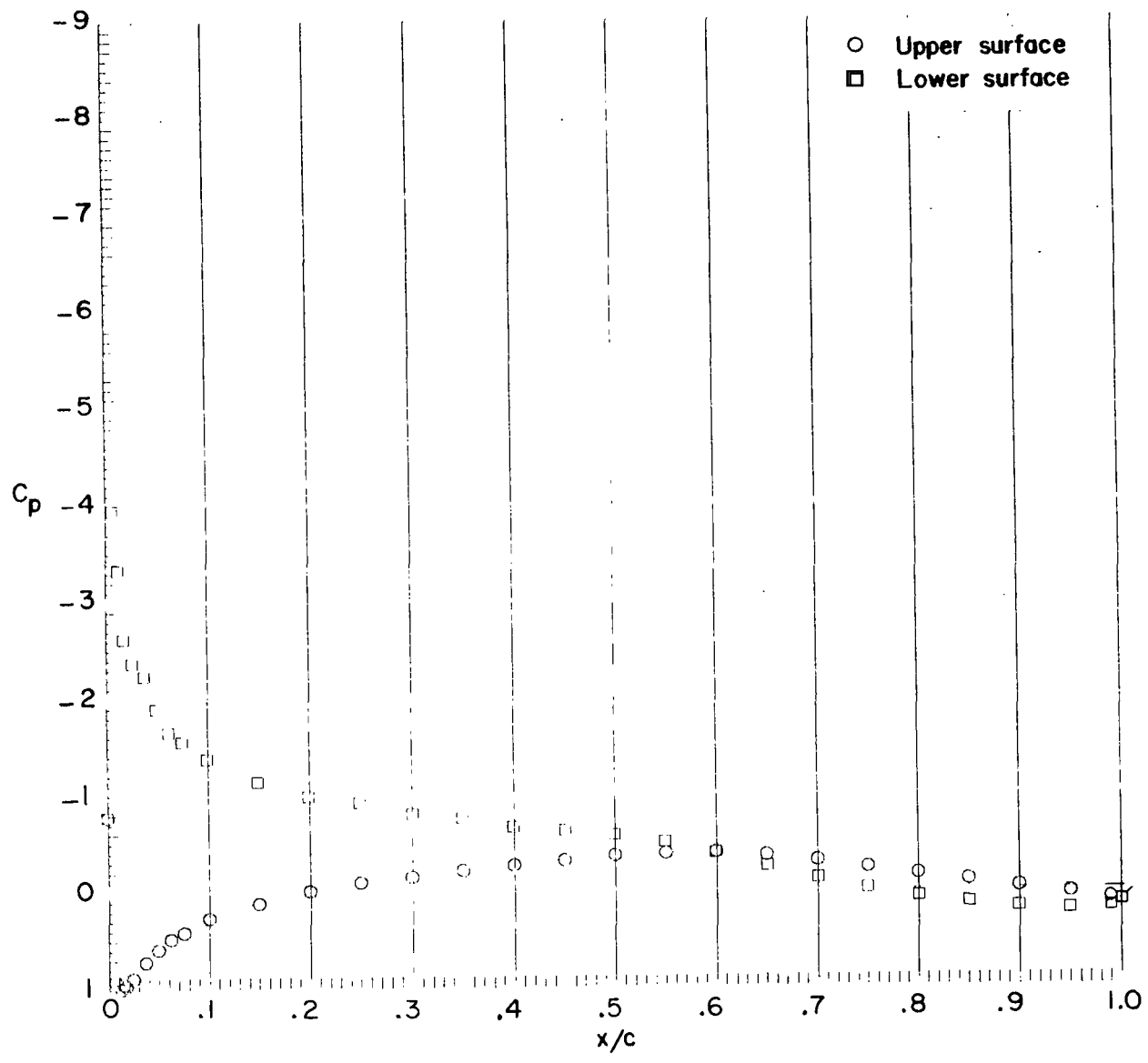


Figure 17.- Section characteristics for $0.20c$ simulated split flap deflected 60° . $M = 0.20$.

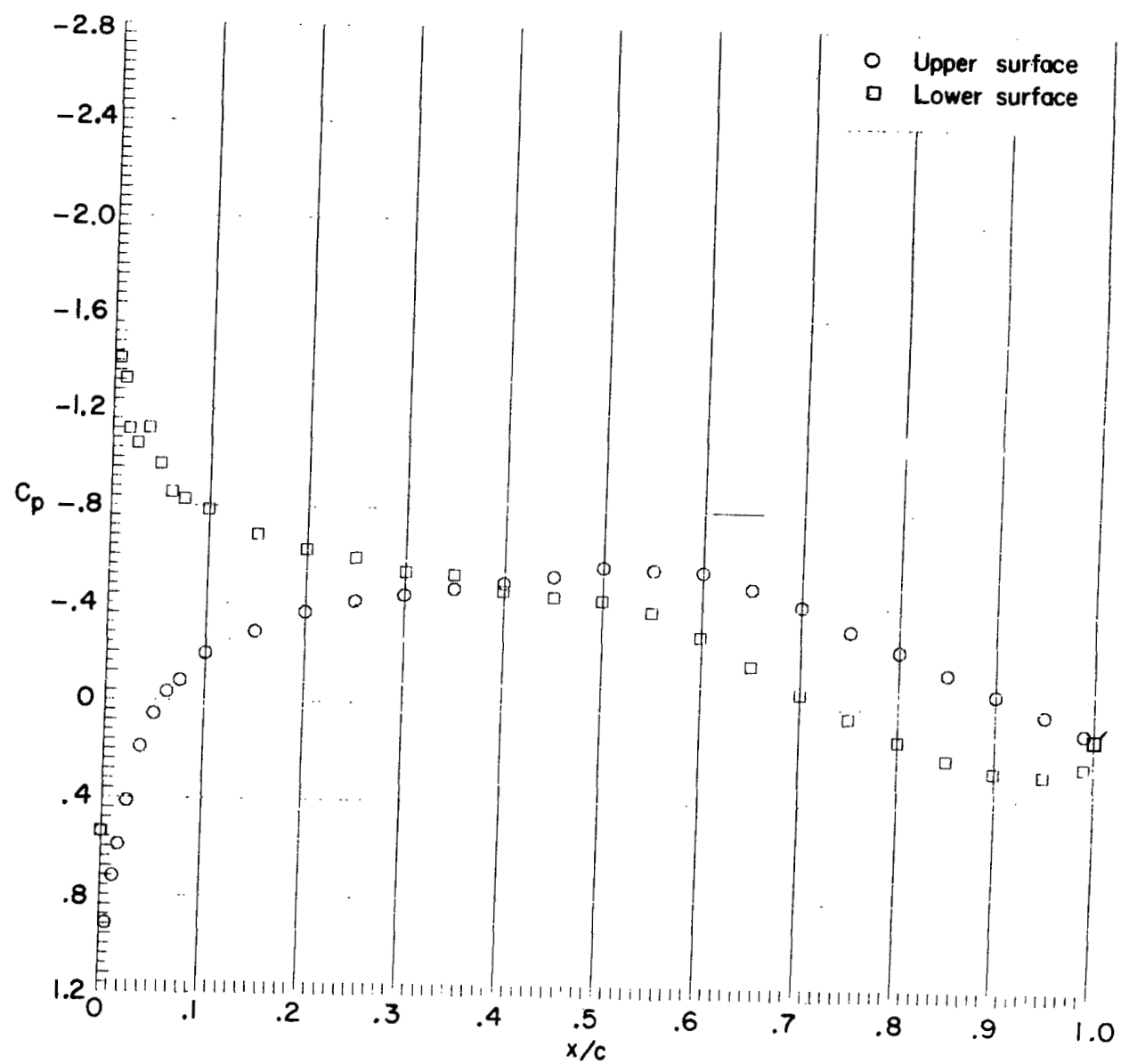


(a) $\alpha = -7.99^\circ$.

Figure 18.- Effect of angle of attack on chordwise pressure distributions.

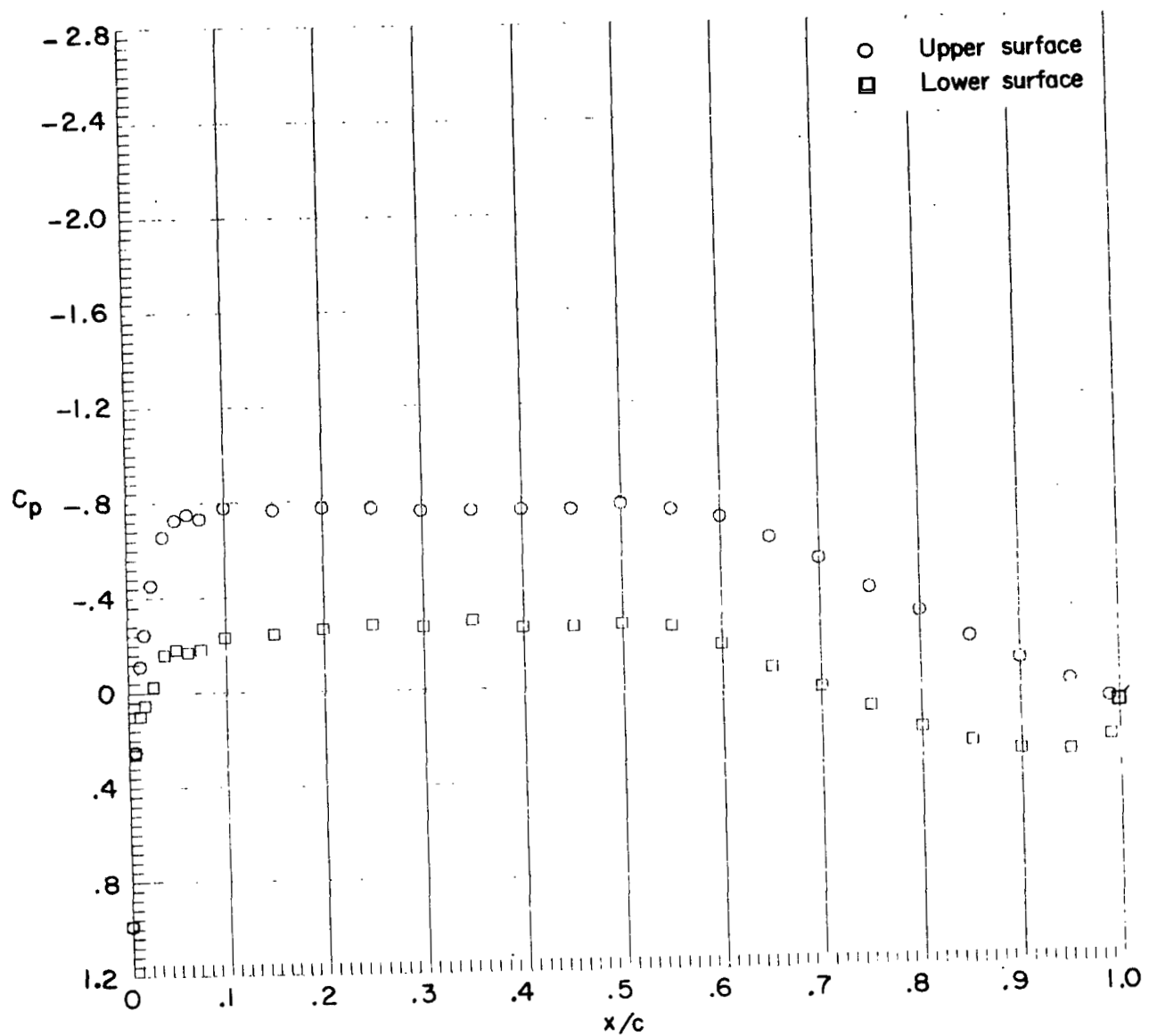
Number 80 roughness located at $0.08c$. $M = 0.15$; $R = 6.3 \times 10^6$.

(Flagged symbol indicates base pressure orifice.)



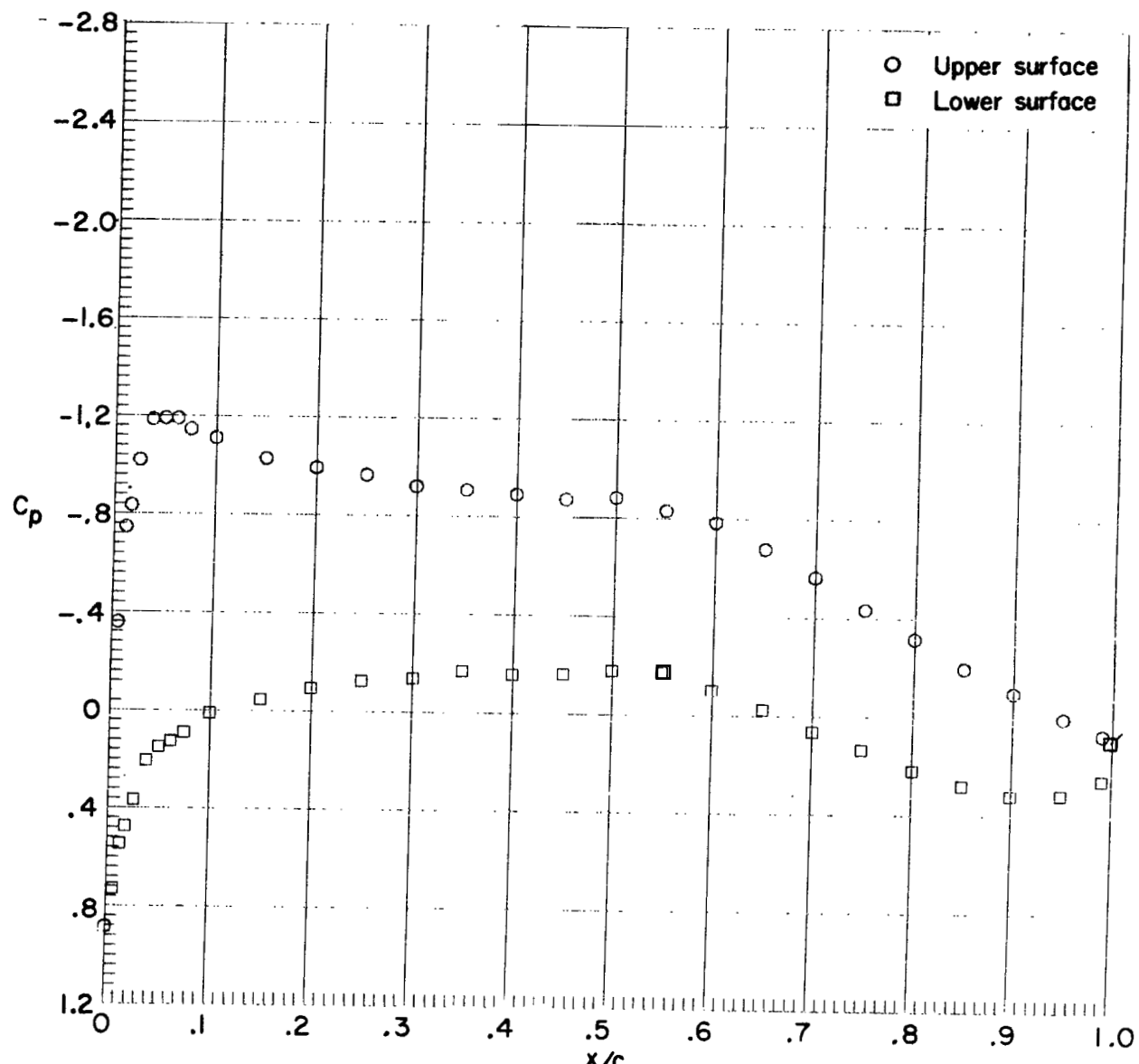
(b) $\alpha = -4.11^\circ$.

Figure 18.- Continued.



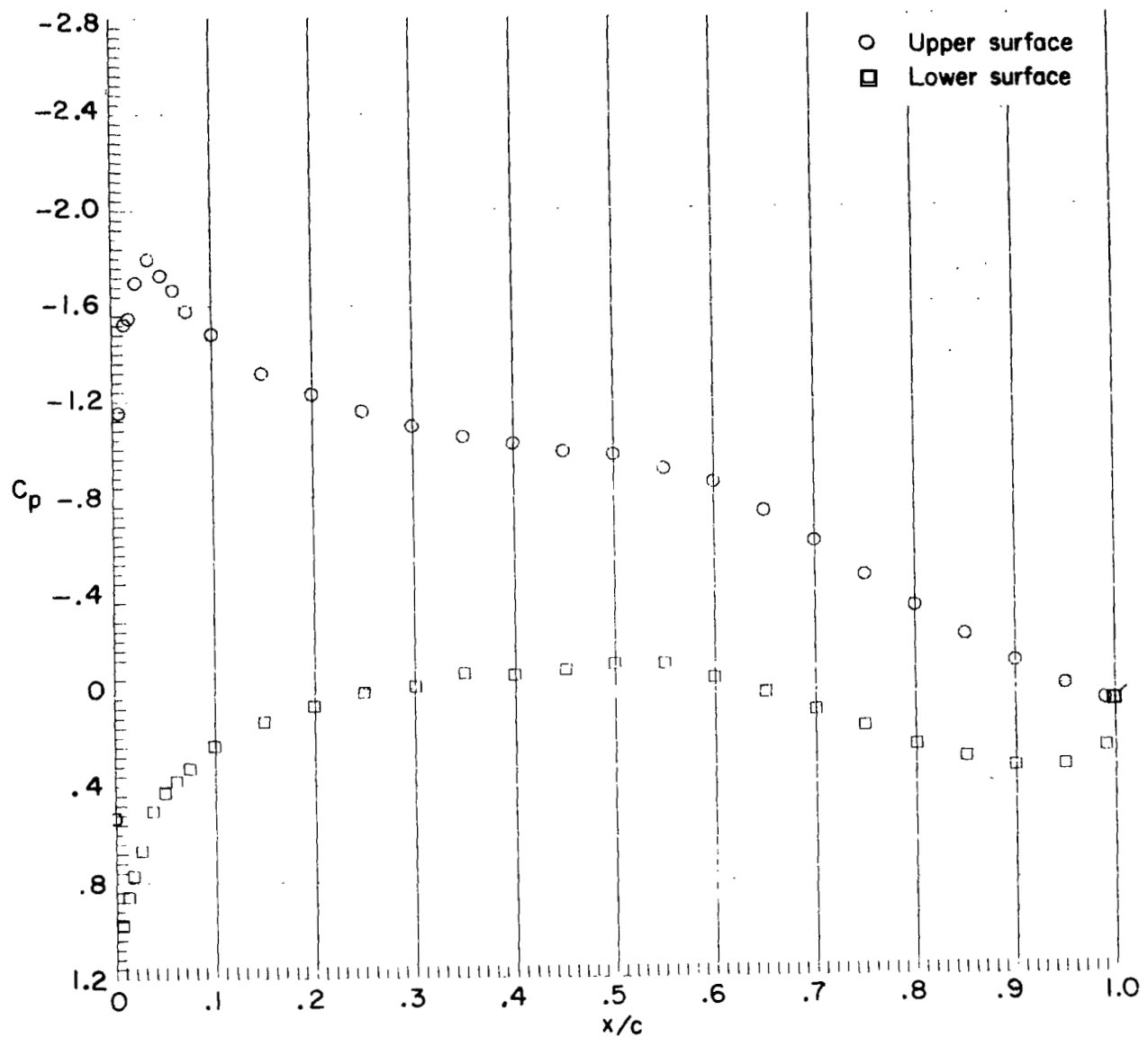
(c) $\alpha = 0^\circ$.

Figure 18.- Continued.



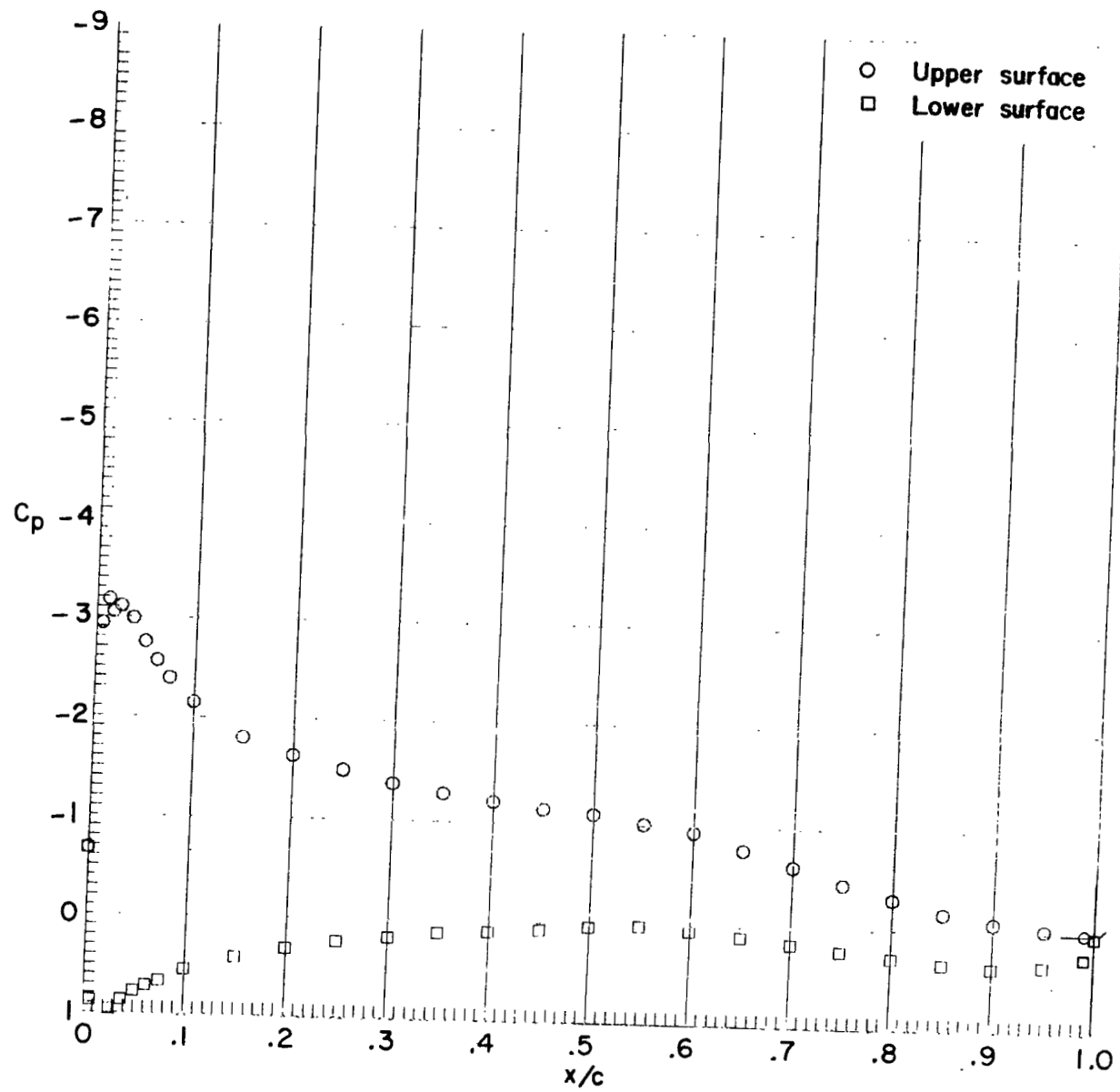
(d) $\alpha = 2.06^\circ$.

Figure 18.- Continued.



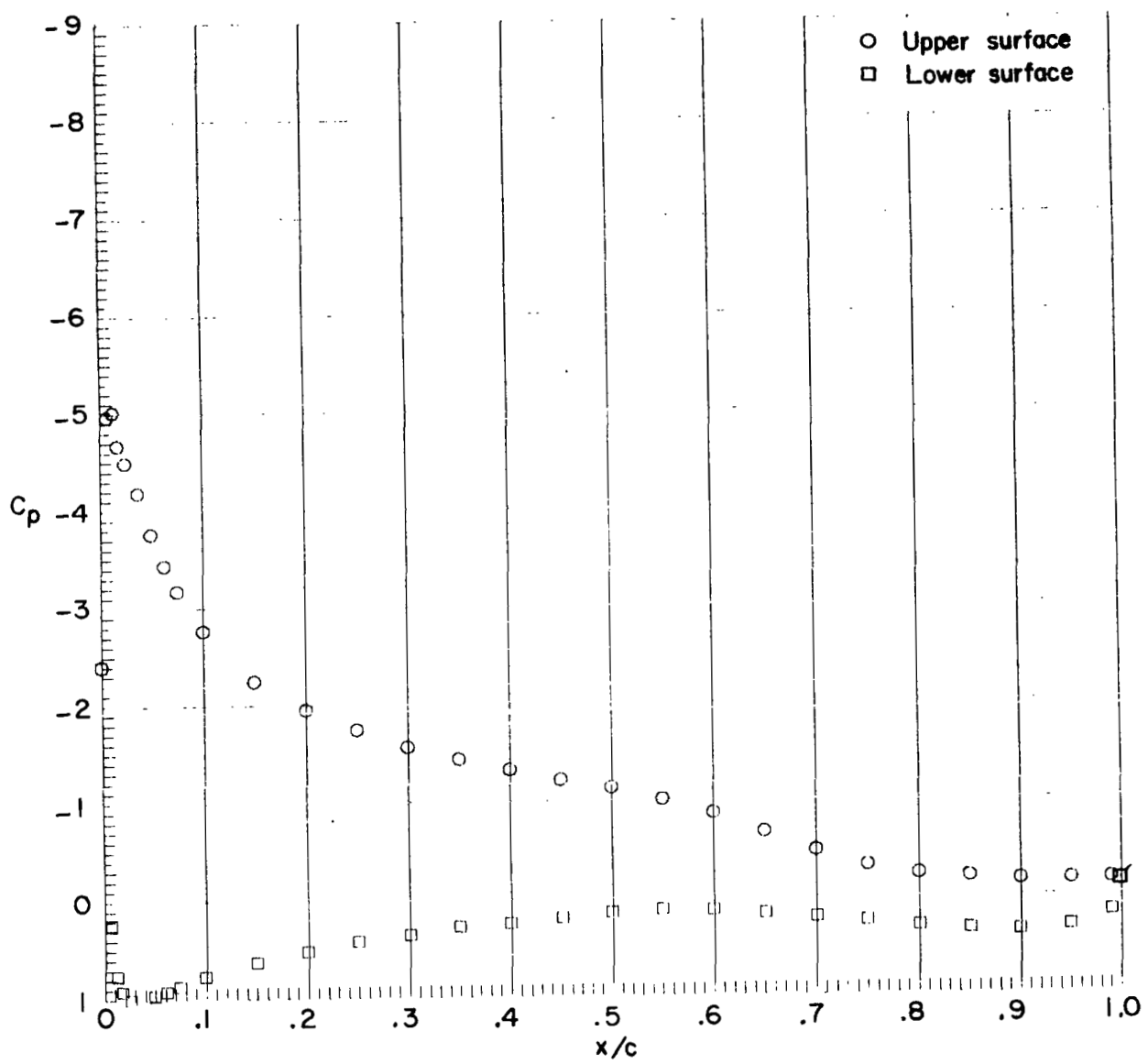
(e) $\alpha = 4.17^0$.

Figure 18.- Continued.



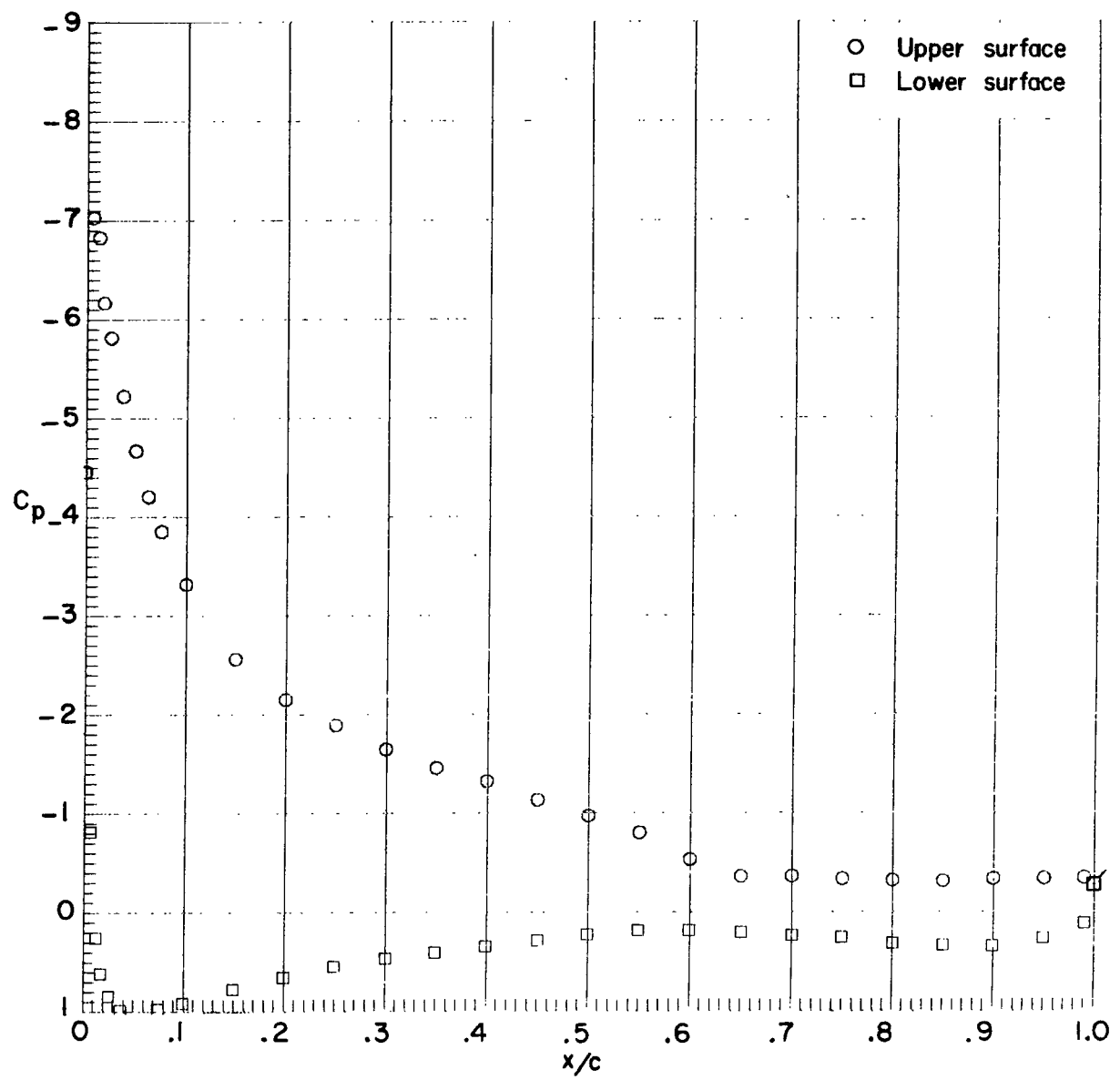
(f) $\alpha = 8.02^\circ$.

Figure 18.- Continued.



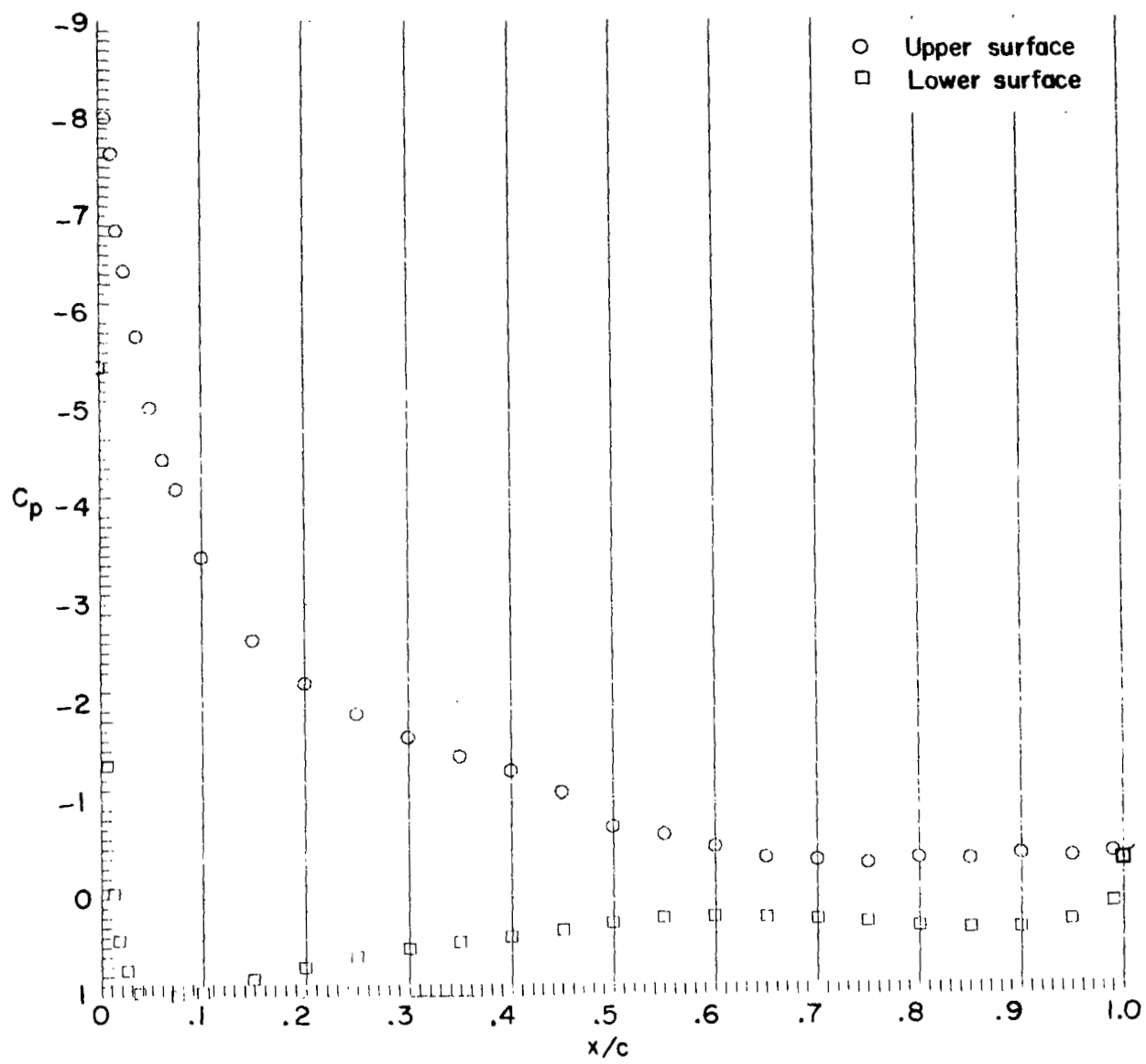
(g) $\alpha = 12.04^\circ$.

Figure 18.- Continued.



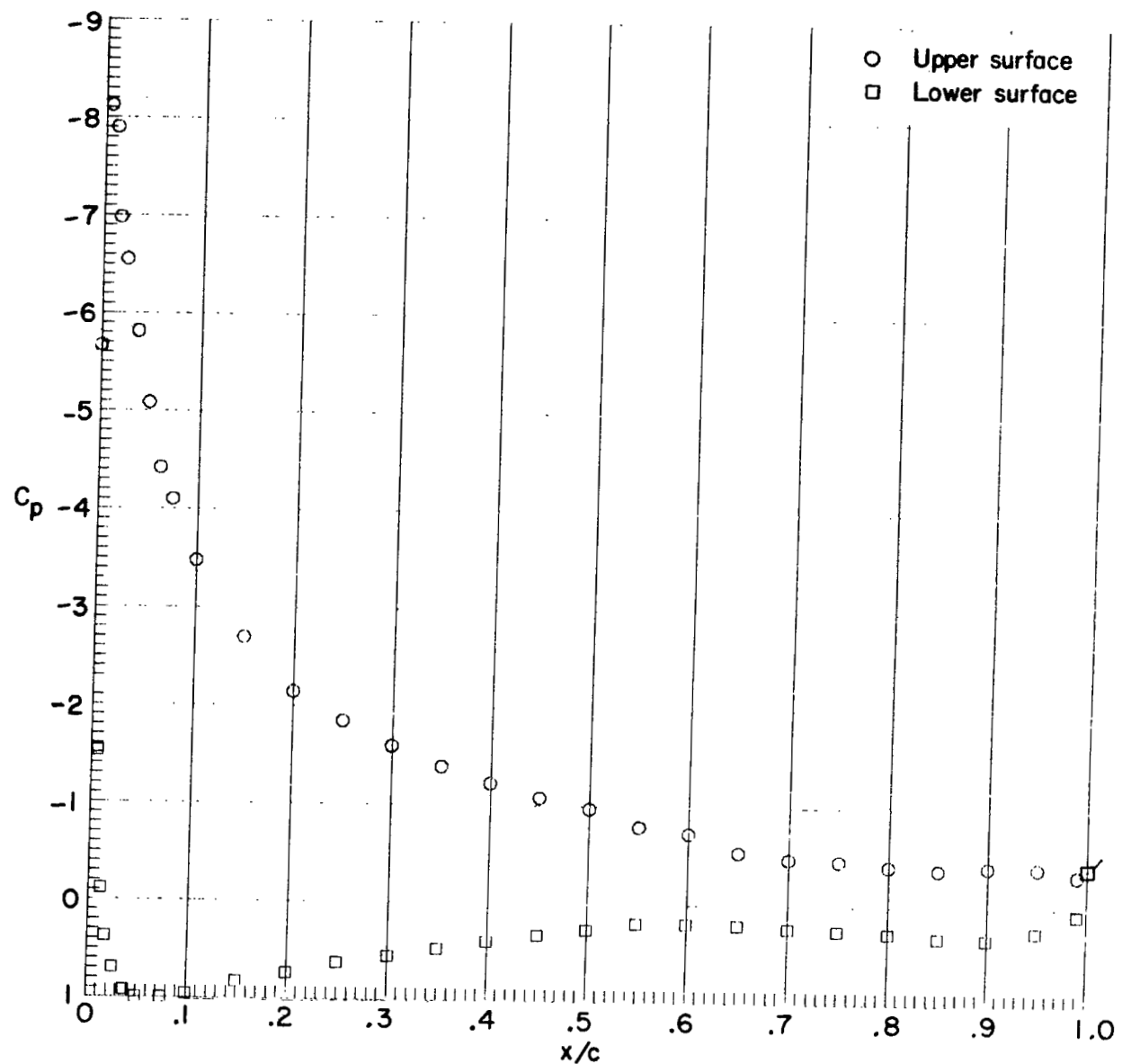
(h) $\alpha = 16.04^\circ$.

Figure 18.- Continued.



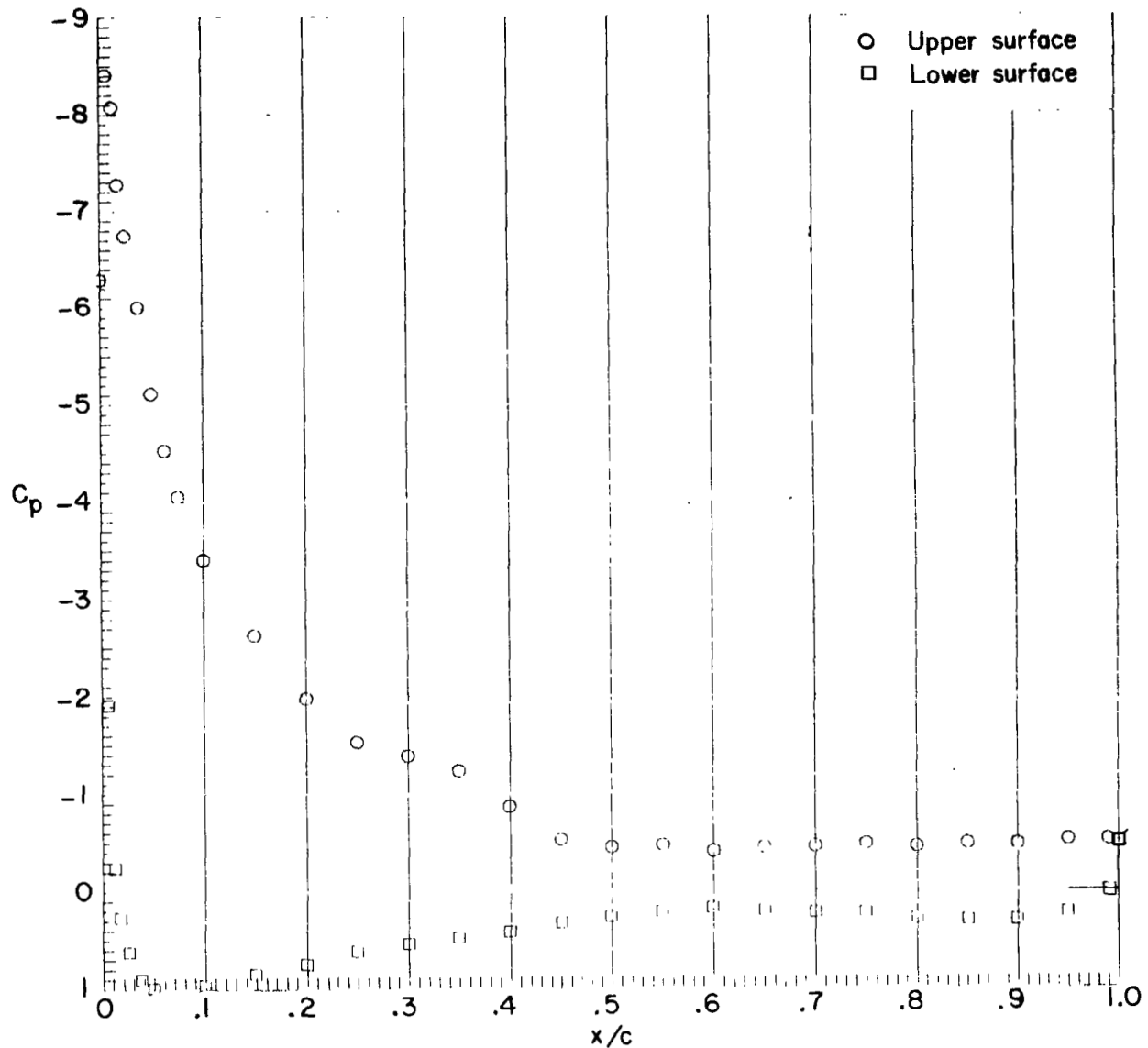
(i) $\alpha = 18.25^\circ$.

Figure 18.- Continued.



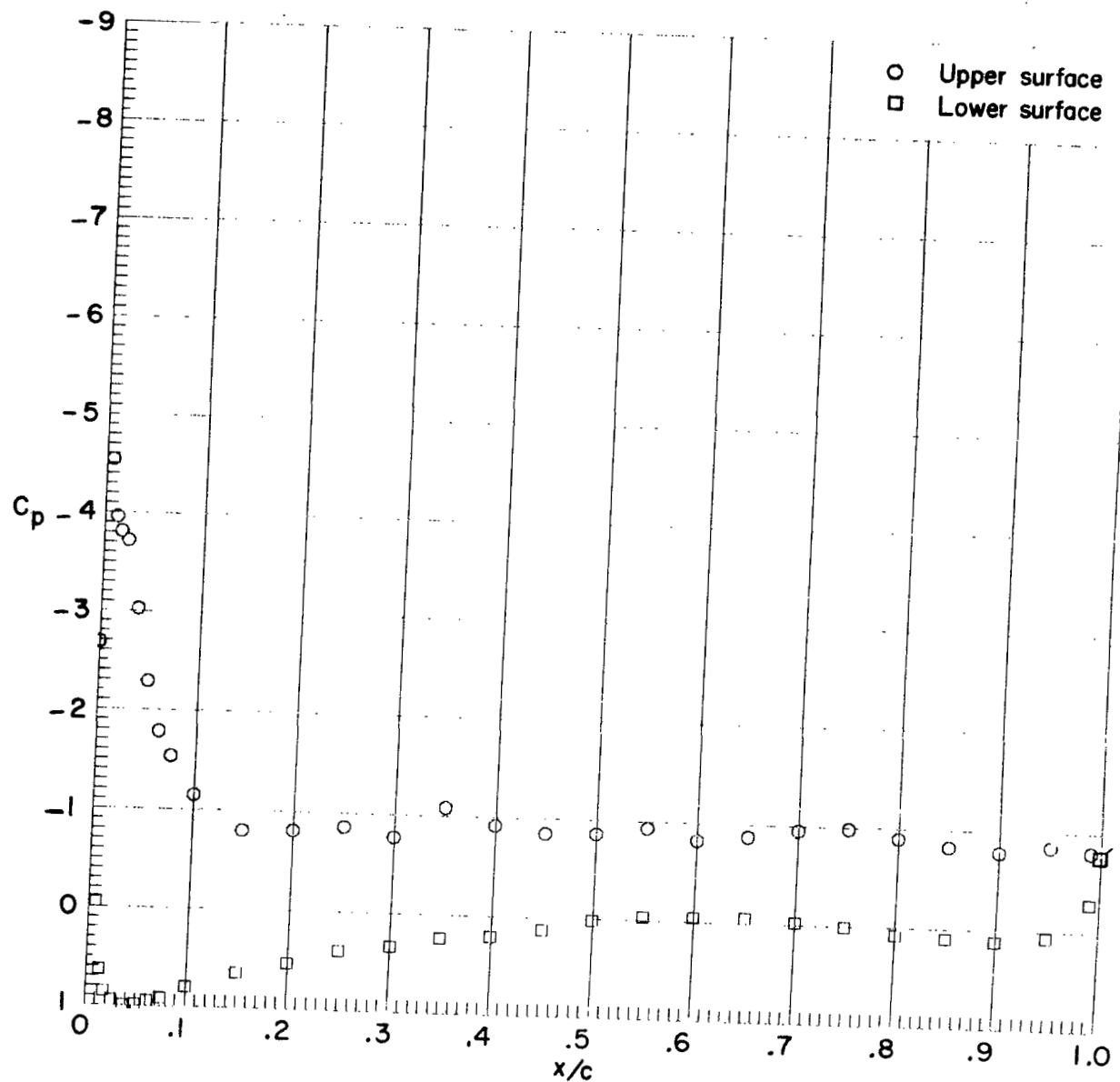
(j) $\alpha = 19.06^\circ$.

Figure 18.- Continued.



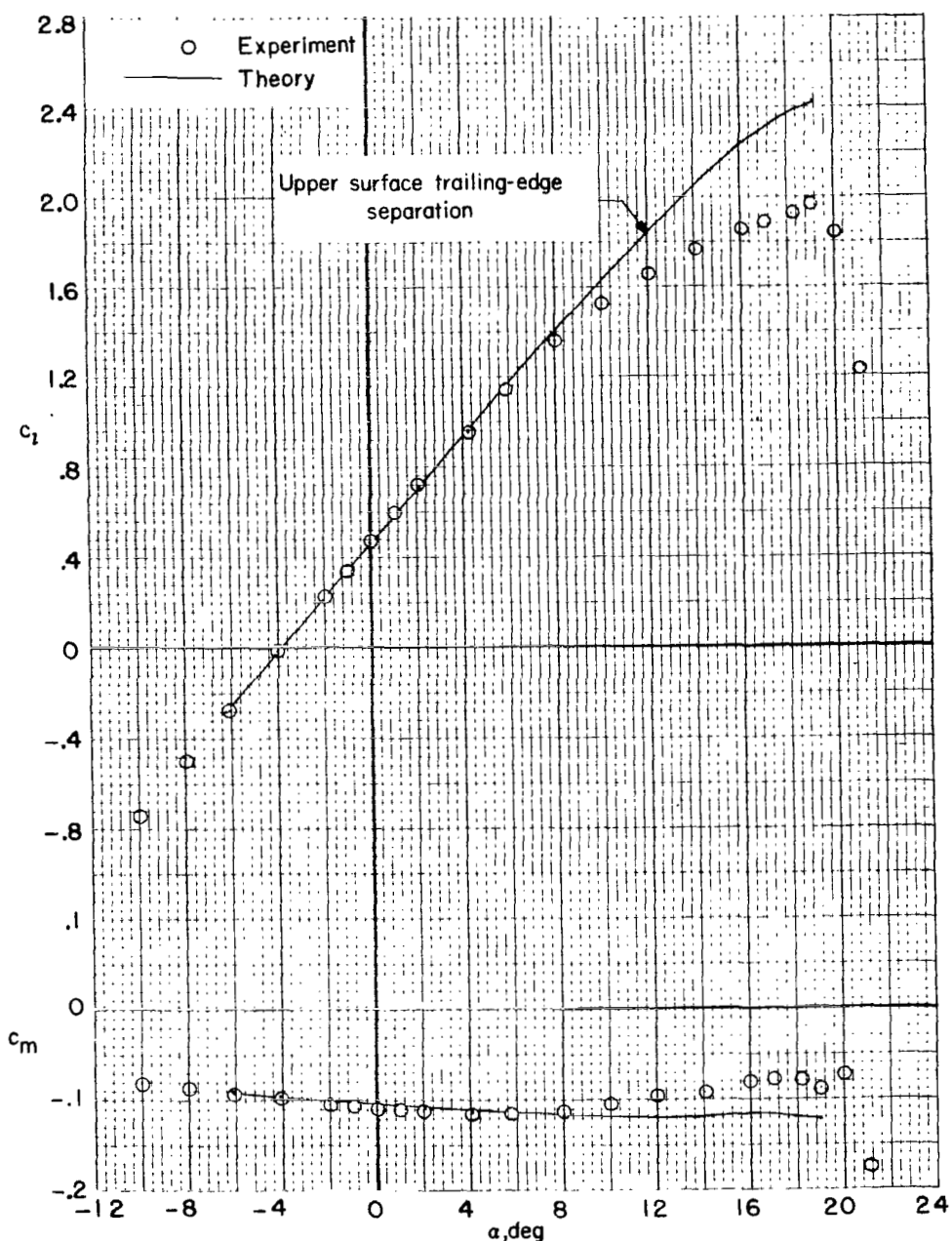
(k) $\alpha = 20.05^\circ$.

Figure 18.- Continued.



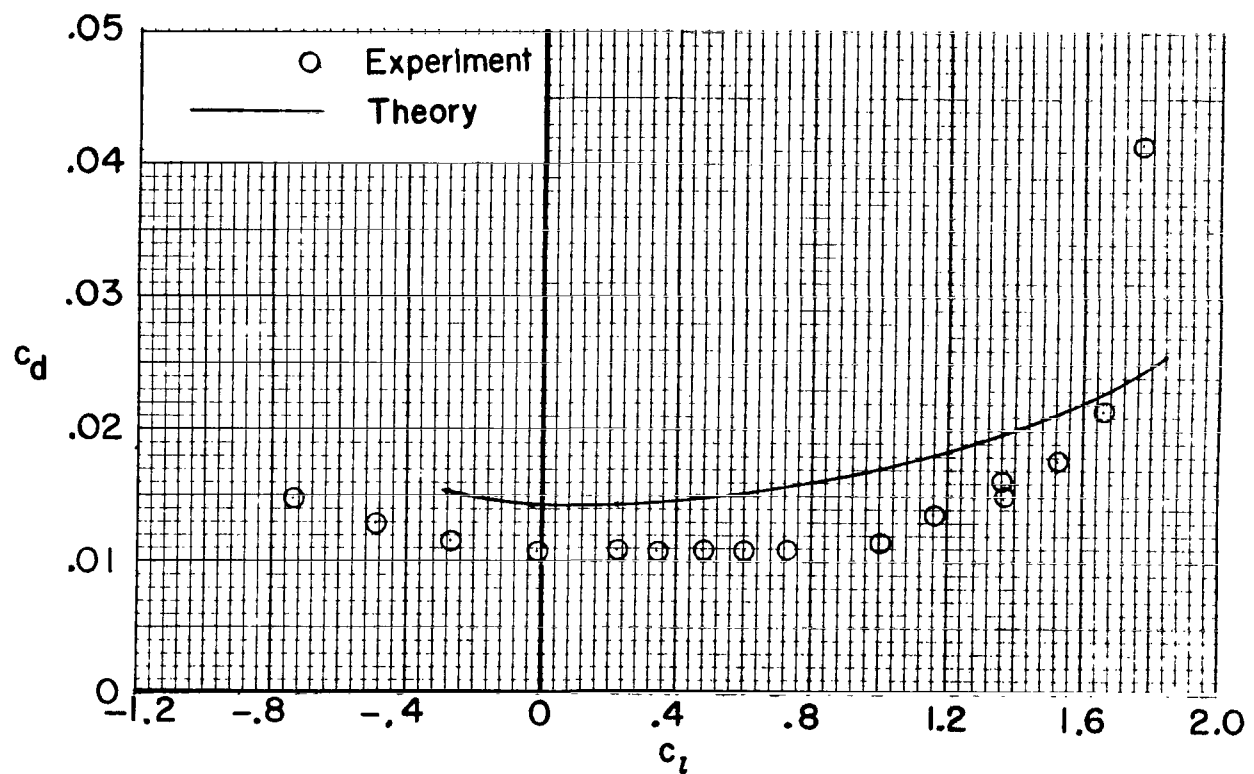
(1) $\alpha = 21.14^\circ$.

Figure 18.- Concluded.



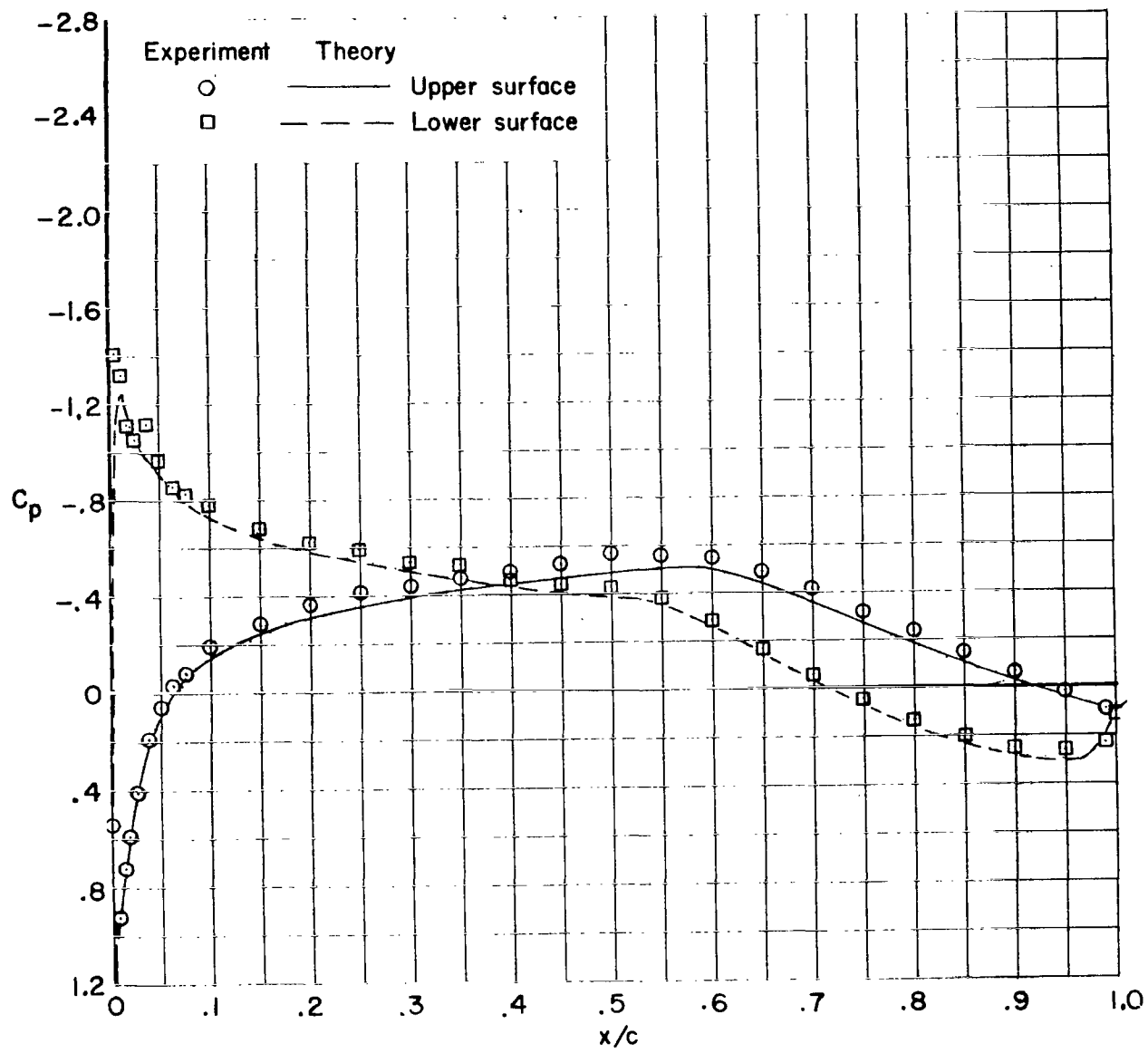
(a) Variation of c_l and c_m with α .

Figure 19.- Comparison of experimental and theoretical aerodynamic characteristics.
Transition fixed at $0.08c$; $M = 0.15$; $R = 6.3 \times 10^6$.



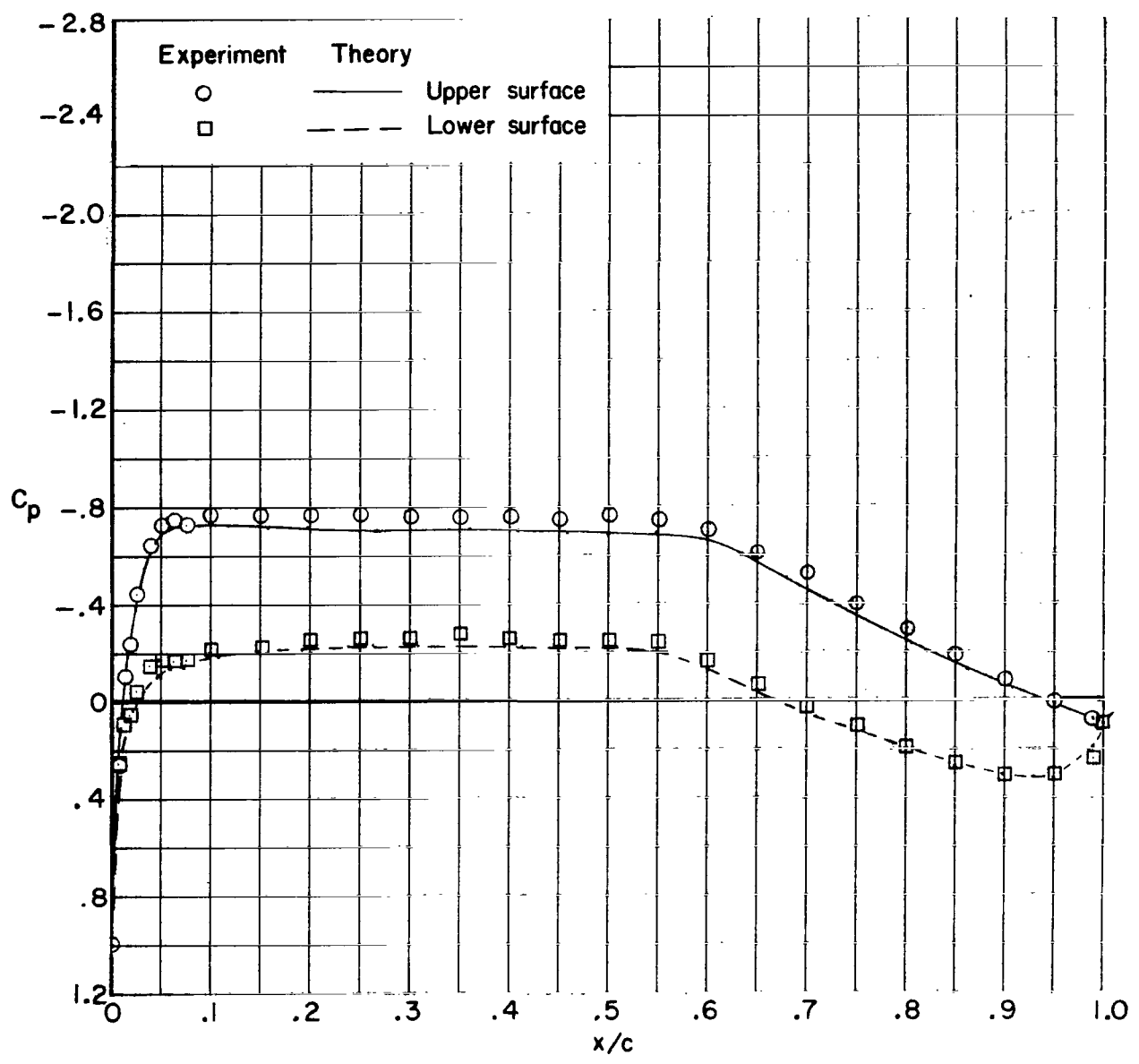
(b) Variation of c_d with c_l .

Figure 19.- Concluded.



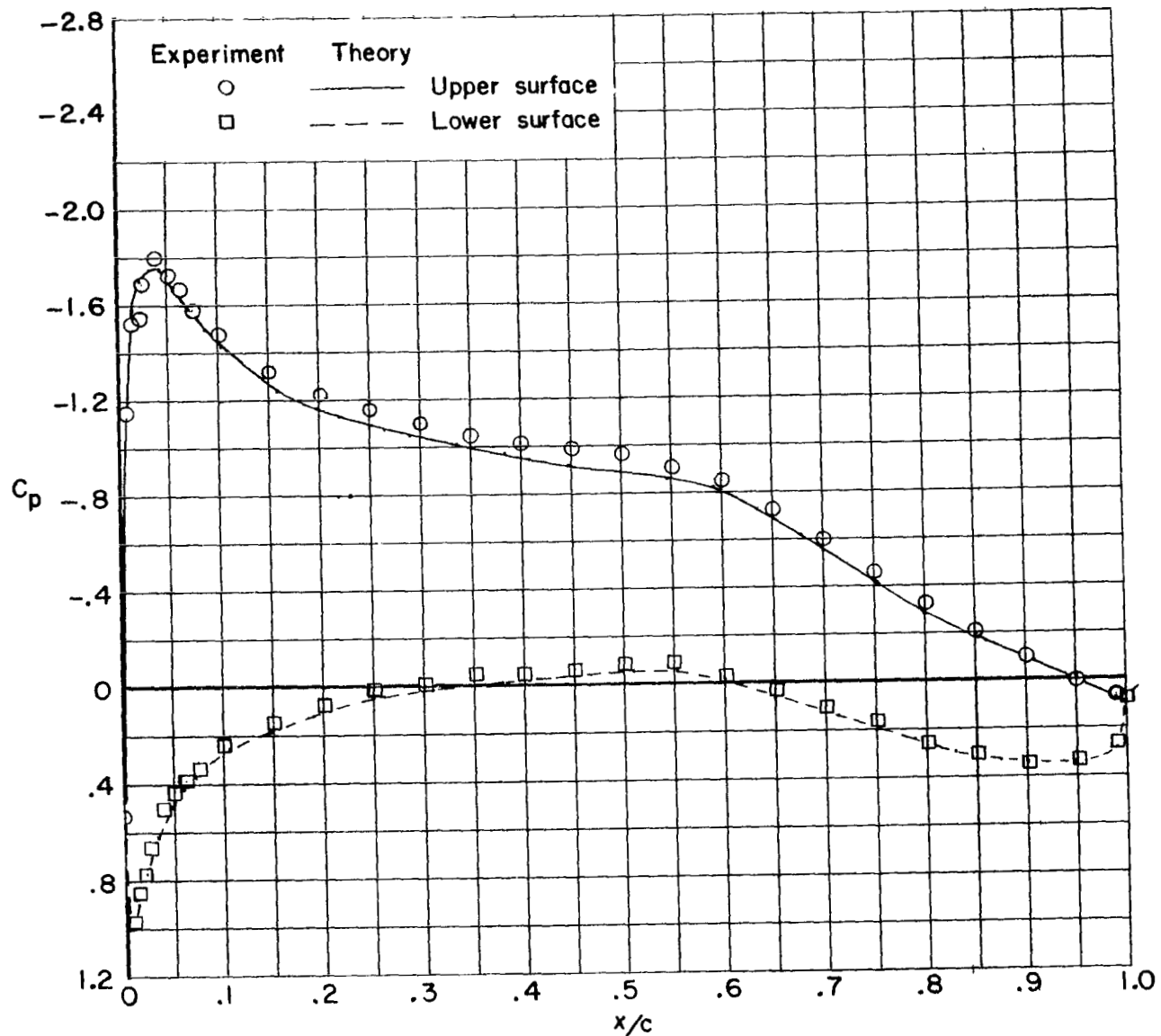
(a) $\alpha = -4.11^\circ$.

Figure 20.- Comparison of experimental and theoretical chordwise pressure distributions. Transition fixed at $0.08c$; $M = 0.15$; $R = 6.3 \times 10^6$.
 (Flagged symbol indicates base pressure orifice.)



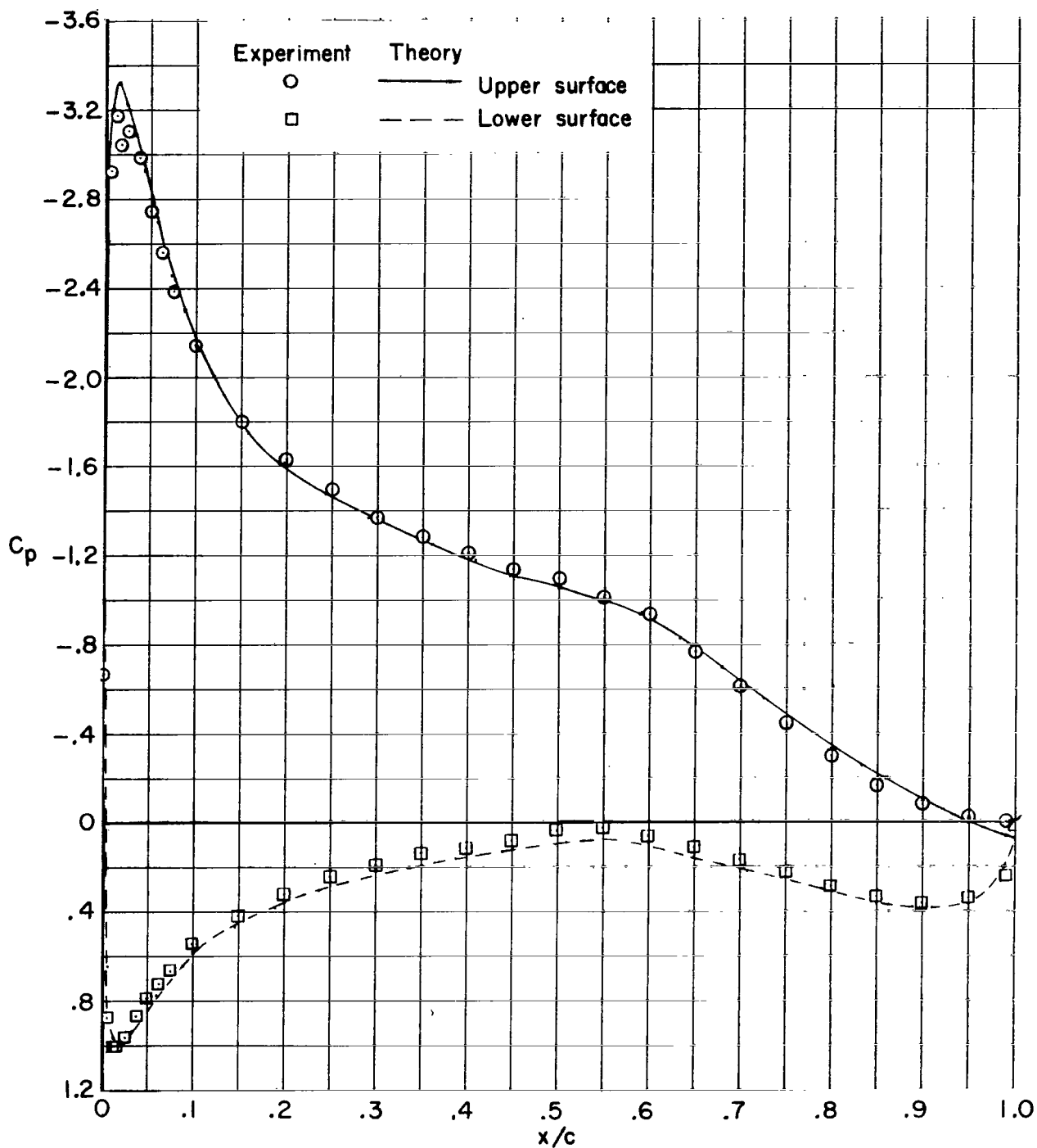
(b) $\alpha = 0^\circ$.

Figure 20.- Continued.



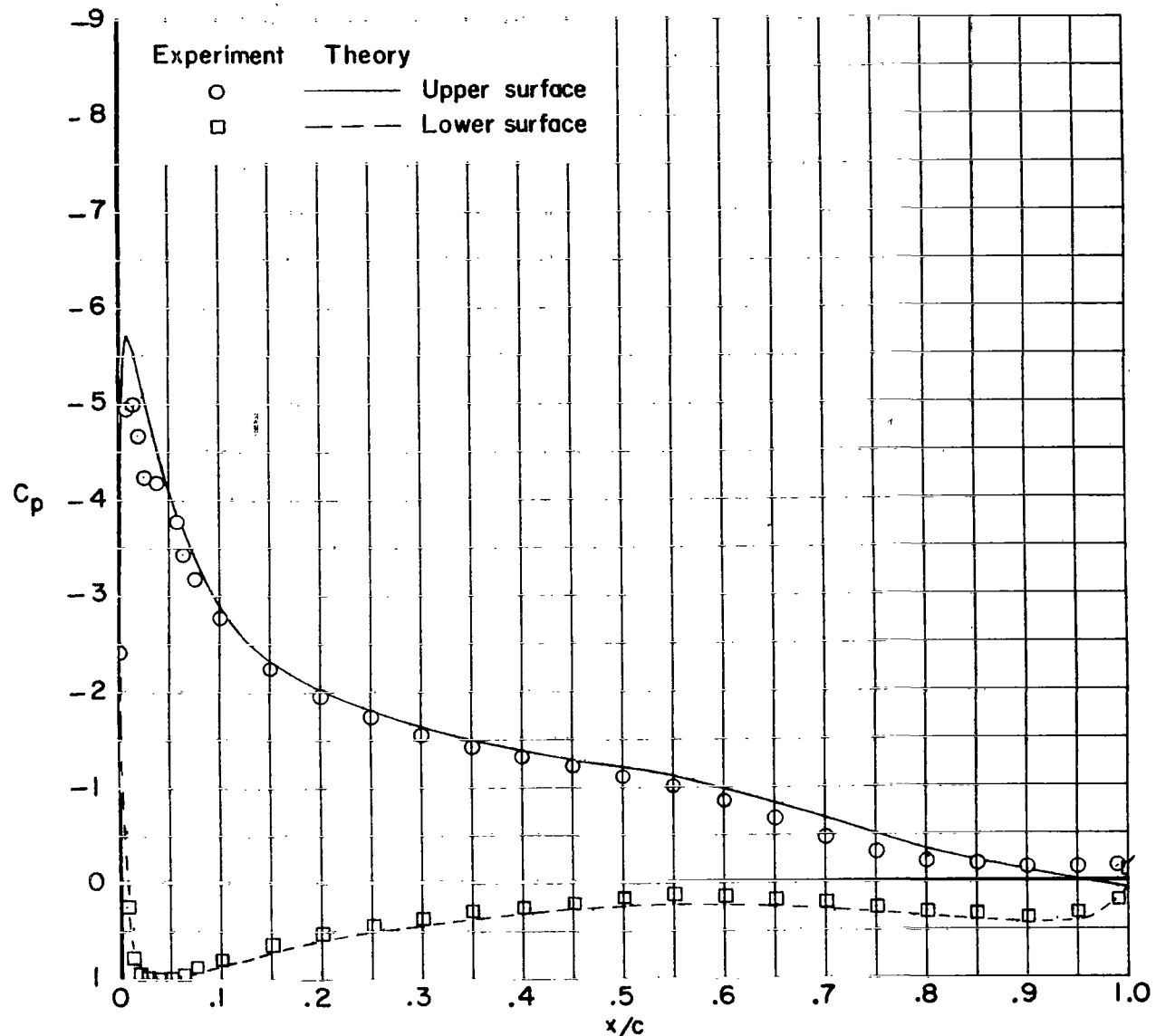
(c) $\alpha = 4.17^\circ$.

Figure 20.- Continued.



(d) $\alpha = 8.02^\circ$.

Figure 20.- Continued.



(e) $\alpha = 12.04^\circ$.

Figure 20.- Concluded.